Gravitational Instability of Galactic Discs

Joachim Wiegert
Supervisor: Alessandro Romeo

One-year Master's thesis in Physics
60 hec

Department of Physics
University of Gothenburg

Host institution: Department of Earth and Space Sciences
Chalmers University of Technology

Faculty of Science

UNIVERSITY OF GOTHENBURG

Gravitational Instability of Galactic Discs

One-year Master's thesis in Physics

Joachim Wiegert
guswiegj@student.gu.se

Supervisor
Alessandro Romeo
alessandro.romeo@chalmers.se

Department of Physics
University of Gothenburg
and
Department of Earth and Space Sciences
Chalmers University of Technology

November, 2010

Gravitational instability of galactic discs
JOACHIM WIEGERT

©JOACHIM WIEGERT, 2010

Master's thesis
Department of Physics
University of Gothenburg
SE-412 96 Gothenburg, Sweden
Telephone: + 46 (0)31-786 0000

Department of Earth and Space Sciences
Chalmers University of Technology
SE-412 96 Gothenburg, Sweden

Onsala Space Observatory
SE-439 92 Onsala, Sweden
Telephone: +46 (0)31-772 1000 (switchboard)

Cover: NGC 628 (M 74) from NED (NASA/IPAC Extragalctic Database) operated by the Jet Propulsion Laboratory, California Institute of Technology.

Abstract

Gravitational instability of galactic discs has been studied for several decades and is still of great importance. It gives understanding of the physics of disc dynamics, stellar formation rates and most relevant today, understanding of formation and evolution of galactic discs. However, this is a very complex theory to study in detail as there are plenty of processes available to consider. The standard approach is to use the simple Toomre stability criterion $Q > 1$ where Q is a parameter depending on the surface density and velocity dispersion of the gas disc.

In this thesis we study in detail the gravitational stability of galactic discs taking into account both stars and interstellar gas. We also apply our stability analysis to the galaxy samples of Leroy et al. (2008) to determine the importance of the stellar and gaseous components in the gravitational instability of the galactic discs. In particular we show that, in certain regimes of surface densities and velocity dispersions, the two components behave as if they are dynamically decoupled in the instability process. Our analysis also include the dynamical effects of disc thickness.

Besides, we propose a new approximation of the effective stability parameter for a two-dimensional disc of stars and gas which is simple and accurate.

Acknowledgements

First of all I would like to thank my supervisor, Alessandro Romeo for suggesting this thesis, for everything he has been able to teach me during this last year and of course also for his good support, extremely inspiring discussions and the many advice he has given. There is no way I can show how grateful I really am for his help.

I am also grateful for the cooperation and friendship with Volker Hoffmann. It has been appreciated and helpful to have someone available to discuss ideas and brainstorm with when trying a new angle on a problem or when just simply being stuck.

Next I would like to thank Farhad Aslani in the Hilbert room of the Physics Department for his many good advice with how to effectively use MATLAB. I am also extremely grateful for the many years of friendship and strange discussions with all the students that also spends time in the Hilbert room. These have been years I will always remember nostalgically.

I also want to thank the staff at the Onsala Space Observatory for the relaxed and friendly atmosphere during my stay there. Especially the other MSc-students, the PhD-students and the postdocs that have been around and willing to give advice when needed. And of course also the fans of the coffee breaks.

Finally I especially want to thank my caring and supporting parents, my older two brothers and sister who always seems to be around and available when needed, especially everytime I encounter a computer break-down.

Göteborg November, 2010
Joachim Wiegert

Nil volentibus arduum

Contents

Abstract **i**

Acknowledgements **iii**

1 Introduction **1**

2 Classical disc instability **5**
2.1 Local stability criterion 5
2.2 The marginal stability curve 6

3 Gravitational instability of stellar and gaseous discs **9**
3.1 Definitions 9
3.2 Analysis of Bertin & Romeo (1988) 10
3.3 The approximation of Wang & Silk (1994) 13
3.4 A new approximation 14
3.5 Summary 18

4 Application to observed galaxies **19**
4.1 Recent surveys 19
4.2 Two galaxy samples 20
4.3 Deriving useful quantities 24
4.4 Results for the first sample 25
4.5 Results for the second sample 27
4.6 Is there a threshold for star formation? 31
4.7 Summary 36

5 Dynamical effects of disc thickness **37**
5.1 Relevant parameters for two-component thick discs 38
5.2 The marginal stability curve 39
5.3 The two-phase region 40
5.4 The stability threshold 42
5.5 Summary 44

6 Conclusions **47**

A Numerical methods: thin discs **49**
A.1 Finding the two-phase region 49
A.2 Determining the stability threshold 50

B Radial profiles of the stability quantities **55**
B.1 Surface density and velocity dispersion ratios 55
B.2 Stability parameters 58
B.3 Radial profiles 59

C Numerical methods: thick discs **71**
C.1 Computing the marginal stability curve 71
C.2 Finding the two-phase region 73
C.3 Determining the stability threshold 74

References **79**

Chapter 1

Introduction

Gravitational instabilities of stellar and fluid discs is a rather old subject that has been studied extensively for almost 50 years since the foundation-laying works of Safronov (1960) and Toomre (1964) who made their discoveries with two different approaches. As will be shown shortly is this still an important field of study with much room for extension.

However, what is the importance of understanding large scale gravitational instabilities of galactic discs? In the past this subject was studied mainly for understanding the dynamics of discs as the formation of spiral arm structures. However, more common today is to try to understand the connection between gravitational instability and stellar formation rate. Both these areas are in turn important for understanding the formation and evolution of galactic discs.

We know from earlier work dating back to that of Schmidt (1959) that it is possible to observe an imperical relation between the gaseous mass densities of galactic discs and the stellar formation rate. Different formulations of these have been written where the most common one is known as the *Schmidt law* and there exist others as one formulated by Kennicutt that takes into account orbital time. The reader might be interested in a summary written by Burkert (2009) on modelling galactic discs that also mentions such stellar formation laws.

It is evident that gravitational stability must be used to explain the physics of stellar formation (Elmegreen 1999; McKee & Ostriker 2007; Leroy et al. 2008) however the phenomenom is highly complex and not well understood yet. There are many processes involved here, many not fully understood yet so those studying this must restrict what processes they are taking into account.

Another problem, perhaps the main problem of studies of instability is the complexity of the models. Even previous theories are very complex to formulate as those from the 60s that involves infinitesimally thin discs of one component, either gaseous or stellar. These approximations however gave very simple results that are easy to use and have been adequate for possible observations so far.

Today are on the other hand new observational possibilities emerging. We are today able to get high resolution of local galaxies and will soon with construction of observatories as ALMA (the Atacama Large Millimeter Array)[1] obtain higher resolutions of high-redshift galaxies. Al-

[1] *http://science.nrao.edu/alma/index.shtml*

ready are studies conducted by e.g. Puech (2010); Burkert et al. (2009) who are using previously formulated thin disc approximations and available resolution of high-redshift galaxies and by Leroy et al. (2008) who are using data from several large surveys of local galaxies to conduct a study of stellar formation rate and instability of a large sample.

Figure 1.1 is an example of two plots by Leroy et al. (2008) of the stability of their sample of spiral galaxies. These plots demonstrates the importance of knowing what aspects to take into account as there is a huge difference in the stability parameter when they only consider the gas component and when they consider both the stellar and gaseous components. The gas-only case seems inconclusive while in the stars+gas case several of the galaxies are marginal stable at several radii.

The problem comes with these new possibilities. The previously used approximations will not be sufficient anymore with the higher resolutions and more precise studies possible. However, we are also posed with the problem that more exact models of gravitational instability that as an example takes into account both gas and stars and uses three dimensional discs with finite thickness are very complicated to use. What is required is a study of these models and an attempt to formulate some analytical approximation with adequate accuracy for the coming observational possibilities.

Such studies have already been conducted by several authors. An expansion of the field by studying two-component infinitesimal thin discs have been done by e.g. Jog & Solomon (1984); Bertin & Romeo (1988); Wang & Silk (1994); Jog (1996); Rafikov (2001) so there is alot of foundation for a further study of the dynamics of these discs. What is required is an extensive study of the numerical solutions of this model to formulate some simple analytical expression that fit these.

Furthermore have also extensive analytical and numerical studies been done in the field of discs with finite thickness by especially Vandervoort (1970); Romeo (1990, 1992, 1994). These studies opens up possibilities for extensions and are possible to compare with previous approximations.

The outline of this thesis is as follows.

In Chapter 2 we revisit the works of Safronov (1960); Toomre (1964) concerning one component infinitesimal thin discs for an introduction into the theories of this field. Thus we are also able to define and explain important quantities that affect the stability and concepts as stability threshold, marginal stability curve and what assumptions allows this kind of approximation.

In Chapter 3 we will study the effects of taking into account a disc constising of two components, namely stars and gas as previously done by already mentioned authors. Here we get the opportunity to evolve a previously found approximation by Wang & Silk (1994) and formulate a new almost as simple and more accurate one to meet the coming observational requirements.

In Chapter 4 we apply observational data of galaxies on the model of Chapter 3. This is possible due to the extensive data provided by the study of Leroy et al. (2008) and thus we in this chapter conduct a similar gravitational stability study as them.

In Chapter 5 we finally study the effects of thickness as done by previous mentioned authors. We conduct a similar study as in Chapter 3 and study how the different concepts that arises from a two-component disc are affected by thickness.

This is followed by a short summary of the most important conclusions we can draw in

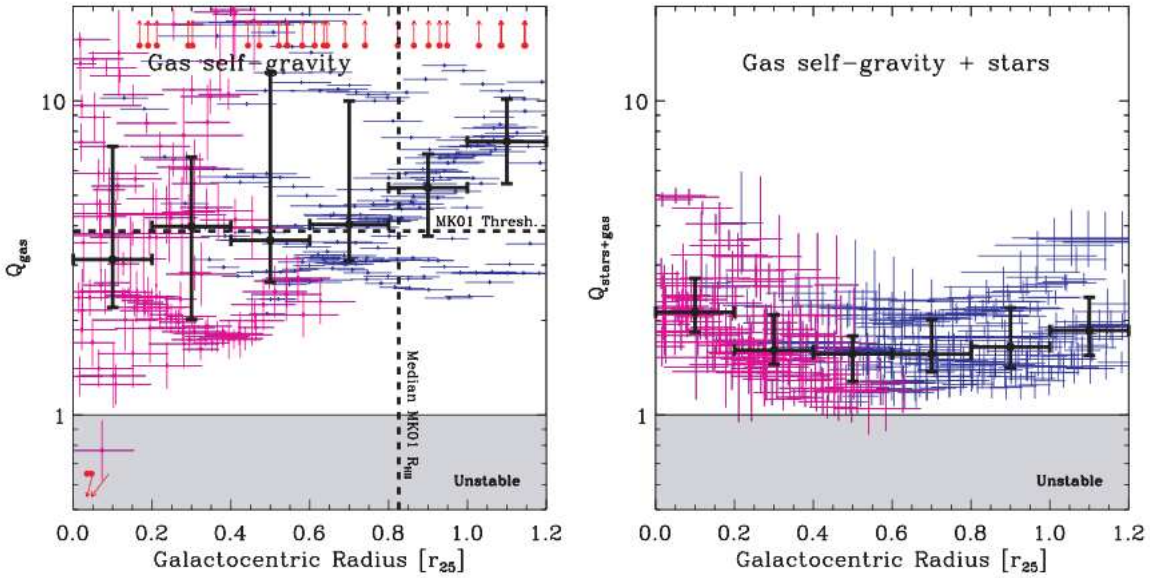

Figure 1.1: Two frames of Figure 9 from Leroy et al. (2008). A perfect example of how gravitational instability is analysed in local galaxies. The left frame is with only taking gas into account and the right frame takes both the stellar and gaseous components into account for their sample of spiral galaxies. In magenta points the gas component is dominated by H_2, in blue points the gas is dominated by HI and the black crosses are the median of the binned data. The grey areas indicate conditions for instability.

Chapter 6 and in the specific appendices are details surrounding the numerical methods and observational data used.

Chapter 2

Classical disc instability

Before we are able to consider stability of galactic discs consisting of both stellar and gaseous material and taking into account disc thickness we should study the classical cases. For this we will consider a stability model of a galactic disc with no thickness and constisting of only one component, or one fluid. By doing so will the terminology used throughout this thesis be defined and understood more easily.

2.1 Local stability criterion

The classical case considered in the 1960's by e.g. Safronov (1960) assumes a disc with no thickness as previously mentioned and consisting of one fluid, usually gas which is collisional. It needs to be differentially rotating with a non-zero radial velocity dispersion and have axisymmetric perturbations. With these assumptions it is possible to derive what is known as a dispersion relation consisting of stabilising and destabilising terms.

In this case the dispersion relation is defined as

$$\omega^2 = \kappa^2 - 2\pi G\Sigma k + \sigma^2 k^2 \tag{2.1}$$

(Binney & Tremaine 2008, p. 495). Also see Fridman et al. (1984, p. 393), however they are using an older notation. The κ is the epicyclic frequency, i.e. the frequency of oscillation of a perturbed circular orbit, Σ is the surface density, k is the wavenumber of the perturbation and σ is the velocity dispersion. The disc we are studying will be unstable if the solution to this is imaginary, i.e. $\omega^2 < 0$. However, to derive a stability criterion we first need to find what wavenumber corresponds to when the minima of ω is zero. As this is a quite simple quadratic equation we can derive this to be when

$$k = \frac{\pi G\Sigma}{\sigma^2}. \tag{2.2}$$

Keeping $\omega = 0$ and using the minima we can derive the stability criterion. What we end up with is that the disc is locally stable for all wavenumbers if

$$\frac{\kappa\sigma}{\pi G\Sigma} > 1, \tag{2.3}$$

usually written as $Q > 1$. This is commonly known as the *Toomre stability criterion* where Q is known as the *Toomre parameter*. However, the more correct name is in fact the *Safronov-Toomre criterion*. Toomre derived a model of kinematic discs (stellar discs) instead of fluid discs. His stability criterion is very similar to equation (2.3),

$$\frac{\sigma\kappa}{3.36G\Sigma} > 1 \tag{2.4}$$

(Binney & Tremaine 2008, p. 496). However, in this thesis we consider only fluid discs.

2.2 The marginal stability curve

We have now been introduced to the concept of a stability parameter which shows us if the disc is locally stable for all wavenumbers of the perturbation. However it is also useful to study how the stability depends on the wavenumber. For this we will derive a function $Q(\Lambda)$ which is known as the *marginal stability curve*.

We derived the stability criterion earlier directly from the dispersion relation. This is not always possible when we consider the more complex cases later in this thesis. The marginal stability curve is on the other hand possible to derive both analytically and numerically and a stability criterion is in turn possible to derive either analytically or numerically from this curve. The marginal stability curve is also very powerful when trying to understand how the special conditions of the cases we study affect the behaviour of the stability criterion.

Previously we looked at the dispersion relation, equation (2.1) at the minima and set $\omega = 0$. Now we instead study how the relation behaves along $\omega = 0$. The whole boundary of stability commonly known as the line of neutral stability.

However, we first need to define a useful dimensionless wavelength,

$$\Lambda = \frac{\lambda}{\lambda_{\mathrm{T}}} = \frac{k_{\mathrm{T}}}{k} \tag{2.5}$$

where k_{T} (λ_{T}) is a critical wavenumber (wavelength) or *Toomre wavenumber*, defined by Toomre (1964) as

$$k_{\mathrm{T}} = \frac{\kappa^2}{2\pi G\Sigma}. \tag{2.6}$$

By setting $\omega = 0$ in equation (2.1) and dividing by k_{T}^2 we obtain

$$\frac{\kappa^2}{k_{\mathrm{T}}^2} - 2\frac{\pi G\Sigma}{k_{\mathrm{T}}}\frac{1}{\Lambda} + \frac{\sigma^2}{\Lambda^2} = 0 \tag{2.7}$$

where we insert equation (2.6) and rewrite in the form of the Toomre parameter Q so that we obtain the expression

$$\frac{4}{Q^2} - \frac{4}{Q^2}\frac{1}{\Lambda} + \frac{1}{\Lambda^2} = 0 \tag{2.8}$$

which is easily rearranged to our final goal,

$$Q = 2 \cdot \sqrt{\Lambda(1-\Lambda)}. \tag{2.9}$$

This is the marginal stability curve of the classical Toomre stability and it is plotted in figure 2.1. A Q anywhere above the curve means that the system is locally stable while anywhere under the curve it is unstable.

In this classical case the peak of the curve is always at $Q = 1$. However this is not true for more complex models, that is why we define a parameter known as the *stability threshold*, denoted $\bar{Q}$. This determines how stable the system is (it is interesting to read Polyachenko et al. 1997 who expands this classic case and studies the stability threshold). We also have for the peak of the curve a corresponding *most unstable wavelength*, denoted as $\bar{\Lambda}$. Usually in the classical one component case this is situated at one half of the Toomre wavelength λ_{T}. And again, in more complex models the behaviour of this could be interesting to study.

It is Important here to remember that this classical Toomre stability criterion is reliable only if the most unstable wavelength is much shorter than the disc scale length R_{d} and if $kh \ll 1$, where h is the disc scale height (Binney & Tremaine 2008, p. 496). So this model is just an early approximation of a galactic disc. However, it is still commonly used when conducting stability analyses and in studies of stellar formation rates. It gives a general picture, though rather inprecise and also a good understanding of the very complicated behaviour of gravitational unstable discs.

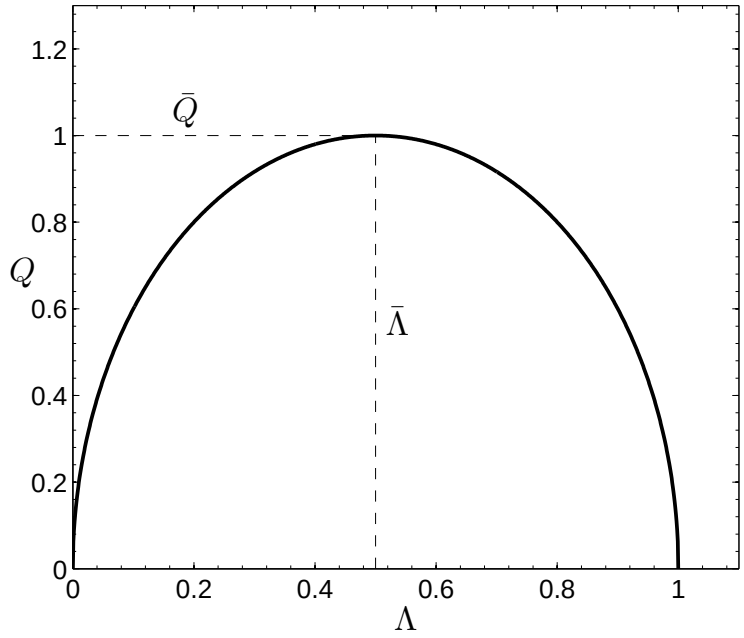

Figure 2.1: Marginal stability curve for tightly wound axisymmetric perturbations in a zero-thickness one component fluid disc.

Chapter 3

Gravitational instability of stellar and gaseous discs

The first more complex case we are going to study is a zero thickness galactic disc consisting of two components, i.e. stars and gas (the interstellar medium). This has been studied several times before by e.g. Jog & Solomon (1984); Bertin & Romeo (1988); Wang & Silk (1994); Jog (1996); Rafikov (2001).

In this chapter I have studied the analysis carried out by Bertin & Romeo (1988). However, the definitions have been adapted to a less theoretical and more modern parametrization. This analysis has been compared to the approximation done by Wang & Silk (1994) which is very commonly used today (Martin & Kennicutt 2001; Hitschfeld et al. 2009; Puech 2010; Burkert et al. 2009; Krumholz & Burkert 2010). However Martin & Kennicutt (2001) do not use the approximation in their study, they only consider what conclusions they could have drawn by using it on their selection of galaxies. The Wang & Silk (1994) approximation is unfortunetaly not adequately accurate (see Jog 1996), a new approximation is instead formulated with the help of Alessandro Romeo that might be very useful.

3.1 Definitions

In the classical case we had a marginal stability curve as a function of the fluid surface density, the velocity dispersion and a dimensionless wavelength Λ for axisymmetric perturbations. Obviously we need for a disc containing two fluids also two surface densities and velocity dispersions. Following what was done by Bertin & Romeo (1988) we define two parameters,

$$\mathcal{A} = \frac{\Sigma_{\rm g}}{\Sigma_{\rm s}} \tag{3.1}$$

and

$$\mathcal{B} = \frac{\sigma_{\rm g}}{\sigma_{\rm s}} \tag{3.2}$$

where the Σ's are the surface densities for the gaseous (g) and stellar (s) components respectively and the σ's are the velocity dispersions. The dimensionless wavelength was previously defined in equations (2.5) and (2.6) and is similary defined here as

$$\Lambda = \frac{k_{\mathrm{s}}}{k} = \frac{1}{k} \cdot \frac{\kappa^2}{2\pi G \Sigma_{\mathrm{s}}} \tag{3.3}$$

where k_{s} is the corresponding Toomre wavenumber for the stellar component.

We also need to define a Q-parameter that is adaptable for this more complicated situation. We do this by introducing the stability threshold, $\bar{Q}$. In analogy with the Toomre stability criterion, equation (2.3) we rewrite $Q > 1$ to $Q_{\mathrm{s}} > \bar{Q}$ and introduce the effective Q-parameter which follows the classical criterion,

$$Q_{\mathrm{eff}} \equiv \frac{Q_{\mathrm{s}}}{\bar{Q}} > 1. \tag{3.4}$$

The stability threshold $\bar{Q}$ is a function of only our parameters, $\mathcal{A}$ and $\mathcal{B}$ defined in equations (3.1) and (3.2) and the Q_{s} is the corresponding stellar Toomre parameter as in equation (2.3). In this way we have reduced the equations so what we need to do is to find a physical correct stability threshold and then derive the effective Q-parameter to define an expression for a two-component stability criterion.

Finally we need to see the two-component dispersion relation before continuing. This was derived by Jog & Solomon (1984) and can be written for a disc consisting of gas and stars as

$$(\omega^2 - \Omega_{\mathrm{g}}^2)(\omega^2 - \Omega_{\mathrm{s}}^2) = 2\pi G \Sigma_{\mathrm{g}} k \cdot 2\pi G \Sigma_{\mathrm{s}} k \tag{3.5}$$

where

$$\Omega_{\mathrm{i}}^2 = \kappa^2 - 2\pi G \Sigma_{\mathrm{i}} k + \sigma_{\mathrm{i}}^2 k^2 \tag{3.6}$$

which we recognise from the classical one-component dispersion relation, equation (2.1).

3.2 Analysis of Bertin & Romeo (1988)

The study of the two component case mainly used in this chapter will be the previously mentioned one done by Bertin & Romeo (1988). In the process of finding the stability threshold here we first look at the neutral stability curve $Q = Q(\Lambda)$ (see Section 2.2 for comparison). This is in terms of our parameters given by

$$\begin{aligned} Q^2 = & \frac{2\Lambda}{\mathcal{B}^2} \Big[\mathcal{A} + \mathcal{B}^2 - \Lambda(1 + \mathcal{B}^2) \\ & + \sqrt{\Lambda^2(1 - \mathcal{B}^2)^2 - 2\Lambda(1 - \mathcal{B}^2)(\mathcal{A} - \mathcal{B}^2) + (\mathcal{A} + \mathcal{B}^2)^2} \Big] \end{aligned} \tag{3.7}$$

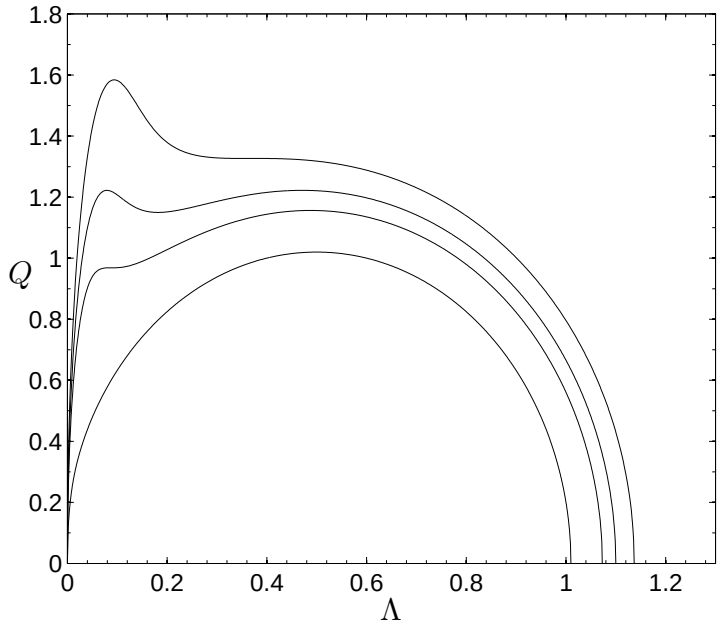

Figure 3.1: Four cases of the marginal stability curve with constant $\mathcal{B} = 0.1$ and from the below, with $\mathcal{A} = 0.010$, 0.073, 0.100 and 0.137.

in analogy with equation (2.9). This marginal stability curve is considered in the range $0 \leq \Lambda \leq 1+\mathcal{A}$ and the stability threshold is, exactly as with the classical case defined by the peak Q-value (in the classical case this is always 1).

Four different cases of the marginal stability curve is shown in figure 3.1. We immediately notice when studying the curves how there is a second peak occuring at low wavelengths when we have a higher gas density (or smaller stellar density). This peak is an instability due to the gaseous component while the wider peak at higher wavelengths is due to the stellar component. The lower wavelength and prominent height of the gaseous peak indicate how powerful the instability can be if the gaseous velocity dispersion is low enough. We also see that there occurs a transition to a lower most unstable wavelength when the gaseous peak is the global maxima.

This transition from high wavelengths (stellar-dominated) to lower (gas-dominated) occurs along the line $\mathcal{A} = \mathcal{B}$ in our parameter space. Also the occurence and disappearence of the gaseous and stellar peaks at specific densities and velocities create transitions between gas-dominated and stellar-dominated peculiar zones in the parameter space, i.e. zones where the marginal stability curve exhibit both peaks. These transitions form what is called the *two-phase region* and is presented in figure 3.2 in log-log scale.

The point where the transition lines converge is known as the *triple point*. Here in the two-component and zero-thickness case it is positioned at approximately $\mathcal{A}_0 \simeq 0.17$ and $\mathcal{B}_0 \simeq 0.17$ where the stability threshold is $\bar{Q}_0 = \sqrt{2} \simeq 1.41$ and the most unstable wavelength is $\Lambda_0 \simeq 0.29$ as analytically calculated by Bertin & Romeo (1988).

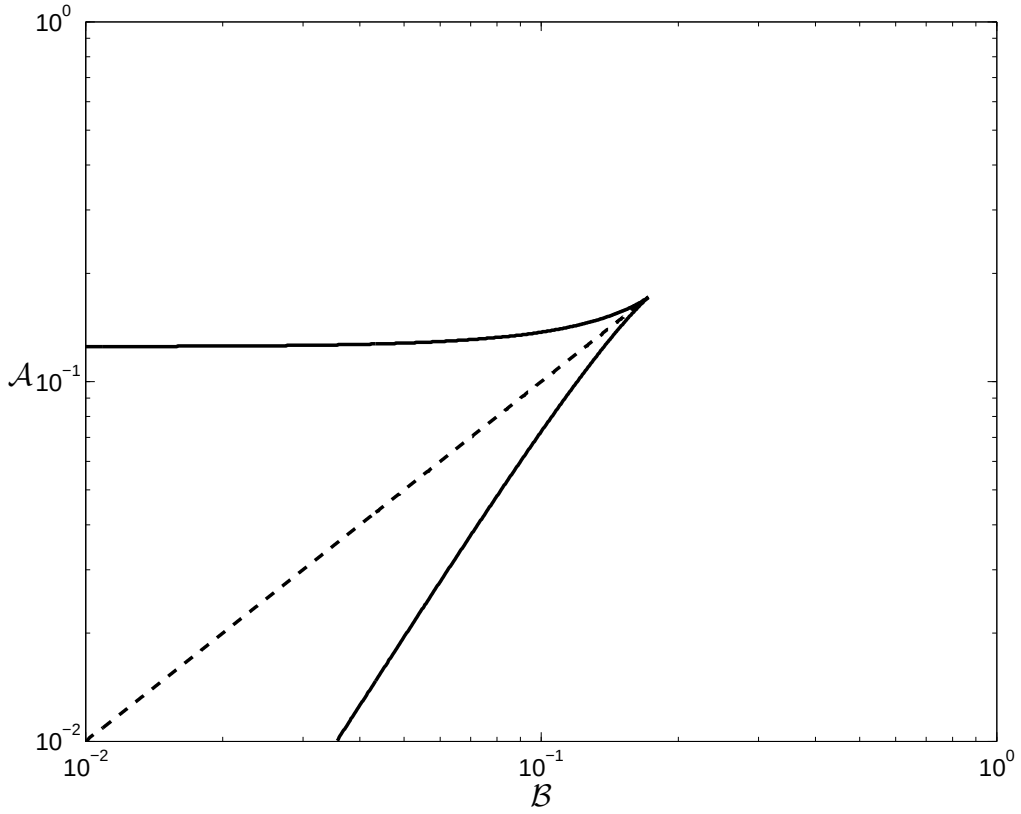

Figure 3.2: two-phase region of thin discs. The region where the marginal stability curve exhibits two peaks and transition between the stellar-dominated (below the dashed line) and gas-dominated instability (above the dashed line)

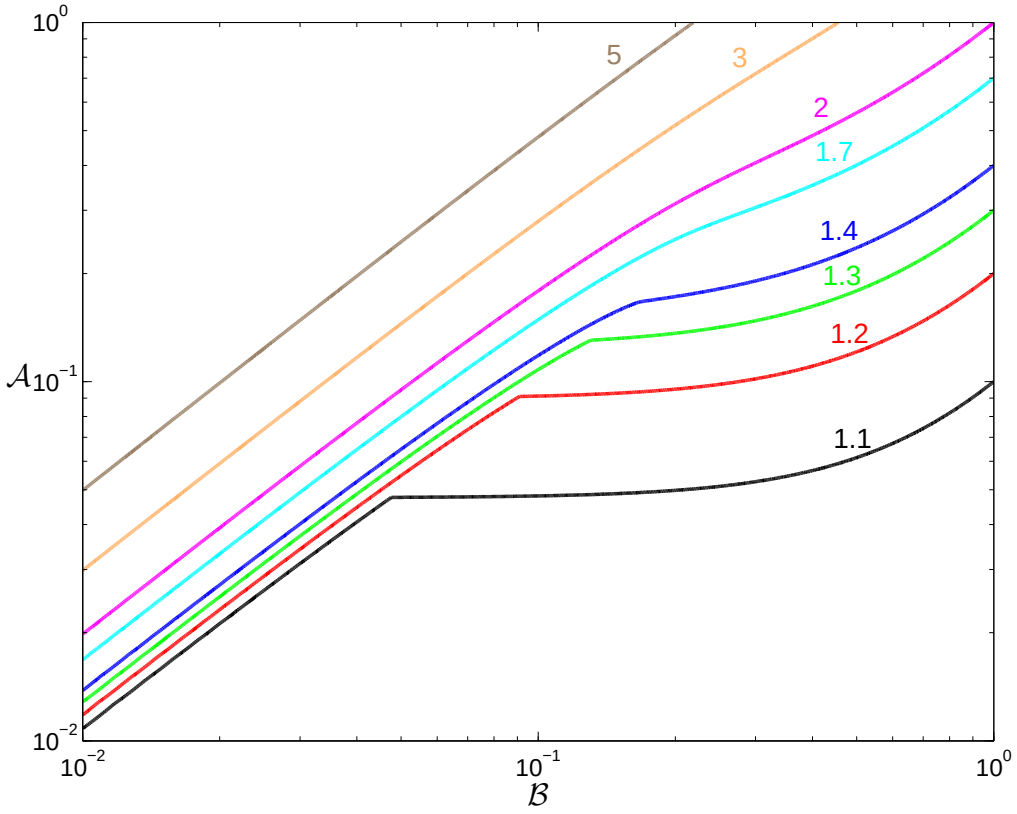

Figure 3.3: Contour plot of the stability threshold $\bar{Q}$ of Bertin & Romeo (1988).

Figure 3.3 shows a selection of contour lines of the stability threshold $\bar{Q}$. In the contour lines is the previously mentioned main transition between stellar-dominated and gas-dominated instabilities along $\mathcal{A} = \mathcal{B}$ clearly visible.

3.3 The approximation of Wang & Silk (1994)

Wang & Silk (1994) attempted to derive a stability criterion directly from the dispersion relation defined by Jog & Solomon (1984) for two weakly interacting fluids, equation (3.5). They used a Taylor expansion around the wavenumber corresponding to the peaks for the stellar and gaseous components respectively. What they got was a stability criterion for a two fluid disc defined as

$$Q_{\text{eff}} \equiv \frac{\kappa}{\pi G}\left(\frac{\Sigma_{\text{s}}}{\sigma_{\text{s}}} + \frac{\Sigma_{\text{g}}}{\sigma_{\text{g}}}\right)^{-1} = \left(\frac{1}{Q_{\text{s}}} + \frac{1}{Q_{\text{g}}}\right)^{-1} > 1. \tag{3.8}$$

This analytical expression is obviously simple and useful, unfortunetaly it lacks accuracy. As stated by Jog (1996) the error is in the fact that they used neutral wavenumbers for each fluid

respectively instead of a common two-fluid wavenumber and also that they used a wrong definition of Q as a function of F. F is a function used by Jog & Solomon (1984) (their equation 21 and 22) from their dispersion relation which gives that there are instabilities if $F > 1$. This is problematic as this approximation, as mentioned earlier is still quite commonly used today (Puech 2010; Hitschfeld et al. 2009; Martin & Kennicutt 2001).

To demonstrate this error we will make a short comparison between the corresponding stability threshold of the Wang & Silk (1994) approximation with the numerically derived stability threshold of figure 3.3.

To derive the corresponding Wang & Silk (1994) stability threshold we use equation (3.4) and obtain quite quickly that

$$\bar{Q}_{\mathrm{WS}} = \frac{Q_{\mathrm{s}}}{Q_{\mathrm{eff}}} = \left(1 + \frac{\sigma_{\mathrm{s}}}{\sigma_{\mathrm{g}}}\frac{\Sigma_{\mathrm{g}}}{\Sigma_{\mathrm{s}}}\right) \tag{3.9}$$

and using our parameters from equations (3.1) and (3.2) this is

$$\bar{Q}_{\mathrm{WS}} = 1 + \frac{\mathcal{A}}{\mathcal{B}}. \tag{3.10}$$

In figure 3.4 are the corresponding contour lines from the Wang & Silk (1994) approximation plotted together with the contour lines from the study by Bertin & Romeo (1988) (figure 3.3). It is quite clear that there is a huge discrepancy at low velocity dispersion ratios. However, when $\mathcal{B}$ goes to 1 we notice how the model and approximation correspond quite well. This is simply due to when $\mathcal{B} = 1$ the gas and stellar velocity dispersions are equal and the two component model and approximation both collapses into a classical one component model containing the sum of our densities. This is written as

$$Q_{\mathrm{eff}} = \frac{\kappa\sigma}{\pi G(\Sigma_{\mathrm{s}} + \Sigma_{\mathrm{g}})} \tag{3.11}$$

where σ is the velocity dispersion of either the gas or the stellar component.

3.4 A new approximation

We are now in a position where we have a quite inaccurate approximation and a model which might not be straightforward to use effectively and very difficult to derive an analytical expression of $\bar{Q}$ from and thus also for Q_{eff}. Instead we need to find an analytical approximation of the study by Bertin & Romeo (1988) that is easy to use and write it in the more practical parameters of Q_{s} and Q_{g} instead of our theoretically practical parameters $\mathcal{A}$ and $\mathcal{B}$, inspired by the parametrization of Wang & Silk (1994).

To start we must first consider the contour lines of $\bar{Q}$ in figure 3.3. The obvious challenge is to consider the transition. Unfortunetaly to be able to have one analytical expression for the whole $\mathcal{B}$ - $\mathcal{A}$ space that also takes into account the transition between stellar and gaseous dominated instabilities we would need an expression equally complicated (and not very useful) as equation

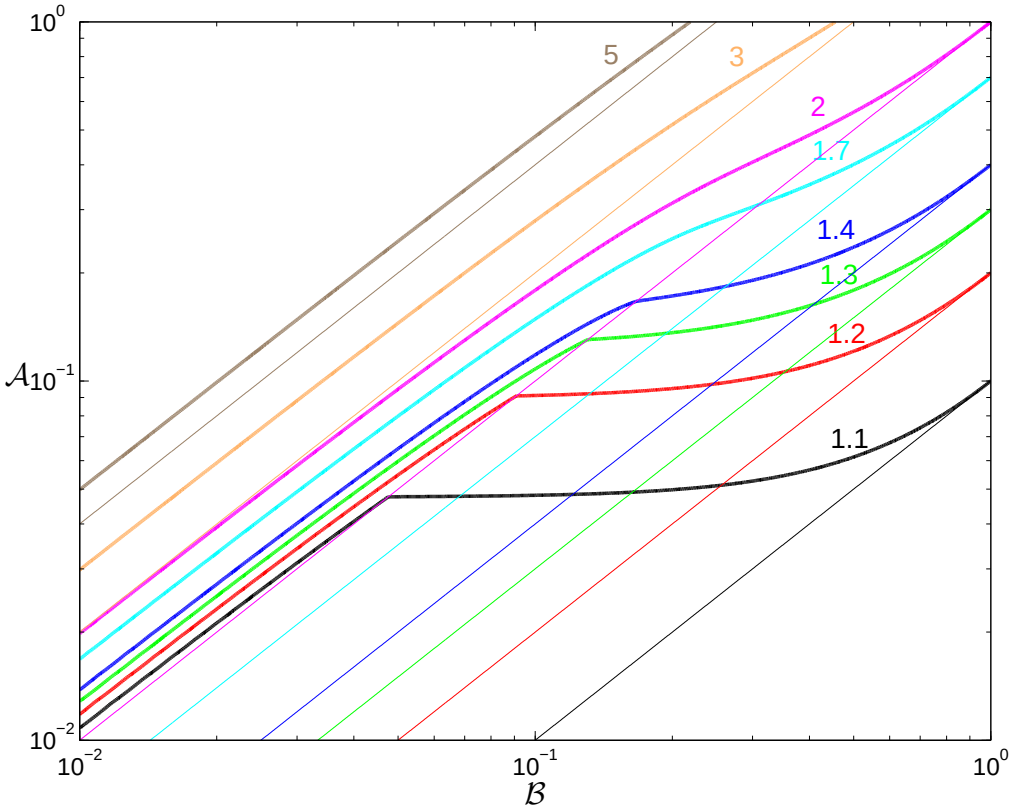

Figure 3.4: Contour plot of the stability threshold $\bar{Q}$ from the study by Bertin & Romeo (1988) (thick lines) and the Wang & Silk (1994) approximation (thin lines).

(3.7). Instead we will find two expressions, one approximation for the stellar regime and one for the gaseous regime.

Consider the stellar $\bar{Q}$ contour lines of figure 3.3. If we consider the contours as functions $\mathcal{A}(\mathcal{B})$ then these can be expressed as quadratic expressions and even simpler if we express each contour line as a function $\mathcal{A}(\bar{Q}, \mathcal{B}^2)$. Then it is possible to use straight lines that fulfil two requirements. They should collapse to the one component case, $\mathcal{A} = \bar{Q} - 1$ when $\mathcal{B} = 1$ and when extending the line to $\mathcal{B} = 0$ it should collapse to $\mathcal{A} = (\bar{Q} - 1)/2$ so that the line crosses approximately the right transition point along the $\mathcal{A} = \mathcal{B}$ line. With this in mind it is possible to express

$$\mathcal{A} = \frac{\bar{Q} - 1}{2} + \frac{\bar{Q} - 1}{2}\mathcal{B}^2 = \frac{1}{2}(\bar{Q} - 1)(\mathcal{B}^2 + 1) \tag{3.12}$$

which we rearrange to

$$\bar{Q} = \frac{2\mathcal{A}}{\mathcal{B}^2 + 1} + 1 = 2 \cdot \frac{\Sigma_{\rm g}}{\Sigma_{\rm s}} \cdot \frac{\sigma_{\rm s}^2}{\sigma_{\rm s}^2 + \sigma_{\rm g}^2} + 1. \tag{3.13}$$

Finally we apply equation (3.4) to obtain the stellar approximation of $Q_{\rm eff}$. We end up with

$$\frac{1}{Q_{\rm eff}} = 2\frac{\sigma_{\rm s}\sigma_{\rm g}}{\sigma_{\rm s}^2 + \sigma_{\rm g}^2} \cdot \frac{\pi G\Sigma_{\rm g}}{\kappa\sigma_{\rm g}} + \frac{\pi G\Sigma_{\rm s}}{\kappa\sigma_{\rm s}} \tag{3.14}$$

that we can write in terms of $Q_{\rm s}$ and $Q_{\rm g}$ so that

$$\frac{1}{Q_{\rm eff}} = \frac{1}{Q_{\rm s}} + \frac{\rm CF}{Q_{\rm g}} \quad ({\rm star - dominated\ regime}). \tag{3.15}$$

This final equation, the stellar approximation of the effective stability parameter is obviously very similar to the original Wang & Silk (1994) approximation, equation (3.8). Except that we now have a simple correction-factor we denote $\rm CF$ and define as

$${\rm CF} = \frac{2\sigma_{\rm s}\sigma_{\rm g}}{\sigma_{\rm s}^2 + \sigma_{\rm g}^2}. \tag{3.16}$$

This stellar regime approximation only applies within the limit of $\mathcal{A} < \mathcal{B}$ or when $Q_{\rm s} < Q_{\rm g}$.

The gaseous regime is somewhat more complicated to describe. However, if we follow the previous method of formulating a function $\mathcal{A}(\bar{Q}, \mathcal{B}^2)$, use the approximations formulated by Bertin & Romeo (1988) and what we can learn from equation (3.13) we are able through some trial and error to formulate

$$\mathcal{A} = \bar{Q}\mathcal{B} - 2\frac{\mathcal{B}^2}{1 + \mathcal{B}^2} \tag{3.17}$$

and by following the previous conduct we can write the stability threshold

$$\bar{Q} = \frac{\mathcal{A}}{\mathcal{B}} + \frac{2\mathcal{B}}{1 + \mathcal{B}^2} \tag{3.18}$$

which gives the effective stability parameter

$$\frac{1}{Q_{\rm eff}} = \frac{\rm CF}{Q_{\rm s}} + \frac{1}{Q_{\rm g}} \quad ({\rm gas-dominated\ regime}), \tag{3.19}$$

where the correction factor, CF is exactly the same as in equation (3.16). This by construct also collapses to the one component case $\bar{Q} = \mathcal{A} + 1$ when $\mathcal{B} = 1$ and approximately connects with the right transition point when $\mathcal{A} = \mathcal{B}$. This expression is instead valid when $\mathcal{A} > \mathcal{B}$ or when $Q_{\rm s} > Q_{\rm g}$.

It is now that we see the power of this approximation. It is very similar to the Wang & Silk (1994) approximation except that in the stellar regime we multiply the gas term with a simple correction factor and in the gaseous regime instead we multiply the stellar term with the same correction factor. In figure 3.5 we see how well the approximated stability threshold contours correlates with the contours of the original model and also how well the two approximations connect along the $\mathcal{A} = \mathcal{B}$ line.

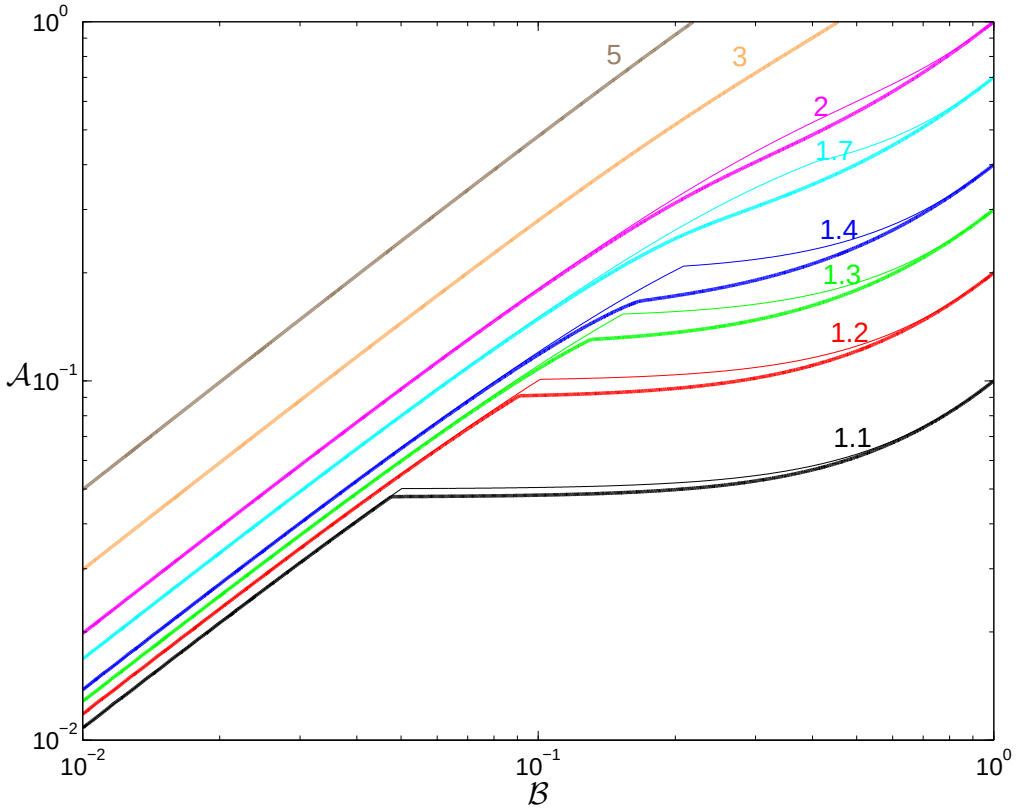

Figure 3.5: Contour plot of the stability threshold $\bar{Q}$ from the study by Bertin & Romeo (1988) (thick lines) and the approximations (thin lines) of the stellar and gaseous regimes with the transition along $\mathcal{A} = \mathcal{B}$.

3.5 Summary

In this chapter we have studied the gravitational instability of galactic discs constisting of a stellar and a gaseous component. For this endevour we defined the parameters $\mathcal{A}$ and $\mathcal{B}$ as in equations (3.1) and (3.2). We also defined a stability threshold $\bar{Q}$ as a function of $\mathcal{A}$ and $\mathcal{B}$ from which we can derive an effective stability parameter, equation (3.4).

We continued to look at the study by Bertin & Romeo (1988) where we see both a powerful transition between stellar-dominated instability when $\mathcal{A} < \mathcal{B}$ and gas-dominated instability when $\mathcal{A} > \mathcal{B}$. We also see that there is a two-phase region in the $\mathcal{B}$ - $\mathcal{A}$ parameter space where the marginal stability curve (equation (3.7)) exhibits two maximas, one stellar at larger wavelengths and one gasoues at lower wavelengths. The two-phase region has a triple point where the transition curves converge at $\mathcal{A}_0 \simeq 0.17$ and $\mathcal{B}_0 \simeq 0.17$, where the stability threshold is $\bar{Q}_0 = \sqrt{2} \simeq 1.41$ and the most unstable wavelength is $\Lambda_0 \simeq 0.29$. The question we ask ourselves is how important the two-phase region and transition line are when considering observational data and this we will study in Chapter 4.

We also made a comparison with the stability parameter derived by Wang & Silk (1994) and verify the conclusion by Jog (1996) that this simple equation unfortunetaly is invalid. Instead we formulate a new approximation of the stability parameter which takes into account the transition between stellar and gaseous dominated regimes. This is a simple improvement of the previously defined approximation and is defined as

$$Q_{\text{eff}} = \left(\frac{1}{Q_{\text{s}}} + \frac{\text{CF}}{Q_{\text{g}}} \right)^{-1} \tag{3.20}$$

when $\mathcal{A} < \mathcal{B}$ (or $Q_{\text{s}} < Q_{\text{g}}$) and

$$Q_{\text{eff}} = \left(\frac{\text{CF}}{Q_{\text{s}}} + \frac{1}{Q_{\text{g}}} \right)^{-1} \tag{3.21}$$

when $\mathcal{A} > \mathcal{B}$ (or $Q_{\text{s}} > Q_{\text{g}}$). The correction factor CF is defined as

$$\text{CF} = \frac{2\sigma_{\text{s}}\sigma_{\text{g}}}{\sigma_{\text{s}}^2 + \sigma_{\text{g}}^2}. \tag{3.22}$$

Chapter 4

Application to observed galaxies

In the previous chapter we noticed discrepancies between the approximation of Wang & Silk (1994) and the study by Bertin & Romeo (1988) and how there is a two-phase region for two-component discs where both the gaseous and the stellar components gives rise to instabilities. However, the question is how these facts relates to concrete cases.

We will in this chapter look shortly at the different surveys done and use data supplied by one of the more extensive and recent surveys. This will be used to make a similar survey using the analysis by Bertin & Romeo (1988).

I also mention an example of large discrepancies in the data of different surveys on the same source. A reminder of the importance of caution when selecting sources of data.

4.1 Recent surveys

There are several observational articles written where stability of disc galaxies is analysed. Some of these are done by Leroy et al. (2008) who looks at a large sample of nearby galaxies, Hitschfeld et al. (2009) who studies NGC 5194 solely, Wong et al. (2009) who studies the Large Magellanic cloud (LMC), Yang et al. (2007) who also studies the LMC and Martin & Kennicutt (2001) who looks at star formation thresholds in observed disc galaxies.

The most extensive survey suitable for this chapter I found in my research was done by Leroy et al. (2008). They have done a survey of 23 nearby galaxies with data from THINGS (The HI Nearby Galaxy Survey), HERACLES (HERA CO-Lines Extragalactic Survey), BIMA SONG (Berkeley-Illinois-Maryland Association Survey of Nearby Galaxies), SINGS (*Spitzer* Infrared Nearby Galaxies Survey) and GALEX (Galaxy Evolution Explorer). Using the intensity maps from these surveys they are able to calculate the surface densities of the gases and stars of each galaxy and obtain radial profiles. Using both the classical Toomre stability criterion and the two-fluid stability criterion as defined by Jog & Solomon (1984) and rewritten in new terms by Rafikov (2001), they conduct a stability survey of these galaxies and derive the stellar formation rates. For details surrounding the data and calculations done by Leroy et al. (2008), see Appendix B. The complete radial profiles for each galaxy in the survey of Leroy et al. (2008) is published

publicly in an online version of their article.[1]

Leroy et al. (2008) states that they publish their data in tables online "to provide a database that can be used to test theories of galaxy-wide star formation or to explore the effects of varying our assumptions". As this is a large collection of very detailed data I have decided to use a sample of galaxies from it in my survey. In Appendix B there are tables (tables B.1 to B.11) with the data used for each chosen galaxy combined with details I have derived from the given data.

In my search for relevant data I also studied the survey done by Hitschfeld et al. (2009). They have done a surface density and gravitational stability analysis of only NGC 5194 (or M 51). When comparing their data with the corresponding data on NGC 5194 in the survey by Leroy et al. (2008) we notice large discrepancies. The stellar surface densities of Hitschfeld et al. (2009) is on the order of 5 to 10 times smaller than those of Leroy et al. (2008). As an example is the central stellar surface density of Hitschfeld et al. (2009) around $810 M_{\odot} \mathrm{pc}^{-2}$ while Leroy et al. (2008) gives $4910 M_{\odot} \mathrm{pc}^{-2}$. The gas surface density of Hitschfeld et al. (2009) however, is closer to that of Leroy et al. (2008), being only on the order of 3 to 1 times smaller.

I attempted to contact the main author, M. Hitschfeld as this is the more recent article, asking what he thinks could be the cause of this discrepancy. However, I was only able to get a response from the second author, C. Kramer, who referred to section 4 and section 5 of their article where they explain how they derived the stellar surface densities and the stellar velocity dispersions. These sections however, does not explain any possible reasons for such large discrepancies.

I mention this here as a reminder of the importance of caution when selecting, studying and comparing sources of data.

The study made by Martin & Kennicutt (2001) is also important to mention more closely. They have studied the stellar formation efficiency of 32 galaxies and define a stellar formation "threshold radius" denoted R_{HII}. We will attempt to try and identify the threshold radius in our sample of galaxies by studying the behaviour of our stability parameter in the sample chosen from Leroy et al. (2008) later in this chapter.

4.2 Two galaxy samples

The data acquired from the article by Leroy et al. (2008) have as mentioned radial profiles of stellar densities, HI densities and H_2 densities for 23 different galaxies from which I chose two samples.

The first sample consists of six galaxies. The four spiral galaxies, NGC 3521, NGC 5055 (M 63, the *Sunflower galaxy*), NGC 5194 (M 51, the *Whirlpool galaxy*) and NGC 6946 (Arp 29, the *Fireworks galaxy*) and two irregular galaxies for comparison, HO II (Arp 268, *Holmberg II*) and IC 2574 (*Coddington's nebula*).

NGC 5194 is interacting with the galaxy NGC 5195 which affect its radial profile in an interesting way shown later in this chapter. NGC 6946 is a peculiar galaxy with one heavy arm (Arp 1966) and several supernovae have been observed there. The two other spiral galaxies, NGC 3521 and NGC 5055 seems to be without any heavy interaction or any other peculiar behaviour.

[1] Table 7 at *http://iopscience.iop.org/1538-3881/136/6/2782/fulltext*.

A trait that will here after be described as them being “normal galaxies”.

The second sample contains four normal galaxies, NGC 628 (M 74), NGC 3184, NGC 3198 and NGC 7331. These will be compared together with NGC 3521 and NGC 5055 from the first sample. Thus we have a sample of ten galaxies in total to study where two are irregulars, two have interaction or other peculiarities and six which seems to be without interaction or any other peculiarities.

Prada et al. (1996) suggests that the bulge of NGC 7331 is rotating retrograde and not co-rotating with its disc. This however does not seem to affect the results in any way.

The criteria used when selecting galaxies were that they must first of all have many data points, the data must contain some H_2 data and many HI data to not be biased towards small $\mathcal{A}$. However, none of the irregulars have H_2 data so the two irregulars with most data available were chosen.

In tables 4.1 and 4.2 there are some general information about the galaxy samples and figures 4.1 and 4.2 are photos of each galaxy. Tables with the complete data used are in Appendix B (tables B.1 to B.11).

Table 4.1: General information on the first sample of galaxies.[2]

Galaxy	Morph.	Dist. (Mpc)	Radius (kpc)	v_{flat} (km/s)	l_{flat} (kpc)	R_{d} (kpc)	R_{25} (kpc)
HO II	Irr	3.4	4.4	36	0.6	1.2	3.7
IC 2574	Irr	4.0	8.8	134	12.9	2.1	7.5
NGC 3521	SBbc	10.7	15.3	227	1.4	2.9	12.9
NGC 5055	Sbc	10.1	20.8	192	0.7	3.2	17.4
NGC 5194	SBc	8.0	10.7	219	0.8	2.8	9.0
NGC 6946	SBc	5.9	11.6	186	1.4	2.5	9.8

Table 4.2: General information on the second sample of galaxies.[2]

Galaxy	Morph.	Dist. (Mpc)	Radius (kpc)	v_{flat} (km/s)	l_{flat} (kpc)	R_{d} (kpc)	R_{25} (kpc)
NGC 628	Sc	7.3	12.2	217	0.8	2.3	10.4
NGC 3184	SBc	11.1	14.3	210	2.8	2.4	11.9
NGC 3198	SBc	13.8	15.1	150	2.8	3.2	13.0
NGC 7331	SAb	14.7	23.2	244	1.3	3.3	19.6

[2] All data are from Leroy et al. (2008), the radii mentioned is the largest radii with data.

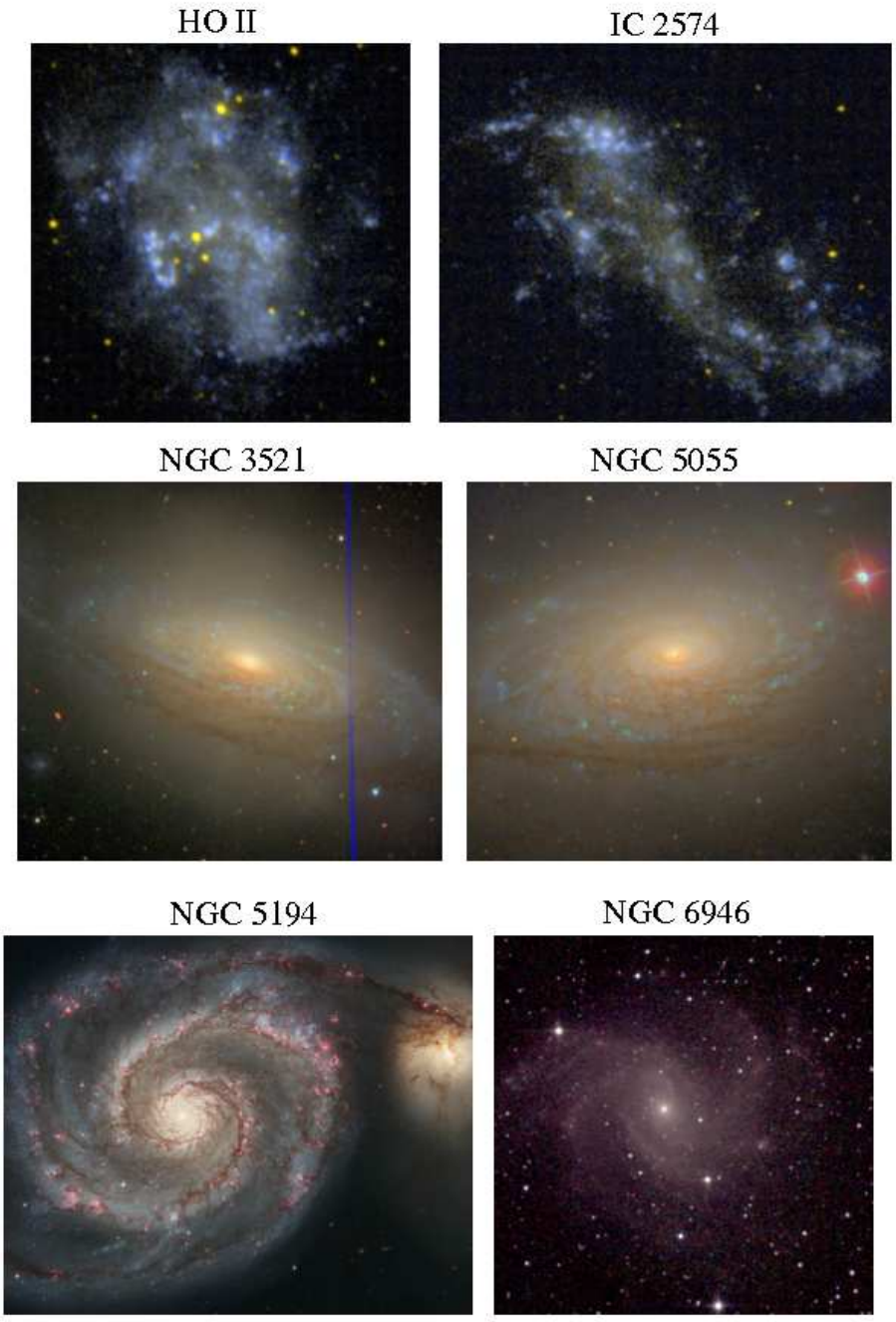

Figure 4.1: Photos of the first sample, from *NASA/IPAC Extragalactic Database* (NED) which is operated by the Jet Propulsion Laboratory, California Institute of Technology, under contract with the National Aeronautics and Space Administration and NGC 5194 is from the *Hubble Heritage project*.

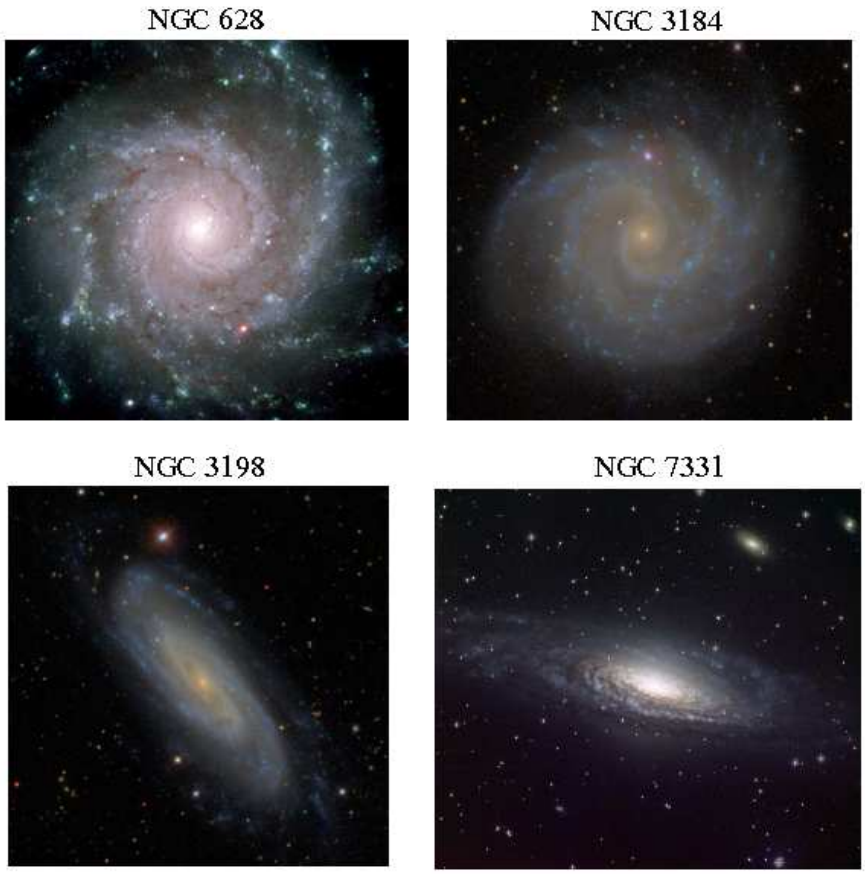

Figure 4.2: Photos of the second sample, photos are again from NED and the NGC 7331 photo is credited to Daniel Bramich (ING) and Nik Szymanek (The Isaac Newton Group of Telescopes, La Palma).

4.3 Deriving useful quantities

As we are using the same data as Leroy et al. (2008) we also need to use the same methods and equations to adapt the data into the parameters we use to apply it to the study by Bertin & Romeo (1988).

The density ratio parameter $\mathcal{A}$ is easy to derive from this data set. The stellar densities are given directly in the data tables (Appendix B) and the gaseous densities are simply the sum of the HI and H_2 densities also given directly in the same tables.

The second parameter, the velocity dispersion ratio $\mathcal{B}$ is a more complicated matter. Leroy et al. (2008) never measured or used measurements of the velocity dispersions directly. Instead the stellar velocities are derived from the stellar densities and the gaseous velocity dispersions is assumed to have a constant value of $\sigma_{\rm gas} = 11$ km s^{-1}. This is an unusually high value and more commonly used is around 6 to 8 km s^{-1} as Martin & Kennicutt (2001) who used $\sigma_{\rm g} = 6$ km s^{-1} in their study. 11 km s^{-1} is however a typical value in the HI-dominated outer parts of the THINGS-galaxies which is why Leroy et al. (2008) uses it.

To derive the radial stellar velocity dispersion needed (see Appendix B.3 of Leroy et al. (2008) for further details if interested) we look at the vertical velocity dispersion given by

$$\sigma_{\rm zs}(R) = \sqrt{2\pi G \Sigma_{\rm s} h_{\rm s}} \tag{4.1}$$

where $\Sigma_{\rm s}$ is the stellar surface density and $h_{\rm s}$ is the stellar disc scale height. As the disc scale height is assumed to be radially constant only the surface density gives a radial dependence for the velocity dispersion.

The disc scale height is assumed to be related to the disc scale length with $R_{\rm d} = (7.3 \pm 2.2) \cdot h_{\rm s}$ which is given for each galaxy in tables 4.1 and 4.2. The vertical velocity dispersion is assumed to be related to the radial velocity dispersion by $\sigma_{\rm zs} = 0.6\sigma_{\rm rs}$. Disregarding the error of the scale height we now have

$$\sigma_{\rm rs}(R) = \frac{1}{0.6}\sqrt{\frac{2\pi G R_{\rm d}}{7.3}}\Sigma_{\rm s}^{1/2}(R). \tag{4.2}$$

Now we have the required radial profiles of the densities and velocity dispersions that gives us the radial profiles of $\mathcal{A}(R)$ and $\mathcal{B}(R)$. However, we also need to calculate our Q-parameters, the stability threshold $\bar{Q}$ and the two component stability parameter $Q_{\rm eff}$ from equation (3.7). For this we do not only need the densities and velocities but also the epicyclic frequency κ of each galaxy. This is derived theoretically by Leroy et al. (2008) and as usual we follow their example.

Normally when calculating the epicyclic frequency of a galaxy a flat rotation curve is assumed so that

$$\kappa = 2\pi \cdot \Omega = \sqrt{2}\frac{V(R)}{R} \tag{4.3}$$

where Ω is the angular velocity and the $V(R)$ is the linear velocity. Leroy et al. (2008) instead defines the epicyclic frequency as

$$\kappa = 1.41 \frac{V(R)}{R} \sqrt{1+\beta} \tag{4.4}$$

where

$$\beta = \frac{d \log V(R)}{d \log R}. \tag{4.5}$$

This is a correction term that compensates for a non-flat rotation curve. When $\beta = 0$ we have a flat rotation curve (occurs in the disc) and when $\beta = 1$ we have solid body rotation (occurs in the center of the disc).

The velocity curve, $V(R)$ is derived from an analytical expression defined as

$$V(R) = v_{\text{flat}} \left(1 - \exp\left(-\frac{R}{l_{\text{flat}}}\right)\right) \tag{4.6}$$

where the parameters v_{flat} and l_{flat} are given in tables 4.1 and 4.2. This emulate a more natural velocity curve.

For further details concerning the calculation of our parameters and corresponding error bars, refer to Appendix B. In Appendix B are also the radial profiles given by Leroy et al. (2008) presented together with the profiles I have derived for each chosen galaxy in tables B.1 to B.11.

4.4 Results for the first sample

The first sample is as previously mentioned HO II, IC 2574, NGC 3521, NGC 5055, NGC 5194 and NGC 6946. This is a mix of two irregular galaxies, two normal disc galaxies and two interacting or peculiar disc galaxies.

In figure 4.3 are the radial profiles of our parameters $\mathcal{A}$ and $\mathcal{B}$ of the first sample shown. The optical radius (*de Vaucouleur radius*) R_{25}, disc scale length R_{d} and stellar disc scale height h_{s} are also designated as vertical lines for each galaxy.

We immediately notice the chaotic behaviour of the two irregulars (HO II and IC 2574). We also see how our parameters are larger than unity for these which means that we have a higher velocity dispersion for the gas than the stars. This is not physically possible as the gas component forms the stellar component. However, these are not disc galaxies and a model for a thin disc is not really applicable for these two. It is still quite interesting to compare these with the behaviour of disc galaxies where instead both parameters in this sample are smaller than unity.

In the two normal galaxies, NGC 3521 and NGC 5055 we see a rather regular behaviour. A rise in the velocity dispersion ratio ($\mathcal{B}$) with the radius. The velocity dispersion of the gas is constant so this is due to stellar velocity, which is dependent of the density and both goes down with the radius.

In NGC 5194 there is a huge wave pattern visible in the profile of the density parameter ($\mathcal{A}$). This is probably due to how density profiles are usually derived. Using an intensity map to derive

the mean of rings around the center can be heavily affected by the arm structure of the disc and seems to be the case here.[3]

We also see in NGC 5194 how the velocity dispersion ratio rises with the radius exactly as in the other disc galaxies. However, at large radii there is a sudden drop. This is probably due to the neighbouring galaxy, NGC 5195 which gives a sudden increase of the mean of the stellar density and of the stellar velocity dispersion. Perhaps it is also due to this neighbouring galaxy that maybe induces the spiral structure of NGC 5194 that the spiral arm structure affects the mean gas densities so greatly.

NGC 6946 also seems to behave a bit strangely. This is a peculiar galaxy with the designation Arp 29. According to the original database article by Arp (1966) this galaxy have one heavy arm. However, the velocity dispersion profile behaves very similar to the other disc galaxies. It is just the density ratio that exhibits some strange behaviour around the galactic center.

In figure 4.4 are the stability threshold ($\bar{Q}$) and the effective stability parameter (Q_{eff}) defined in equation (3.4) shown for each galaxy in this sample. Again are the optical radii (R_{25}), disc scale length (R_{d}) and stellar disc scale height (h_{s}) designated, and also the stability criterion for the effective stability parameter $Q_{\text{eff}} = 1$ is marked with a horisontal red line.

The shaded areas are the regions of each galaxy that are inside the two-phase region (see figure 3.2). The lighter shades marks out where only the error bars of $\mathcal{A}$ and $\mathcal{B}$ are inside the two-phase region while the darker shades are where the mean values are inside the region. Only where two or more data points apply to these criteria are taken into account.

Again are the two irregular galaxies quite different than our disc galaxies of this sample and show no correlation with the two-phase region. This is quite obvious when considering the huge values of the density and velocity dispersion ratios these galaxies have. However, again it is interesting to see the huge difference compared with the disc galaxies.

We also see how both irregulars have rather high stability thresholds. This effect is visible in the effective stability parameter that crosses the stability criterion line several times in these two.

All four disc galaxies of this sample have areas inside the two-phase region. The two more peculiar only have some small irregular areas, this seems to be due to the chaotic behaviour of the density profiles. A gentler density variation would probably put a larger portion of the disc inside the two-phase region like our two normal galaxies.

In any way we still see that a large portion the inner parts of the discs are inside the two-phase region and that this area even extends beyond the disc scale length. So in conclusion does the two-phase region play a significant role in the dynamics of the discs according to this data.

In this data sample the stability threshold seems to have a downward trend with higher radii for all disc galaxies except NGC 3521 where it instead rise with radius. The effective stability parameter seems very similar though, except in NGC 6946 where it instead of being very stable in the center of the galaxy is heavily unstable. Otherwise, not considering the irregularities of the data the effective stability parameter behaves quite similar for all the disc galaxies in this sample and some even have some local instabilities in the disc.

Figure 4.5 is a plot of the $\mathcal{A}$ and $\mathcal{B}$ trails of all six galaxies of this sample in our parameter

[3]The gas density sometimes varies on the order of the mean density due to the spiral structure. This of course affects our $\mathcal{A}$-parameter greatly.

space. In the background are the two-phase region and main transition from figure 3.2 plotted as a comparison in thin black lines.

As the stellar density is in every disc galaxy very high in the center and the stellar velocity dispersion is proportional to the density the center of each disc galaxy is always in the lower left corner of the $\mathcal{B}-\mathcal{A}$ space. This makes it possible to follow the radius outwards by following each data point from the lower left. And most of the two irregular galaxies are outside the considered range.

In figure 4.5 it is much easier to see how the data points are in relation to the two-phase region than in figure 4.4. We quickly notice that all four disc galaxies are quite "crowded" around the triple point. We are also able to see that if NGC 5194 had not had its wave behaviour in its density profile a larger portion of the disc would probably have been inside the region. It is also interesting to see how the outer parts of NGC 5194 behaves very differently to the other galaxies which tend to go to the top right of the range and instead this goes back down to the low values again. Similar as how the central parts of each galaxy behaves. This is probably again just an effect of the neighboring galaxy and we are seeing the edges of the central parts of that galaxy in the data.

Furthermore we also see much more clearly that the two-phase region in fact plays a significant role. Considering how we use the fairly high constant gas velocity dispersion of 11 km s^{-1} we can similar as Leroy et al. (2008) did imagine the effects of a lower gas velocity dispersion of perhaps the more usual 6 km s^{-1}. Such a change would move all the data points to a lower $\mathcal{B}$ which would probably put several more data points, thus larger portions of the discs inside the two-phase region, further strengthening our argument.

4.5 Results for the second sample

The second sample of four normal galaxies, NGC 628, NGC 3184, NGC 3198 and NGC 7331 are presented together with the two previously presented normal galaxies, NGC 3521 and NGC 5055. Thus are all our normal galaxies grouped together and compared.

Figure 4.6 depicts the radial profiles of the density ratio $\mathcal{A}$ and the velocity dispersion ratio $\mathcal{B}$. Again is the optical radius (R_{25}), the disc scale length ($R_{\rm d}$) and the stellar disc scale height ($h_{\rm s}$) marked for each galaxy.

Three of our galaxies have been measured to have $\mathcal{B}$ just larger than unity in the outer parts of the disc, though not as large as the irregulars of the first sample. Again, this is not really physical as this would mean that the gaseous velocity dispersion is higher than the stellar. The error could be either in the fact that we are using a higher than normal constant gaseous velocity dispersion or that the measured stellar density which is used to derive the stellar velocity dispersion is too low.

However, we still see large similarities in the density profiles. All with small $\mathcal{A}$ and $\mathcal{B}$-parameters in the center which then grows larger with the radius. Except for NGC 5055 where the $\mathcal{A}$-parameter (density ratio) grows rather small in the outer parts of the disc. This means that there is a small increase of the stellar density in the these parts. It is unknown to me why, however NGC 5055 is part of the M 51 group, so it is probably not without any interactions.

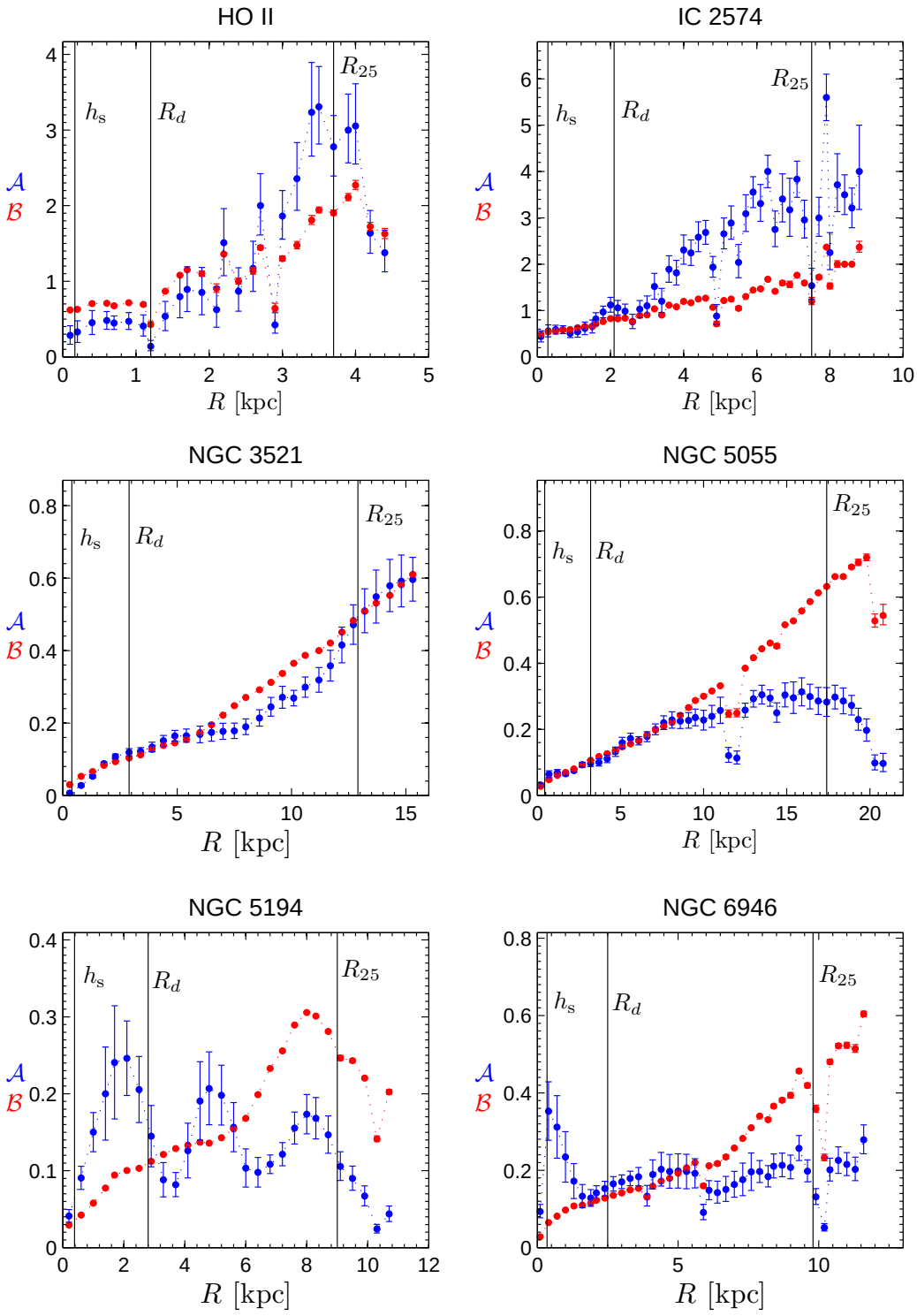

Figure 4.3: Radial profiles of $\mathcal{A}$ and $\mathcal{B}$ for the first sample of galaxies.

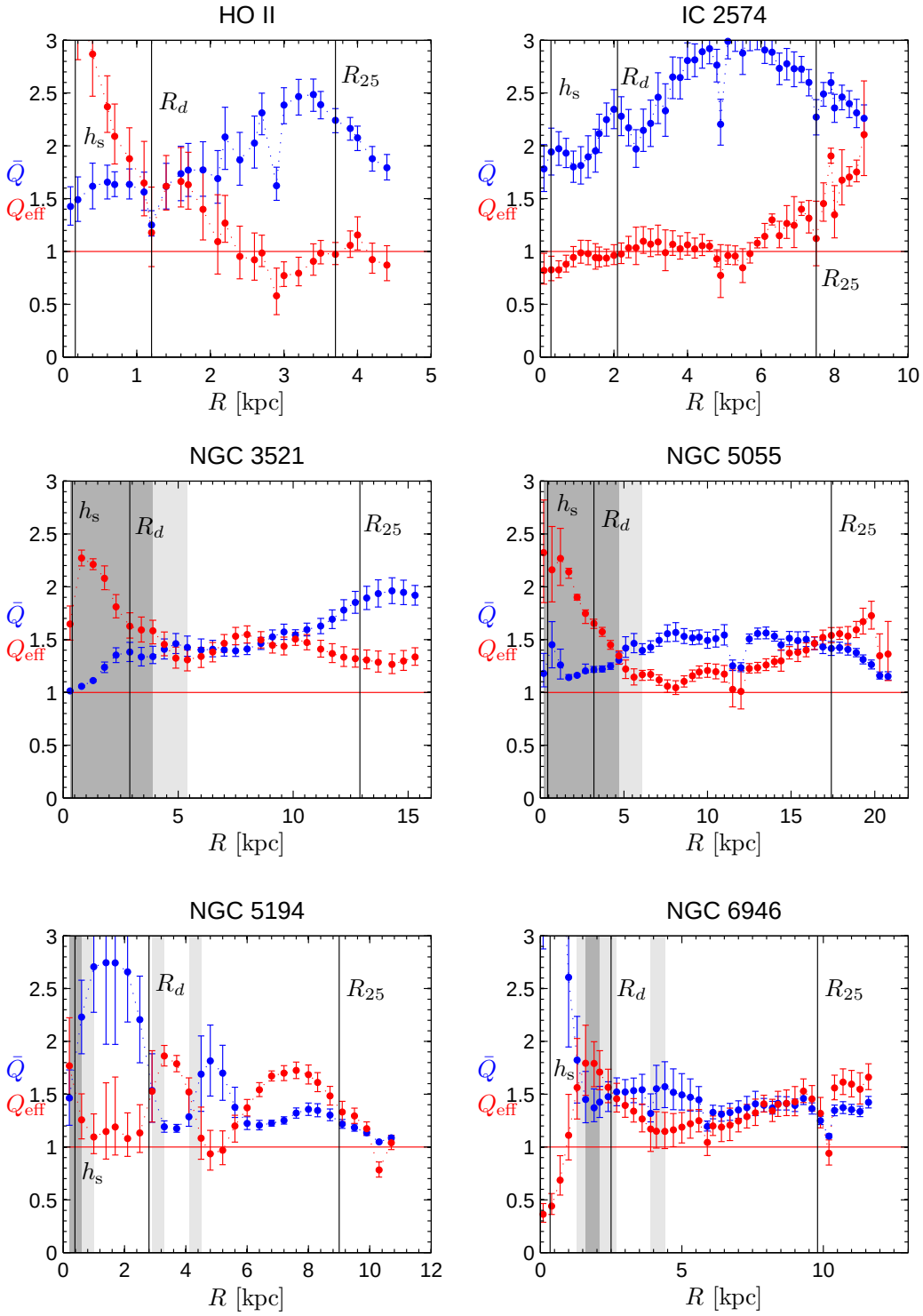

Figure 4.4: Radial profiles of the stability threshold $\bar{Q}$ and the stability parameter $Q_{\rm eff}$ for the first sample of galaxies.

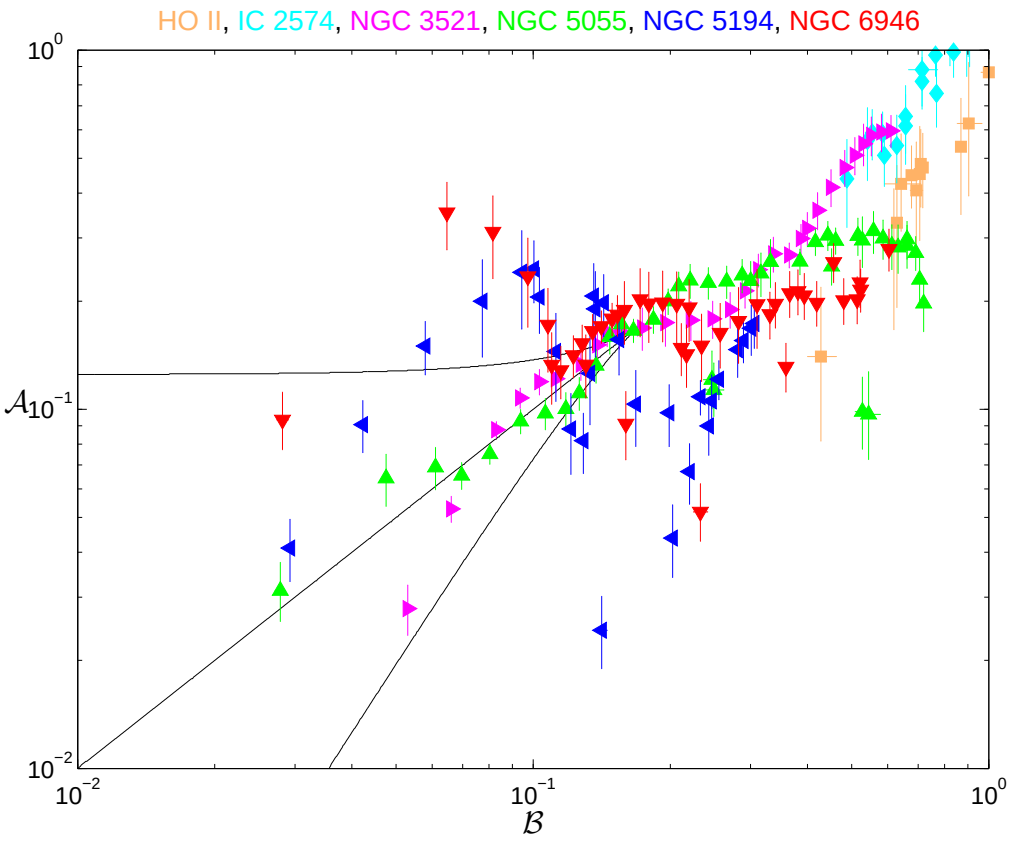

Figure 4.5: $\mathcal{A}$ and $\mathcal{B}$ trails against the two-phase region for the first sample of galaxies.

Figure 4.7 depicts the effective stability parameter Q_{eff} with its corresponding stability criterion along $Q = 1$, the stability threshold $\bar{Q}$, the areas of the discs inside the two-phase region and again the different radii of interest.

In contrast to the first sample there are disc galaxies in this sample with no parts inside the two-phase region, NGC 628, NGC 3184 and NGC 3198. However, we will see that the $\mathcal{B} - \mathcal{A}$ tracks of these galaxies are in the very near vicinity of the region in the parameter space.

Otherwise we see many similarities again. The center of each galaxy is more stable while the discs grow more unstable with some local instabilities at some radii for some galaxies. At the outer parts the effective stability parameter grows slightly and the stability threshold decreases slightly, depicting more stable outer parts of the discs.

Figure 4.8 presents the $\mathcal{B} - \mathcal{A}$ tracks of each galaxy of this sample in our parameter space against the two-phase region. Here we clearly see that our three galaxies without any part in the two-phase region, NGC 628, NGC 3184 and NGC 3198 are all in the vicinity just below the region. NGC 3198 even have the error bar of its central data point in the stellar peculiar regime. However, as before I only take into account when two or more data points are inside the region.

Again we can remind ourselves that a smaller gaseous velocity dispersion would move all the data points of figure 4.8 to smaller $\mathcal{B}$, thus moving the inner parts of the three galaxies in the vicinity into the two-phase region. So we can draw the conclusion that the two-phase region is probably of importance even for these three galaxies.

4.6 Is there a threshold for star formation?

The study by Martin & Kennicutt (2001) was previously mentioned. They have done a very extensive survey on 32 different galaxies where they derive radial profiles of stellar formation efficiency. What they found was a powerful break in stellar formation rates in almost all of their galaxies at specific radii. This is known as the stellar formation threshold radius and is denoted as R_{HII}.

Leroy et al. (2008) attempted to find this break in their sample of galaxies by searching for a drastic increase of stability of the gas disc at some radii and were unsuccessful. Their results seem to contradict that of Martin & Kennicutt (2001), however this is not the case.

The reason stated by Leroy et al. (2008) as to why they were not successful in locating this threshold radius is mainly due to the gaseous velocity dispersion and the estimated amount of H_2. A lower velocity dispersion would drastically destabilise the discs and they also estimated less amount of H_2.

We are using a different stability criterion on these galaxies from Leroy et al. (2008) which made it interesting to search for this threshold radius again. In figure 4.9 the radial profiles of our Q_{eff} for all ten galaxies in our sample are plotted, normalised to the optical radius R_{25}. A stellar formation threshold should be visible as a sudden drastic increase of the stability parameter around a specific radius.

However, even when not considering the two irregular galaxies in the plot are the data inconclusive. There is no clear regular increase of the stability parameter either around the optical radius nor beyond it. A result that is similar to that of Leroy et al. (2008). However we suggest

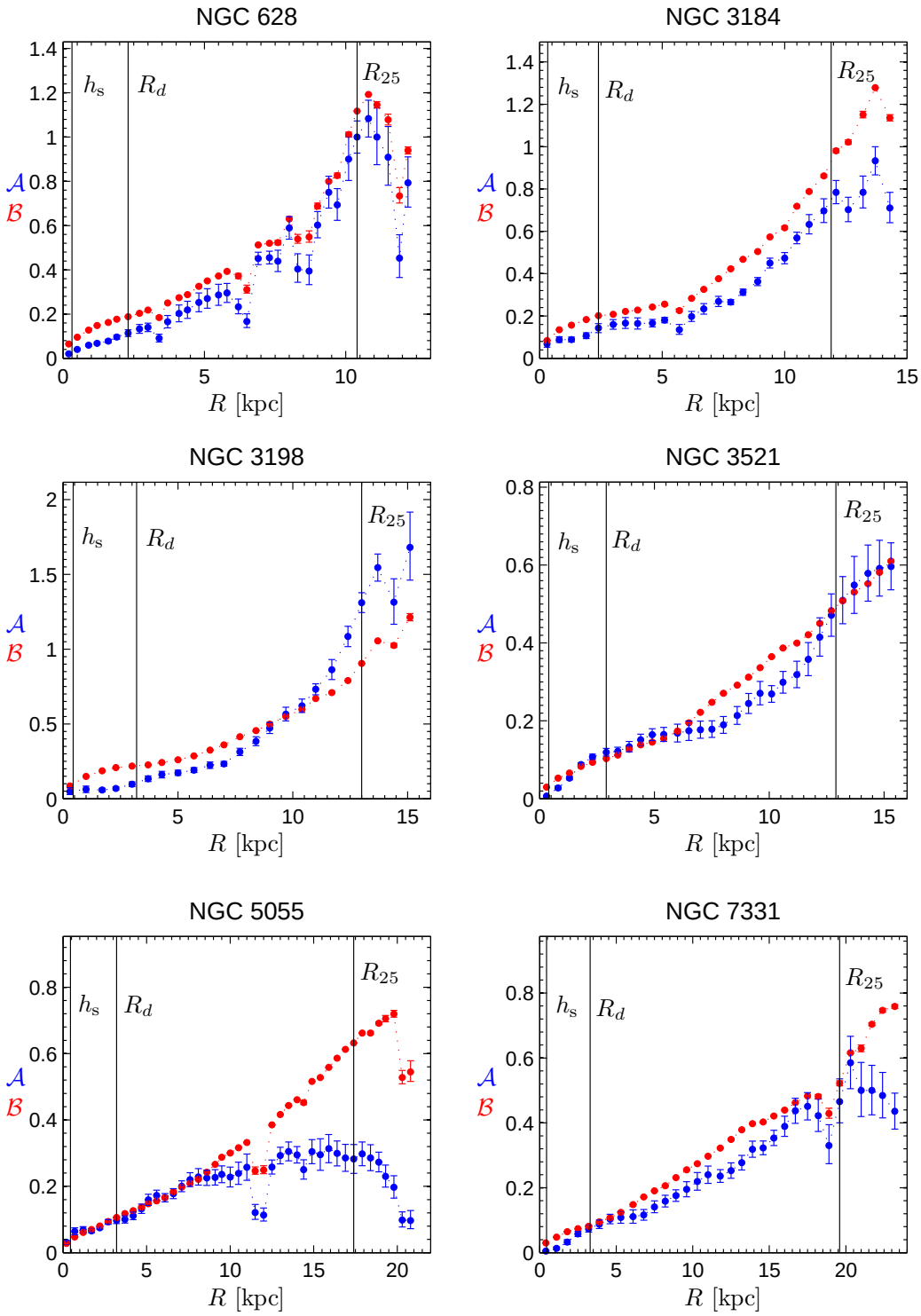

Figure 4.6: Radial profiles of $\mathcal{A}$ and $\mathcal{B}$ for the second sample of galaxies.

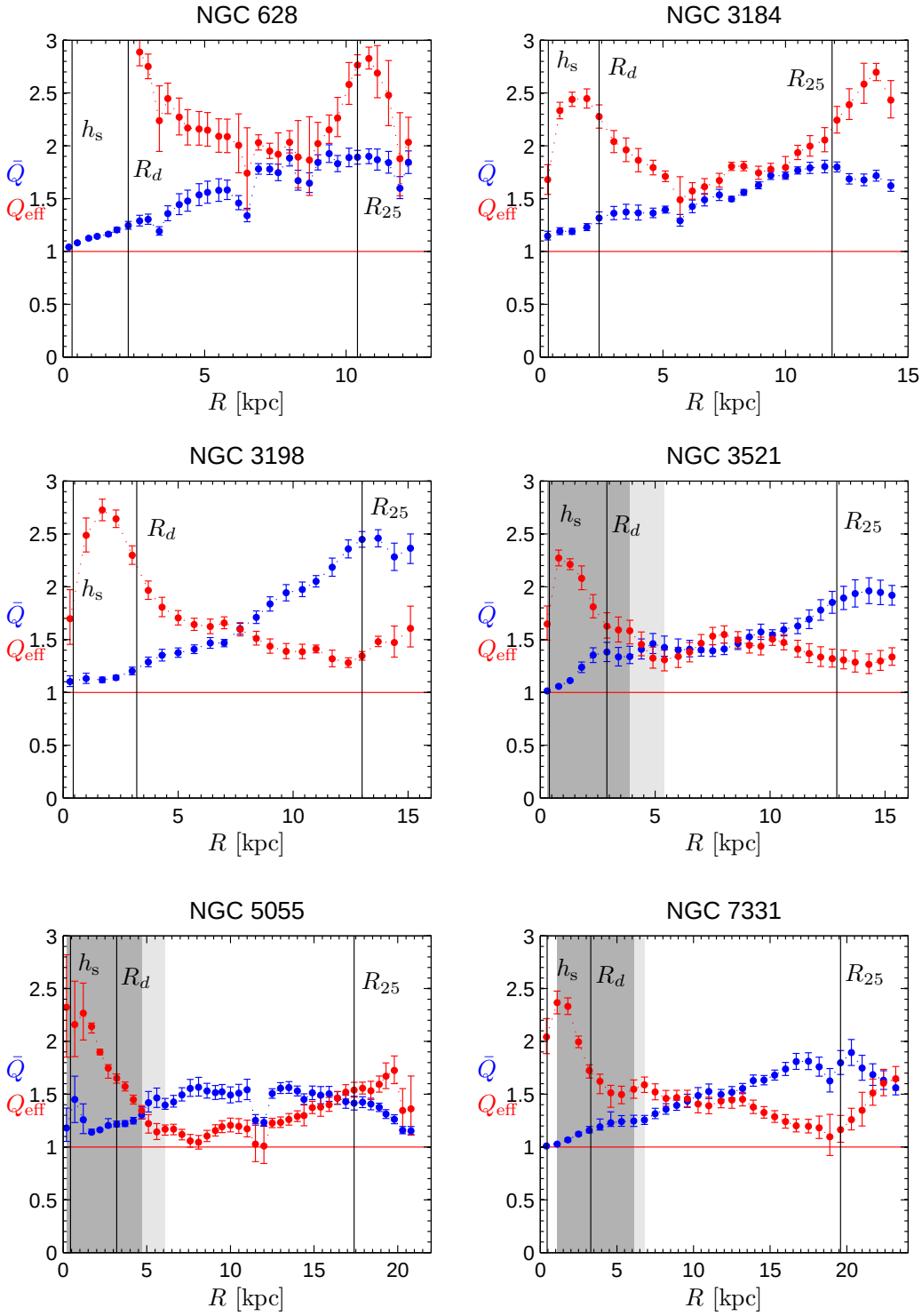

Figure 4.7: Radial profiles of the stability threshold $\bar{Q}$ and the stability parameter $Q_{\rm eff}$ for the second sample of galaxies.

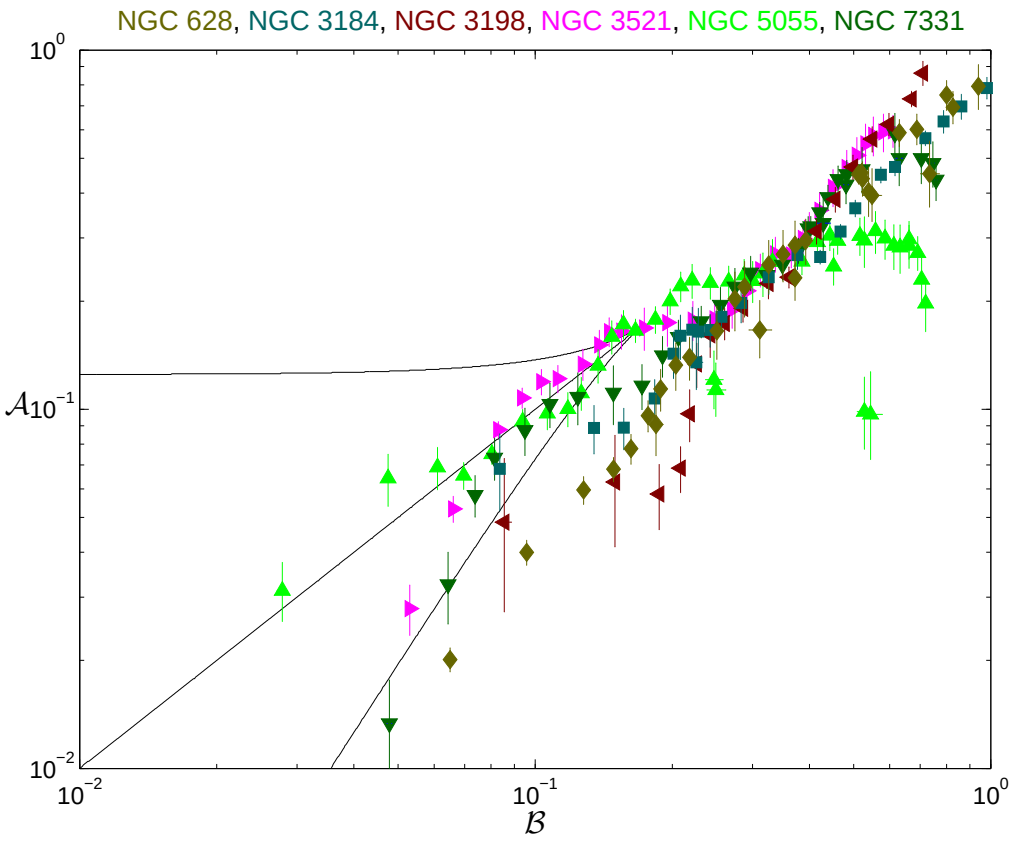

Figure 4.8: $\mathcal{A}$ and $\mathcal{B}$ trails against the two-phase region for the second sample of galaxies.

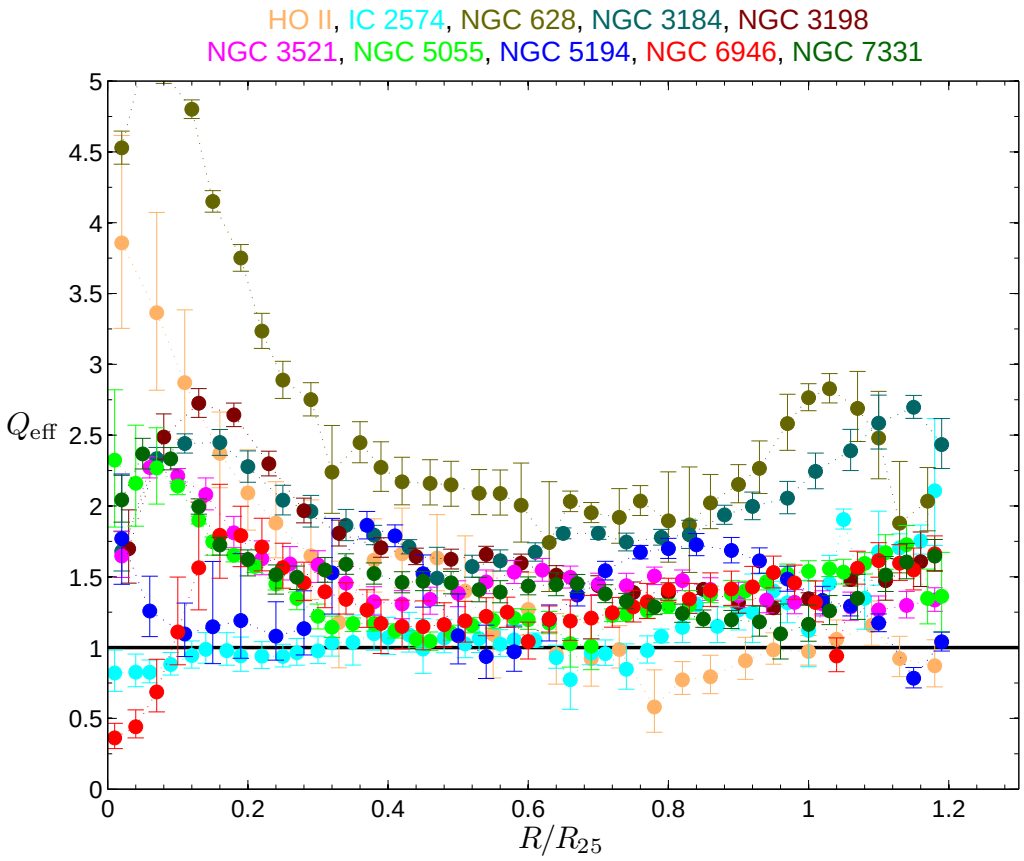

Figure 4.9: Radial profiles of $Q_{\rm eff}$ normalised to the optical radius R_{25} for all ten galaxies in our sample.

two different possible explanations as to why the results seems to contradict that of Martin & Kennicutt (2001).

One reason might simply be that the $R_{\rm HII}$ defined by Martin & Kennicutt (2001) is located at a higher radius than what the data of Leroy et al. (2008) encompasses. The Leroy et al. (2008) data only extends out to 1.2 of the optical radius. In the whole set there is still a significant stellar density at these radii. This should mean that there is still a significant stellar formation rate at these radii and that we have not yet reached the stellar formation threshold radius. However, the median of $R_{\rm HII}$ from Martin & Kennicutt (2001) is roughly $0.8R_{25}$ in the study of Leroy et al. (2008) so this might not be the case.

Another possibility is that newer studies with ultraviolet measurements suggest that there is no sudden powerful increase of the stability parameter and instead a slow increase with the radius in the outer parts of the disc (John S. Gallagher, private communication). Which would also explain the lack of observed threshold radius by both Leroy et al. (2008) and this study. It exists however, just not as powerful as previously observed.

4.7 Summary

To see the possible importance of taking into account two components in a disc of no thickness and if the peculiar two-phase region at density ratios and velocity dispersion ratios smaller than 0.17 is of any relevance we need to apply the model on observational data.

The survey best suited for these needs is the one done by Leroy et al. (2008) where a similar survey of 23 different galaxies is done. However, they are using the classical Toomre criterion and the two component stability formulated by Rafikov (2001). Leroy et al. (2008) have also been kind enough to present their derived radial density profiles of each galaxy in an online version of the article for others to use which further simplified this work.

From the set of data of Leroy et al. (2008) we choose ten galaxies for two samples presented in tables 4.1 and 4.2. These are of six normal, not heavily interacting or peculiar disc galaxies (normal), two peculiar galaxies and two irregulars to see similarities and differences, chosen according to the quality of the data.

We can immediately see how the irregular galaxies do not fit with the thin disc model at all and behave quite chaotic. The two peculiar disc galaxies behave quite chaotic also, however they also show some similarities with the other disc galaxies. These have regions inside the two-phase region and some instabilities. The six normal galaxies all behave more or less regular with many similarities in their radial profiles. Stable centers are found and the discs are also quite stable with a few local instabilities.

All eight disc galaxies have considerable parts either inside or in the vicinity of the two-phase region in the $\mathcal{B} - \mathcal{A}$ parameter space. This indicates that this is in fact of importance when studying disc dynamics. Facts as the high gaseous velocity dispersion used in this set of data strengthens my argument as a lower velocity dispersion would have moved more data points of the center of each galaxy into the two-phase region.

We also attempted to find any signs of the stellar formation threshold radius observed by Martin & Kennicutt (2001). However we were, exactly as Leroy et al. (2008) not successful at this. A few possible reasons were suggested, one simply being that the threshold radius should be at a higher radius than the data of Leroy et al. (2008) encompasses.

Furthermore, we have yet to study the effects of thickness on a two component disc. This is a much more complicated case than the thin two component case and took much effort on my behalf. The question is how taking into account disc thickness might affect the two component disc behaviour of two-phase region, transition line and the stability threshold.

Chapter 5

Dynamical effects of disc thickness

We have so far studied discs with a stellar and gaseous component with no thickness. This is of course a serious approximation. A normal disc galaxy, such as the Milky Way is usually roughly 10 kpc in diameter and on the order of 1 kpc in thickness (Binney & Tremaine 2008). This is a fact we can not easily discard. To demonstrate the importance of disc thickness we will begin by looking at a one-component thick fluid disc.

In a disc of finite thickness we must obviously have a volume density. This is defined by using the scale height h. The stellar disc usually has a constant scale height so the thickness of a disc is defined as $2h$ and the volume density is normally given by (Binney & Tremaine 2008, p. 390; Romeo 1990)

$$\rho(z) = \rho_0 \operatorname{sech}^2\left(\frac{z}{h}\right) \tag{5.1}$$

where ρ_0 is the volume density in the center of the disc, where $z = 0$. And by integrating over z from $-\infty$ to ∞, we obtain the surface density

$$\Sigma = \rho_0 \cdot 2h. \tag{5.2}$$

Note that sometimes, as by Binney & Tremaine (2008, p. 324) is instead a Gaussian law to describe the volume density used. This gives a similar vertical dependence however not as exact as the sech^2 law we are using.

The dispersion relation for a one component thin disc was defined in Chapter 2, equation (2.1) as

$$\omega^2 = \kappa^2 - 2\pi G\Sigma k + \sigma^2 k^2. \tag{5.3}$$

The thick one component dispersion relation can by using a reduction factor be written as (Romeo 1990, 1992, 1994; Vandervoort 1970)

$$\omega^2 = \kappa^2 - 2\pi G\frac{\Sigma}{1+kh}k + \sigma^2 k^2. \tag{5.4}$$

To demonstrate the importance of thickness we will consider the wavenumber where the dispersion relation in the thin case defined above (or equation (2.1)) has a minima. This was found in Chapter 2 to be

$$k_{\min} = \frac{\pi G \Sigma}{\sigma^2}. \tag{5.5}$$

The disc scale height is possible to write as (Binney & Tremaine 2008, p. 324)

$$h = \frac{\sigma_{\mathrm{z}}^2}{\pi G \Sigma} \tag{5.6}$$

where σ_{z} is the vertical velocity dispersion. This gives that

$$k_{\min} \cdot h = \left(\frac{\sigma_{\mathrm{z}}}{\sigma} \right)^2. \tag{5.7}$$

From the study of the classical Toomre criterion in Chapter 2 we learn that the criterion is only reliable if $k_{\min} h \ll 1$. This is visible in equation (5.4) as this limit reduces the relation to the classical dispersion relation, equation (2.1). However, we will see later that the ratio between the radial and vertical velocity dispersions for the stellar component is most commonly around 0.5 and 0.6. $0.5^2 = 0.25$ is smaller than unity, however not much smaller than unity. This small relation shows us that thickness indeed plays a significant role in the stability of discs.

To study discs of two components and finite thickness we will follow the method and equations described by Romeo (1992, 1994) and study the model he described in more detail. In analogy with the zero-thickness case we will look at stability threshold contours, two-phase region and the effects on these. For further details concerning the numerical calculations used, refer to Appendix C.

5.1 Relevant parameters for two-component thick discs

When considering two-component discs with thickness we first need to discuss what kind of parameters might be useful. The obvious is to just use the scale height for each component. This is problematic though as we can only directly measure the thickness of galaxies that are edge-on. Also it is difficult to know the shape of the gaseous disc as this is difficult to measure. It is simpler to consider the velocity ellipsoid and look at the vertical velocity dispersion for each component, following the study by Romeo (1992, 1994). The advantages of using the velocity ellipsoid is that the vertical stellar velocity dispersion is possible to measure along the line of sight and it is possible to make good assumptions around the gaseous velocity dispersion.

Thus we define the following parameter

$$\mathcal{D}_{\mathrm{i}} \equiv \frac{\sigma_{\mathrm{zi}}}{\sigma_{\mathrm{i}}}, \tag{5.8}$$

the ratio between the vertical velocity dispersion and the radial velocity dispersion where the index “i” is as usual either “g” for gas or “s” for stars.

The stellar velocity dispersion ratio has been measured several times. In the literature I was able to find that it is for the Milky Way around 0.5 (Binney & Tremaine 2008, p. 18) or between 0.5 and 0.6 (van der Kruit & de Grijs 1999). NGC 488 seems to have a stellar velocity ratio of 0.7 (van der Kruit & de Grijs 1999; Gerssen et al. 1997). Gerssen et al. (1997) also mentions that the solar neighbourhood has a ratio of 0.52. van der Kruit & de Grijs (1999) also tabulates measurements of the stellar velocity ratio for a number of galaxies and found values ranging from 0.49 to 0.71.

The stellar disc thickness parameter we are going to consider in this chapter are $\mathcal{D}_{\rm s} = 0.5$, 0.7 and 1. $\mathcal{D}_{\rm s} = 1$ is for comparison, an isotropic disc (equal radial and vertical velocity dispersions). $\mathcal{D}_{\rm s} = \mathcal{D}_{\rm g} = 0$ does of course represent the infinitesimal thin case of Chapter 3.

The gaseous velocity dispersion ratio can not be measured, however as we can assume that the gas is collisional $\mathcal{D}_{\rm g}$ should realistically be unity. However, for comparison we are also going to consider a case with $\mathcal{D}_{\rm g} = 0.5$.

The case with $\mathcal{D}_{\rm s} = 0.5$ and $\mathcal{D}_{\rm g} = 1$ should then represent the most realistic case (and the solar neighbourhood). This case will be studied in more detail than the others and also used to, in a similar fashion as in Chapter 3, try to formulate a simple and useful approximation.

In summary are the considered thick cases

- $\mathcal{D}_{\rm s} = 0.5$ and $\mathcal{D}_{\rm g} = 0.5$, the thinnest case.
- $\mathcal{D}_{\rm s} = 0.5$ and $\mathcal{D}_{\rm g} = 1$, the most realistic case, “the solar neighbourhood”.
- $\mathcal{D}_{\rm s} = 0.7$ and $\mathcal{D}_{\rm g} = 1$, the thickest realistic case.
- $\mathcal{D}_{\rm s} = 1$ and $\mathcal{D}_{\rm g} = 1$, the thickest case.

5.2 The marginal stability curve

As with the thin two component case of Chapter 3 we start by considering the marginal stability curve, as derived in the study by Romeo (1992). He derived two different marginal stability curves using two different parametrizations, with the vertical velocity dispersion parameters already defined and one parametrization using the scale heights for each component and the stellar wavenumber. However, visible in his results the velocity dispersion parametrization is more precise, though also more complicated to handle while the wavenumber parametrization gives some unphysical results.

The marginal stability curve as a function of the velocity dispersion parameters is given by a polynomial of the 8th degree. For more details concerning the polynomial, the constants and how they were all solved numerically, refer to Appendix C. The polynomial has the form of

$$A \cdot Q^8 + B \cdot Q^6 + C \cdot Q^4 + D \cdot Q^2 + E = 0 \tag{5.9}$$

which has to be solved numerically for each point of Λ in our range of $0 \leq \Lambda \leq 1 + \mathcal{A}$ to obtain the wanted marginal stability curve,

$$Q(\mathcal{A}, \mathcal{B}, \mathcal{D}_{\rm s}, \mathcal{D}_{\rm g}, \Lambda). \tag{5.10}$$

Figure 5.1 are a few examples of how the marginal stability curves behave in the considered thick cases, using the same $\mathcal{A}$ and $\mathcal{B}$ examples as in figure 3.1 of the thin case. The first plot of the figure is in fact the same as figure 3.1 as it shows the thin cases.

We notice how the curves are quite similar to the thin cases as they also exhibits two peaks for certain densities and velocity dispersions. This obviously again gives us a two-phase region and transitions between stellar and gas-dominated regimes for each thick case.

However, when comparing with the zero-thickness case we see that for thicker discs the marginal stability curve exhibit lower values. Thus the stability threshold evidently grows smaller. Already we can see that the thickness has a stabilising effect on the disc.

Furthermore, we see when studying the curves more closely that not only does the stability threshold change but also the shape of the curves. The transitions between stellar and gaseous regimes apparently also changes with the thickness. We evidently need to study the two-phase region of each case in more detail.

5.3 The two-phase region

The two-phase regions of all our cases are plotted in figure 5.2. The general shape of the regions seem to be conserved, however the size and transition lines are affected by the thickness. The first point to note is how the regions grow larger due to the thickness. This is interesting as it further strengthens the earlier arguments of the region's importance. In Chapter 4 we saw how observations indicate that large portions of the discs of galaxies are in fact inside the two-phase region of the zero-thickness case. Taking into account the thickness may increase the portions of the discs that are inside the region.

It is also visible here that the triple point of the regions are affected by the thickness, though we now encounter problems. The triple point and the size of the two-phase regions are affected by the thickness in a quite irregular manner. The hope was that we could construct a simple and powerful approximation for the two-phase region depending on the thickness parameters. In table 5.1 the effects on the triple point is presented together with the zero-thickness values from Chapter 3 so that it is easier to see the unpredictable behaviour of it.

Instead of formulating an exact approximation I suggest some constant values that envelopes all the regions. As an example we may use $\mathcal{A} < 0.25$ and $\mathcal{B} < 0.2$. This forms a square around the two-phase region and the proximity at low stellar densities for all cases. This is obviously larger than even the two-phase region corresponding to the isotropic disc. However, this is just an approximation and any values are possible to use. As another example we may use the $\mathcal{A}$ and $\mathcal{B}$ triple point values for the Milky Way-like disc, $\mathcal{A} < 0.22$ and $\mathcal{B} < 0.16$ which may be a more realistic constraint.

Furthermore it is possible, if one need to be more exact, to take advantage of the triangle-like shape of the two-phase region and construct an approximation for the necessary thickness of the disc by just postulating some straight lines in the $\mathcal{B} - \mathcal{A}$ parameter space.

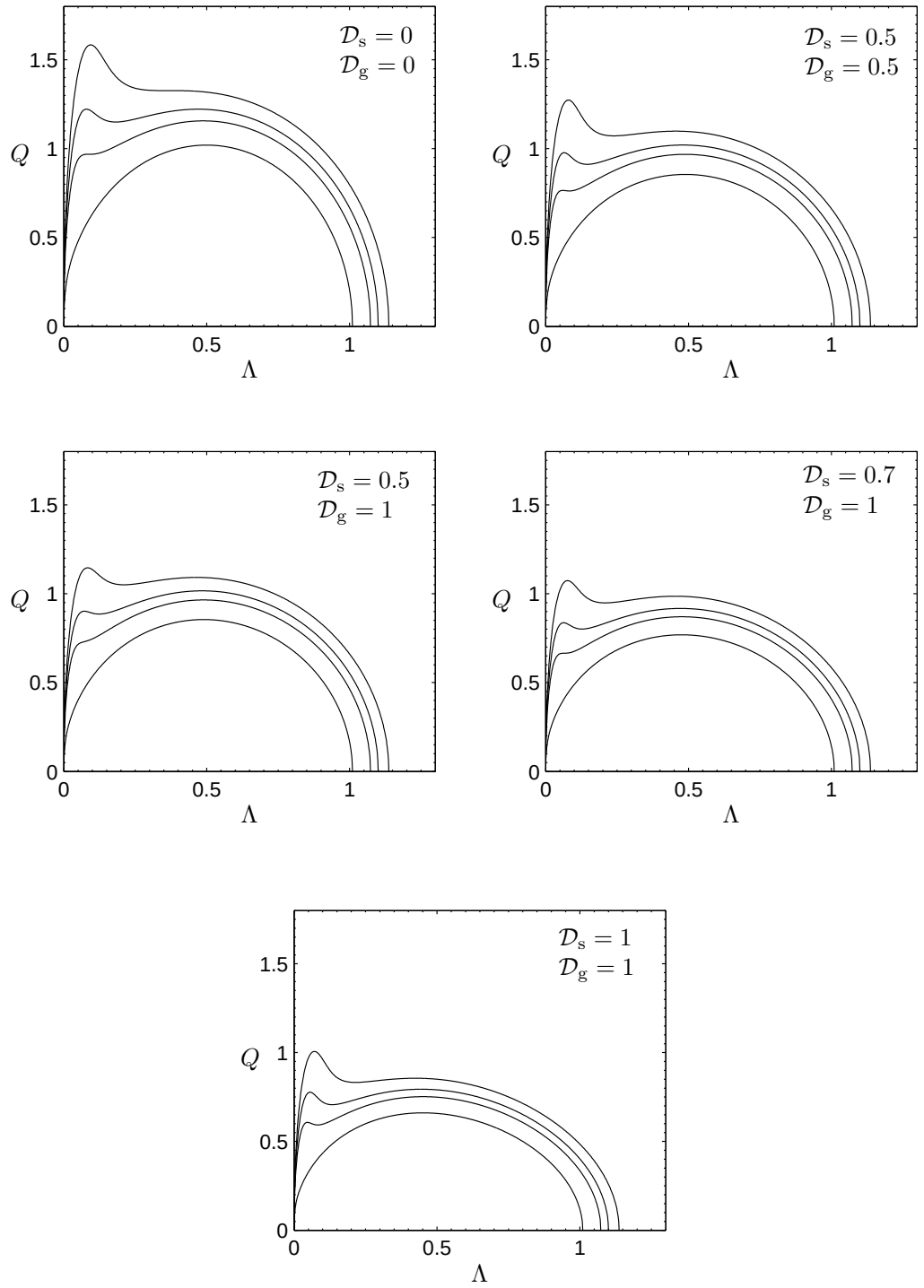

Figure 5.1: The marginal stability curves for different thicknesses, with constant $\mathcal{B} = 0.1$ and $\mathcal{A} = 0.01$, 0.073, 0.1 and 0.137 (lower to uppwer curves) for each plot.

Table 5.1: Effects of thickness on the triple point.

Thickness	$\mathcal{A}_0$	$\mathcal{B}_0$	$\bar{Q}_0$	$\bar{\Lambda}_0$
$\mathcal{D}_\mathrm{s}=0$, $\mathcal{D}_\mathrm{g}=0$	0.17	0.17	1.41	0.29
$\mathcal{D}_\mathrm{s}=0.5$, $\mathcal{D}_\mathrm{g}=0.5$	0.21	0.18	1.26	0.23
$\mathcal{D}_\mathrm{s}=0.5$, $\mathcal{D}_\mathrm{g}=1$	0.22	0.16	1.27	0.21
$\mathcal{D}_\mathrm{s}=0.7$, $\mathcal{D}_\mathrm{g}=1$	0.24	0.18	1.76	0.25
$\mathcal{D}_\mathrm{s}=1$, $\mathcal{D}_\mathrm{g}=1$	0.22	0.19	0.99	0.36

For the Milky Way the region could perhaps be approximated with a lower transition line from $\mathcal{A}=0.01$ and $\mathcal{B}=0.04$ to the triple point and an upper line from $\mathcal{A}=0.01$ and $\mathcal{B}=0.15$ to the same point. Note that as we do not consider anything with $\mathcal{A}$ and $\mathcal{B}$ lower than 0.01 here as this example uses the lowest values available for the two-phase region. This would give the simple lines $\mathcal{A}_\mathrm{high}=0.47\mathcal{B}+0.15$ and $\mathcal{A}_\mathrm{low}=1.75\mathcal{B}-0.06$. This is of course highly affected by the resolution we are using for the triple point and lower values. It would be advisable to be more precise than this example and perhaps use a higher accuracy on the coordinate of the triple point and to extend the two-phase region down to $\mathcal{A}=\mathcal{B}=0$ prior to defining the lines.

5.4 The stability threshold

In figure 5.3 we compare the stability threshold contour lines of the discs with different thickness. The thin black lines in the background are the same contour lines as in figure 3.3, the zero-thickness contour lines of Chapter 3, while the coloured lines are the different thick cases with the stability threshold being $\bar{Q}=1$. In the thin case this contour line only exists along $\mathcal{A}=0$ as it is the classical one-component Toomre case we find there. However, when taking into account the thickness this contour line is quite prominent due to the stabilising effect we obtain which is clearly visible in this plot. The thicker discs have the $\bar{Q}=1$ contour line at very high $\mathcal{A}$-values, so that a much larger area of the parameter space has the threshold $\bar{Q}<1$.

We can also notice both in figure 5.2 and 5.3 how the main transition line is affected by the thickness. However, this is as the two-phase region, also behaving quite unpredictable.

We should also pay extra attention to the Milky Way-like case, when $D_\mathrm{s}=0.5$ and $\mathcal{D}_\mathrm{g}=1$. In figure 5.4 several more contour lines of the stability threshold is plotted for further study. The intention was to use a more detailed analyses of this case to formulate an approximation of the effective stability parameter in a similar fashion as for the thin case in Chapter 3. It seemed quite probable that this would be possible as the behaviour is very similar and it seemed to be a question of correcting the shift of the contour lines. However, to formulate an approximation of the effective stability parameter when not neglecting thickness proved to be much more complex. It is possible to formulate an approximation for the stellar regime. However, connecting this with the transition between stellar and gaseous dominated regimes and formulating a useful approximation of the gaseous regime proved too complex. Details concerning this may be presented

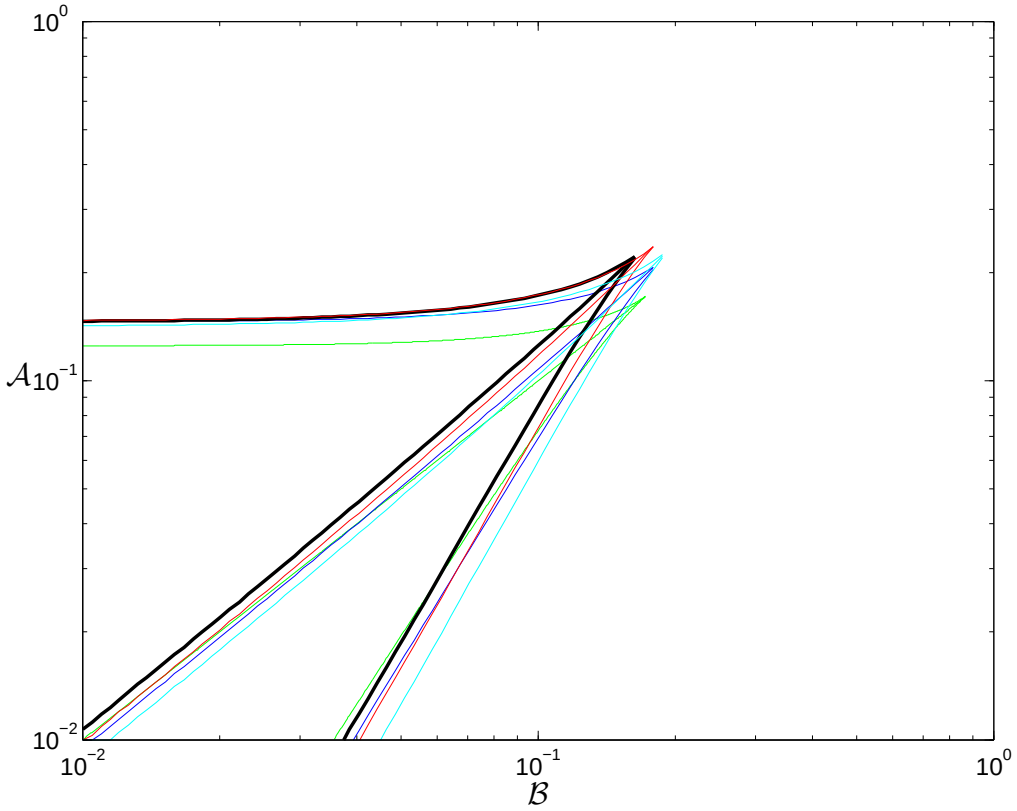

Figure 5.2: Effects of thickness on the two-phase region. Green: zero thickness, blue: $\mathcal{D}_{\rm s} = 0.5$ and $\mathcal{D}_{\rm g} = 0.5$, thick black: $\mathcal{D}_{\rm s} = 0.5$ and $\mathcal{D}_{\rm g} = 1$ (Milky Way-like), red: $\mathcal{D}_{\rm s} = 0.7$ and $\mathcal{D}_{\rm g} = 1$ and cyan: $\mathcal{D}_{\rm s} = 1$ and $\mathcal{D}_{\rm g} = 1$.

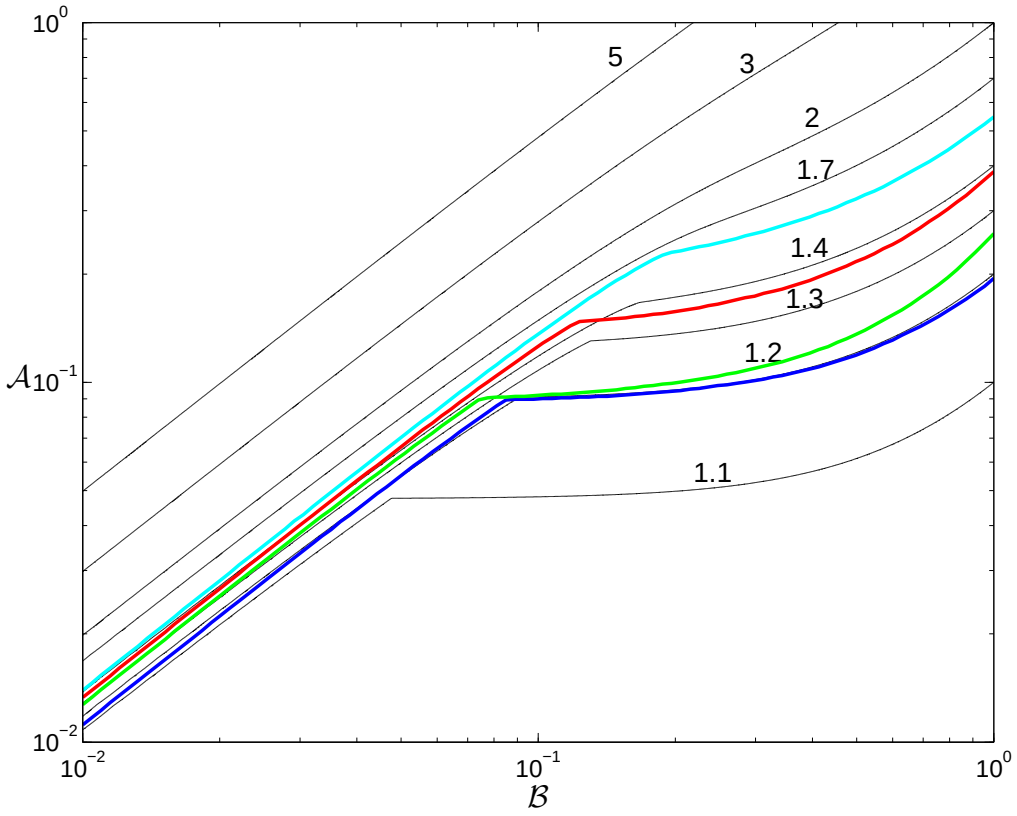

Figure 5.3: Contour lines of the stability threshold $\bar{Q} = 1$ for discs with thickness. Black: zero thickness contour lines as comparison, blue: $\mathcal{D}_\mathrm{s} = 0.5$ and $\mathcal{D}_\mathrm{g} = 0.5$, green: $\mathcal{D}_\mathrm{s} = 0.5$ and $\mathcal{D}_\mathrm{g} = 1$, red: $\mathcal{D}_\mathrm{s} = 0.7$ and $\mathcal{D}_\mathrm{g} = 1$ and cyan: $\mathcal{D}_\mathrm{s} = 1$ and $\mathcal{D}_\mathrm{g} = 1$.

elsewhere.

5.5 Summary

We had not yet discussed the effects of disc thickness on the stability in this thesis. These can be proven to be quite important by finding out if $k_\mathrm{min} h \ll 1$ is really true. By calculating equation (5.7) we however see that $k_\mathrm{min} h = (\sigma_\mathrm{z}/\sigma)^2$ which is commonly measured to be roughly 0.25 to 0.3.

There are different ways to formulate good parameters that describe disc thickness. However, the most useful is to describe it with the help of the velocity ellipsoid. More specifically we use parameters defined by the ratio between the radial and vertical velocity dispersions of our specific components. Such parametrization was used by Romeo (1992, 1994) and we followed his conduct in this study.

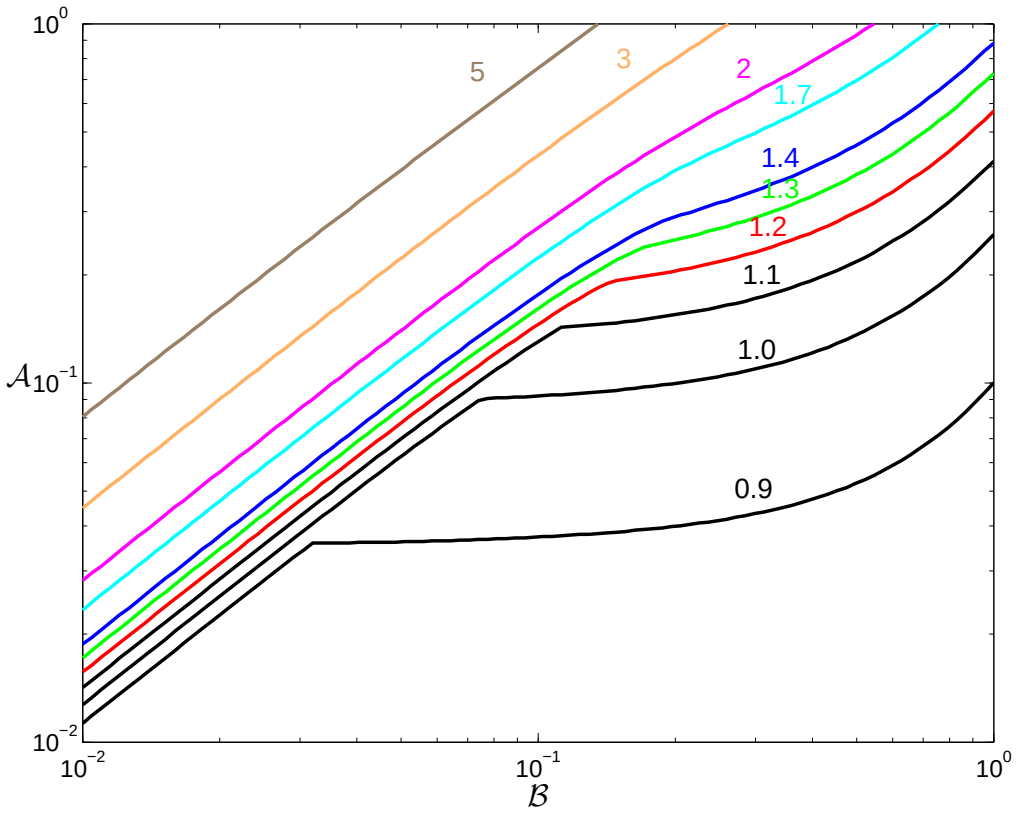

Figure 5.4: Contour lines of the stability threshold $\bar{Q}$ for a disc with $\mathcal{D}_{\rm s} = 0.5$ and $\mathcal{D}_{\rm g} = 1$, the Milky Way-like case.

Romeo (1992) derived how the marginal stability curve can be derived numerically from an polynomial of the 8th order, equation (5.9). As in Chapter 3 we know that it is possible to derive the stability threshold and the two-phase region from the marginal stability curves. Furthermore, we know it is possible to study the stability threshold to attempt to find an approximation of the effective stability parameter. This however, proved more complex than first expected when we are not neglecting disc thickness and this is left for later.

However, it is possible to draw several conclusions from this study. First of all we find that the thick cases that are more realistic according to the literature greatly affects the stability. The thickness strongly stabilises the discs and we see that the two-phase region, which unfortunately behaves rather irregular depending on the thickness, grows larger. This strengthens the arguments of Chapter 4 where we conclude that the two-phase region plays a significant role in a large portion of many disc galaxies.

Even though the two-phase region behaves irregular when using thickness it is still possible to use the general shape of each case to formulate an approximation of it. Either using the triple point of each case (see table 5.1) to form a square around the two-phase region and its vicinity or we can formulate a triangle from the lower $\mathcal{B}$ - $\mathcal{A}$ values to the triple point to obtain a more exact result.

Chapter 6

Conclusions

By revisiting the study of gravitational instability in thin two-component discs as studied by Jog & Solomon (1984); Bertin & Romeo (1988); Wang & Silk (1994); Jog (1996) we are able to formulate a new approximation of a stability criterion similar to that formulated by Wang & Silk (1994). With this approximation however, we are able to take into account previously found behaviours of a two-component disc. The most important for the approximation is the transition between stellar and gaseous dominated instabilities.

What we obtain are two Toomre-like effective stability criterions (see Chapter 3), one for the stellar dominated instability, equation (3.15) and one for the gaseous dominated instability, equation (3.19).

These expressions are with purpose formulated in a similar fashion as how Wang & Silk (1994) formulated theirs. This makes it easy to adapt this quite complex case for application with observations because it just involves using a correction factor, equation (3.16) and taking into account what kind of instability is dominating for the specific data point.

The two-component case exhibits other interesting behaviours also found by previous mentioned authors. There is not only a transition between stellar and gaseous dominated instabilities, however there are also situations where we obtain instabilities from both components at two different wavelengths of perturbation, or at two different scale lengths. The stellar and gaseous components are in a way decoupled. This is usually known as a region of peculiar instability (see the two-phase region, Section 3.2).

To find how important this behaviour may be, we applied the data from ten different galaxies (eight disc galaxies and two dwarf galaxies) from the study by Leroy et al. (2008) and conducted a similar stability analyses as them. We applied the data in exactly the same way as Leroy et al. (2008) though on this model instead and can conclude that the regions of peculiarity appears to be of importance. This is due to that considerable portions of the inner parts of five of the eight considered disc galaxies were measured to have the required densities and velocity dispersions. The other three disc galaxies had densities had velocity dispersions in the vicinity of the required range so other assumptions as a lower gaseous velocity dispersion could have strengthened this result.

Furthermore when taking into account the thickness of discs by following the conduct of Vandervoort (1970); Romeo (1990, 1992, 1994) we can see that the importance of the peculiar

two-component instabilities are strengthened. This is due to the fact that disc thickness widens the ranges of densities and velocity dispersions that gives rise to the peculiar instabilities by a significant amount.

The widened ranges of densities and velocity dispersions are possible to approximate with simple constraints depending on the disc thickness even though the ranges are affected in an irregular manner. This can be done by either using constant densities and velocities for each component or by using simple linear functions, i.e. the velocity dispersions as functions of the densities. Which conduct is favoured depends on what degree of accuracy is required (see Section 5.3 for further details).

Finally we have to note that when applying the data of Leroy et al. (2008) it is important to remember the importance of the conversion factor used for finding the gaseous densities, especially for the densities of molecular hydrogen. This is due to the fact that the existing H_2-data affects the gas density much more than the HI-data near the centre in spiral galaxies while at the same time are the H_2-data the most unreliable data as they are found purely by observing tracers. Leroy et al. (2008) discusses this problem and concludes that there exists no reliable conversion factor which takes into account the different aspects that affects the connection between the tracer intensity and the H_2-density. This fact can however affect our conclusion of how important the two-component effect of having instabilities from both the gaseous and stellar components really is.

For the future it could be interesting to study the disc thickness effects further. However, the question is how useful this would be as it is very difficult to formulate some useful simplification of this quite complex case. We should also note that the main topic in this field these days is the study of the role of turbulence. This on the other hand complicates matters again as the common conduct these days when doing stability analysis of observed galaxies is to adopt one constant velocity dispersion for the gaseous component.

These comments again remind us of how complex these studies can be and the importance of finding simple useful methods of applying these on observations with adequate accuracy, i.e. adequate enough to cover what is possible to measure. This is what our approximation of the infinitesimal thin two-component disc stability criterion provides.

Appendix A

Numerical methods: thin discs

MATLAB was used for all the numerical computations of this thesis.

The problem described in Chapter 3 consists of (1) deriving the marginal stability curve for given values of the relevant parameters $\mathcal{A}$ and $\mathcal{B}$; (2) extracting useful information from these curves to find the two-phase region and transitions; and (3) determing the stability threshold.

A.1 Finding the two-phase region

As the expression describing the marginal stability curve was already given by Bertin & Romeo (1988) it was only a simple matter of plotting the curve to be able to study it. To derive the two-phase region is another matter however as it demands that I am able to derive when the curve exhibits two peaks and also which peak is the global maxima in the whole $\mathcal{B} - \mathcal{A}$ space. This can of course be done in several ways and I have mainly been using two methods.

For the predefined parameters was a resolution of 1000 points used, i.e. for $\mathcal{A}$, $\mathcal{B}$ and Λ. The Λ was defined from 0 to 1.2 when finding the two-phase region in constrast as when plotting the curve from 0 to $1 + \mathcal{A}$, as the two-phase region does not exist at $\mathcal{A} > 0.2$ as already found by Bertin & Romeo (1988). In this way was not a new Λ range required to be defined for each $\mathcal{A}$ value, perhaps saving a bit of time.

The $\mathcal{A}$ and $\mathcal{B}$ parameters were first defined in linear scale from 0 to 1, however when the thesis progressed it was noticed that it would be better to define them in logarithmic scale from 0.01 to 1, still with a resolution of 1000 points each. In this way was only one range needed for the large scale plots instead of the two ranges used by Bertin & Romeo (1988), one small scale for the transitions and two-phase region and one large scale.

The method finally used to find the two-phase region of this thin two-component case was based on one of the earlier codes I wrote for this problem. Thus it is a bit manual and perhaps ineffective. See figure A.1 for a flowchart of the following description.

The routine consists of a double for-loop where the computer, for each defined $\mathcal{A}$ and $\mathcal{B}$ point derive the marginal stability curve. The $\mathcal{B}$ range was confined to $\mathcal{B} \leq \sqrt{0.0294}$ (≈ 0.1715) to save time. This is the theoretical derived $\mathcal{B}$ for the triple point found by Bertin & Romeo (1988).

Each marginal stability curve is sampled by the computer for each Λ, first from the lowest Λ

(blue parts figure A.1) in an attempt to find the gaseous peak as this is always at a wavelength smaller than the stellar peak (see figure A.2). The computer searches for when $Q(\Lambda_1) - Q(\Lambda_2) \leq 0.00001$ where $\Lambda_1 < \Lambda_2$, and saves the Λ_1 in a matrix denoted l1. 0.00001 is an arbitary number used to counter numerical errors.

To find the stellar peak was a similar method used, however I instead let the computer sample the curve from the high Λ (green parts of figure A.1), looking for when $Q(\Lambda_1) - Q(\Lambda_2) \leq 0.00001$. The number 0.00001 is again used to counter numerical errors. It is of greater importance here when searching for the stellar peak as this is much flatter than the gaseous peak (see figure 3.1). The Λ_1 corresponding to the stellar peak was saved in a matrix denoted l2.

Furthermore was a third matrix, ltrans created, where all the Λ corresponding to the global maxima of the marginal stability curve was saved (yellow part in figure A.1) with the help of the MATLAB-function max. In this way we have three different matrices with the Λ of each local maxima (gaseous and stellar peaks) and for the global maxima for each $\mathcal{A}$ and $\mathcal{B}$ in the chosen range saved.

To find the lower curve of the two-phase region (see figure A.2) the l1 matrix is sampled from high $\mathcal{A}$ and low $\mathcal{B}$ until the Λ is larger than 0.293. A value theoretically derived by Bertin & Romeo (1988) to be the wavelength of the single flat maxima of the triple point. The higher transition curve of the two-phase region is found in exactly the same way, however by sampling the l2 matrix instead which has the Λ for the stellar peaks. And finally is the main transition line between the gaseous and stellar regimes found by the same method, however by sampling the ltrans matrix containing the Λ for the global maxima.

The specific $\mathcal{A}$ values for each transition to $\Lambda > 0.293$ for each matrix are saved in vectors and simply plotted against the $\mathcal{B}$ axis. Thus is the two-phase region plotted.

A second method to find the two-phase region was also used. However this was mainly for the thick two-component disc case and it involved using the predefined MATLAB-function denoted findpeaks. That is explained in Appendix C.

A.2 Determining the stability threshold

The contours of the stability threshold $\bar{Q}$ are easily determined by finding the Q value of the global maxima of the marginal stability curve. Again was this done by calculating the marginal stability curve for every $\mathcal{A}$ and $\mathcal{B}$ in the same range used for finding the two-phase region, however the $\mathcal{B}$ was not confined to be $\leq \sqrt{0.0294}$ here. The predefined MATLAB-function max was used to find the global maxima. This command returns both the maximal Q value and the corresponding Λ. However, I was only interested in the stability threshold and thus only saved a matrix with the derived $\bar{Q}$ for every $\mathcal{A}$ and $\mathcal{B}$.

For the plotting of the stability threshold was the contour function for contour plots in MATLAB used. There is not much to write about this except that there are other methods possible to find the contours of the stability threshold that are not equally exact however more effective. These were used in the two-component thick cases and not required in this thin disc-case.

Exactly the same conduct was used for the contour lines of the Wang & Silk (1994) stability threshold approximation. However, for the Romeo and Wiegert approximation (Section 3.4) was

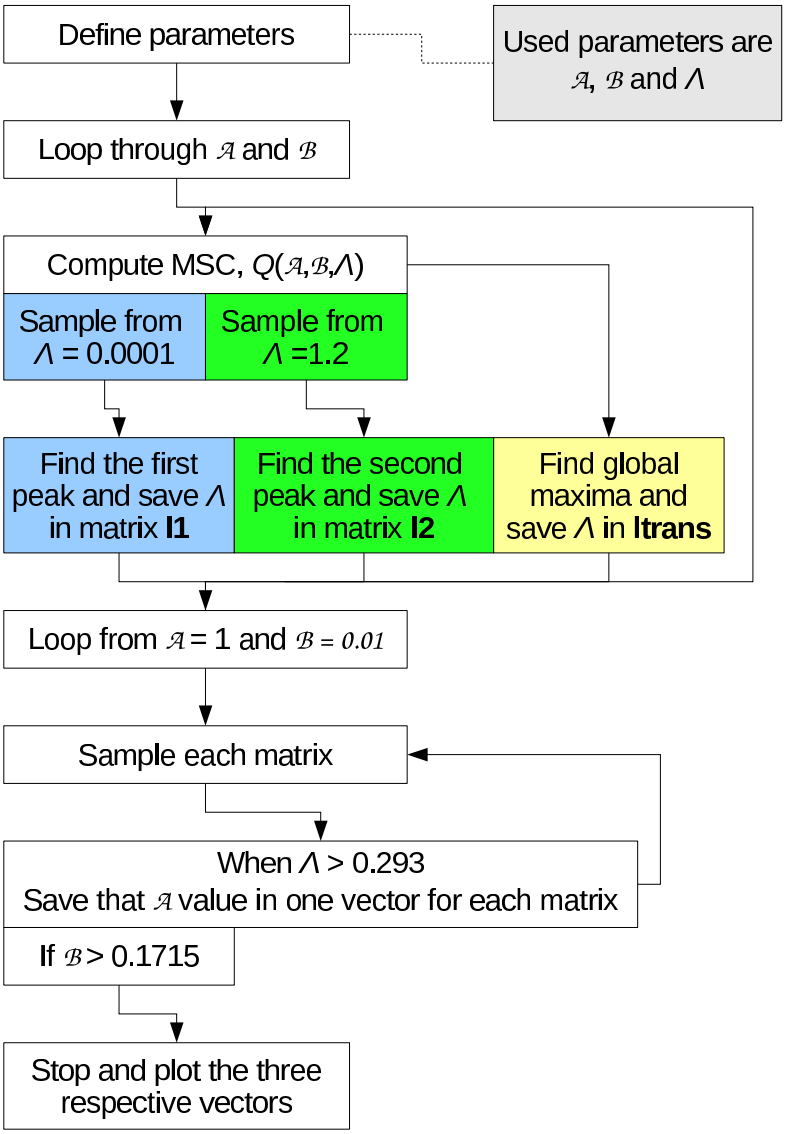

Figure A.1: Flowchart describing the routine used to find the two-phase region. More details are found in the text of Appendix A.1.

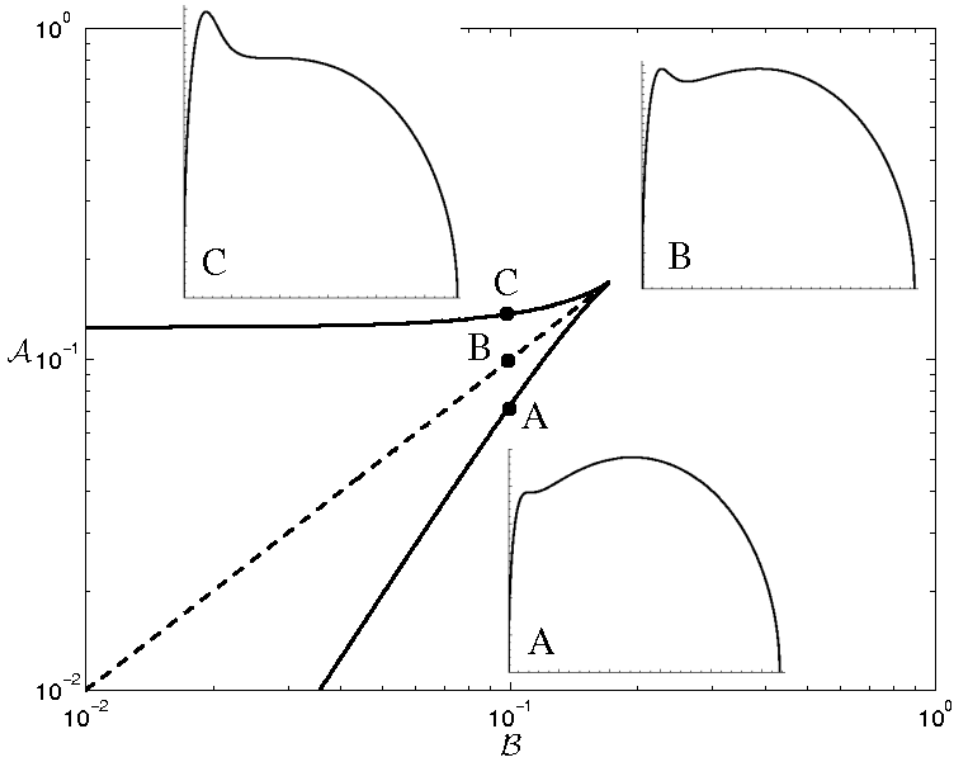

Figure A.2: The two-phase region and the wanted characteristics of the marginal stability curve in the transition lines.

the contour lines plotted as several functions $\mathcal{A}(\bar{Q}, \mathcal{B})$ instead with the corresponding constant $\bar{Q}$ chosen for each contour line without using the contour function. This was due to how the approximation was derived and that we for simplicity looked at these kinds of functions instead of a $\bar{Q}(\mathcal{A}, \mathcal{B})$ for the stellar and gaseous regimes.

Appendix B

Radial profiles of the stability quantities

In the online version of Leroy et al. (2008) all the derived radial density profiles from the galaxies of their survey were presented in their table 7. They also linked to a machine-readable file of the table that was allowed to download. The data were all very extensive so it was only a matter of deriving the wanted quantities, parameters and corresponding error bars when conducting this study. The only troubles were the choices of galaxies and the amount of data to handle. In this appendix are details surrounding how the data was derived by Leroy et al. (2008) and how their data in turn was handled by me. The radial profiles of the chosen galaxies are also presented in tables B.1 to B.11.

B.1 Surface density and velocity dispersion ratios

In Section 4.3 I explained how the mean density ratio and velocity dispersion ratio profiles were derived. However, the densities and velocity dispersions were first derived by Leroy et al. (2008). As mentioned in Chapter 4 were they using intensity maps of galaxies at different wavelengths to derive the densities. The appendices by Leroy et al. (2008) are very extensive on how they derived the density profiles, however I write here a summary of their work and how I used their derived quantities in more detail.

The stellar surface density profiles were derived by Leroy et al. (2008) by using infrared pictures from SINGS (Kennicutt et al. 2003) taken in the 3.6 μm band for most of their galaxies. They gathered intensity profiles denoted $I_{3.6}$ from the median of $10''$ wide tilted rings with the help of earlier derived parameters for each galaxy. From the profiles from the 2MASS (Jarrett et al. 2003) they acquired the ratio between $I_{3.6}$ and the K-band intensity which was found to be $I_{3.6} = 0.55 I_K$. With this they can use the K-band mass-to-light ratio of $\Upsilon_{\rm s}^K = 0.5 M_\odot / L_{\odot,K}$ which they approximate to be constant for all their galaxies at all radii to derive the wanted densities. This gives that the stellar surface densities can be derived from

$$\Sigma_{\rm s} = \Upsilon_{\rm s}^K \frac{I_K}{I_{3.6}} \cos i I_{3.6} = 280 \cos i I_{3.6} \tag{B.1}$$

where i accounts for the inclination given by Leroy et al. (2008), $I_{3.6}$ is in MJy ster^{-1} and $\Sigma_{\rm s}$ is

in $M_\odot$ pc^{-2}.

The choice of mass-to-light ratio is a major uncertainty as this depends on the star formation history, metallicity and initial mass function. It varies less in the near infrared than the optical however it still varies. Leroy et al. (2008) discusses differences in derived densities by different authors due to this.

To derive the gas density profiles Leroy et al. (2008) used THINGS (Walter et al. 2008) maps for HI densities and HERACLES maps for H_2. From THINGS they obtain 21 cm line emissions with a mean angular resolution of $11''$ and mean velocity resolution of 5 km s^{-1} from which they could convert from integrated intensity to surface density with

$$\Sigma_{\rm HI} = 0.020 \cos i I_{21\rm cm} \tag{B.2}$$

where $\Sigma_{\rm HI}$ is given in $M_\odot$ pc^{-2} and the intensity $I_{21\rm cm}$ in K km s^{-1}. This conversion also takes into account the presence of helium with a factor of 1.36.

The molecular hydrogen, H_2 is estimated by measurements of CO emission. This was done with results from HERACLES, with intensity maps of CO $J = 2 \rightarrow 1$ emission for most of the galaxies in their study. These data have an angular resolution of $11''$ and a velocity resolution of 2.6 km s^{-1}.

Such intensity maps from HERA were not available for the galaxies NGC 3627 and NGC 5194 of the study which is important to mention as data on NGC 5194 were used in this thesis. Instead were CO $J = 1 \rightarrow 0$ emission maps from BIMA SONG (Helfer et al. 2003) used for these with an angular resolution of $7''$.

The surface density, $\Sigma_{\rm H_2}$ is derived from the $J = 1 \rightarrow 0$ emissions with the conversion

$$\Sigma_{\rm H_2} = 4.4 \cos i I_{\rm CO}(1 \rightarrow 0) \tag{B.3}$$

where again the density is given in $M_\odot$ pc^{-2} and the intensity is in K km s^{-1}.

The CO $J = 2 \rightarrow 1$ emissions are related to the $J = 1 \rightarrow 0$ emissions. Based on HERACLES and other surveys Leroy et al. (2008) assumes the ratio $I_{\rm CO}(2 \rightarrow 1) = 0.8 I_{\rm CO}(1 \rightarrow 0)$ which is a typical value in their sample. Thus is the H_2 surface density given by

$$\Sigma_{\rm H_2} = 5.5 \cos i I_{\rm CO}(2 \rightarrow 1). \tag{B.4}$$

The errors for the radial profiles of gaseous and stellar densities were derived by Leroy et al. (2008) from

$$\Delta = \frac{\Delta_{\rm rms}}{\sqrt{N_{\rm pix,ring}/N_{\rm pix,beam}}} \tag{B.5}$$

for each quantity. The $\Delta_{\rm rms}$ is the rms scatter within the tilted ring, the $N_{\rm pix,ring}$ is the number of pixels in the ring and $N_{\rm pix,beam}$ is the number of pixels per resolution element. This captures both random scatter in the data and variations due to the azimuthal structure in the ring. It does not however capture systematic errors, as choices of light-to-mass ratios and tracers.

The total gas density is just simply the sum of the HI and H_2 densities. And the total gas error margins are derived from the sum of the given error margins derived by Leroy et al. (2008).

So the $\mathcal{A}$-parameter was simply derived as it is defined, with the ratio between the gaseous and stellar densities. The $\mathcal{A}$-error however were derived so that the highest (and lowest) values possible would be obtained, i.e. with

$$\Delta_{\mathcal{A}+} = \frac{\Sigma_{\rm g} + \Delta_{\rm g}}{\Sigma_{\rm s} - \Delta_{\rm s}} - \mathcal{A} \tag{B.6}$$

for the length of the top error bar where the different Δ's denotes the corresponding density error bars. Similar is the length of the lower error given by

$$\Delta_{\mathcal{A}-} = -\left(\frac{\Sigma_{\rm g} - \Delta_{\rm g}}{\Sigma_{\rm s} + \Delta_{\rm s}} - \mathcal{A}\right). \tag{B.7}$$

For the gaseous velocity dispersion is a constant $\sigma_{\rm g} = 11$km s^{-1} adopted by Leroy et al. (2008). This is due to the fact that $\sigma_{\rm g} = 11 \pm 3$km s^{-1} agrees well with the outer (HI dominated) parts of the galaxies of THINGS. The error is not taken into account here as this was not done by Leroy et al. (2008).

The derivation of the mean stellar velocity dispersions used by Leroy et al. (2008) were explained in Section 4.3 and are given by

$$\sigma_{\rm rs} = \frac{1}{0.6}\sqrt{\frac{2\pi G R_{\rm d}}{7.3}}\Sigma_{\rm s}^{1/2}. \tag{B.8}$$

To obtain this equation was a relation between the disc scale length and disc scale height used, $R_{\rm d} = 7.3 \pm 2.2 h_{\rm s}$. However, in the derivation we stated that we disregarded the margin of error to obtain the mean velocity dispersion. This was done also when deriving the errors of the velocity dispersion as this seems to have been the case in the study by Leroy et al. (2008). Thus the error for the $\mathcal{B}$ parameter is only due to the error of the measured stellar densities as we have a constant gaseous velocity dispersions and disregard the errors of the relations used to find the stellar velocity dispersions.

The top stellar velocity dispersion error was thus given by

$$\Delta_{\sigma\,{\rm s}+} = \frac{1}{0.6}\sqrt{\frac{2\pi G R_{\rm d}}{7.3}}(\Sigma_{\rm s} + \Delta_{\rm s})^{1/2} \tag{B.9}$$

and the lower error was given by

$$\Delta_{\sigma\,{\rm s}-} = \frac{1}{0.6}\sqrt{\frac{2\pi G R_{\rm d}}{7.3}}(\Sigma_{\rm s} - \Delta_{\rm s})^{1/2} \tag{B.10}$$

so that the $\mathcal{B}$ top error is

$$\Delta_{\mathcal{B}+} = \frac{\sigma_{\rm g}}{\sigma_{\rm s} - \Delta_{\sigma\,{\rm s}-}} - \mathcal{B} \tag{B.11}$$

and the lower error is

$$\Delta_{\mathcal{B}+} = -\left(\frac{\sigma_{\rm g}}{\sigma_{\rm s} + \Delta_{\sigma\,{\rm s}+}} - \mathcal{B}\right). \tag{B.12}$$

As the $\mathcal{B}$ error is only dependant of the error of the stellar densities this gives much smaller margins of error in this range than for the $\mathcal{A}$. This is quite visible in the data plots of Chapter 4, especially the $\mathcal{B} - \mathcal{A}$ tracks of figures 4.5 and 4.8. Considering how the gaseous velocity dispersions are set to a constant value and the stellar velocity dispersions are theoretically derived this is not so strange.

B.2 Stability parameters

For the stability threshold $\bar{Q}$ was the thin two-component case studied by Bertin & Romeo (1988) used. As described in Chapter 3 and in Appendix A must the marginal stability curve for each $\mathcal{A}$ and $\mathcal{B}$ used be derived and from these curves are the global maximas taken numerically to find the stability threshold.

As shown in this thesis is the marginal stability curve for a thin two-component disc given by equation (3.7),

$$\begin{aligned} Q^2 =& \frac{2\Lambda}{\mathcal{B}^2}\left[\mathcal{A} + \mathcal{B}^2 - \Lambda(1+\mathcal{B}^2)\right. \\ & \left. + \sqrt{\Lambda^2(1-\mathcal{B}^2)^2 - 2\Lambda(1-\mathcal{B}^2)(\mathcal{A}-\mathcal{B}^2) + (\mathcal{A}+\mathcal{B}^2)^2}\right]. \end{aligned} \tag{B.13}$$

By simply using the mean $\mathcal{A}$ and $\mathcal{B}$ values derived for each galaxy are the mean stability threshold values derived. The margins of error for the stability threshold are given by deriving the marginal stability curves

$$Q = Q(\mathcal{A} + \Delta_{\mathcal{A}+}, \mathcal{B} + \Delta_{\mathcal{B}+}, \Lambda) \tag{B.14}$$

for the top error and

$$Q = Q(\mathcal{A} - \Delta_{\mathcal{A}-}, \mathcal{B} - \Delta_{\mathcal{B}-}, \Lambda) \tag{B.15}$$

for the lower error. The stability threshold errors are again found from the global maximas of these curves and denoted $\Delta_{\bar{Q}+}$ and $\Delta_{\bar{Q}-}$ respectively.

The second important stability parameter applied on the data is the effective stability parameter defined in equation (3.4) to be

$$Q_{\text{eff}} \equiv \frac{Q_{\text{s}}}{\bar{Q}} \tag{B.16}$$

where

$$Q_{\text{s}} = \frac{\kappa\sigma_{\text{s}}}{\pi G\Sigma_{\text{s}}} \tag{B.17}$$

and κ is the epicyclic frequency for each galaxy of the chosen sample. This is derived theoretically by Leroy et al. (2008) and most details were explained in Section 4.3. They used an

adaptation of how the epicyclic frequency for a flat rotation curve is formulated with the help of the term

$$\beta = \frac{d \log V(R)}{d \log R} \tag{B.18}$$

where R is the galactocentric radius and $V(R)$ is the linear velocity. This β we in turn derived numerically in MATLAB by using the simple command diff on both the velocity and radius terms. The following output is a vector one element shorter than the input-vectors, where the output-vector elements are the difference in value of each element of the input-vectors. To counter the problem that the β is now one element shorter than the rest of the input-vectors I simply create one more element in β that is equal the the previously last element. These two elements correspond to the absolutely last data points of each galaxy, i.e. the outer parts of each galaxy and thus also where the rotation curve is normally flatter.

Thus is the margin of error for the $Q_{\rm s}$ given by the errors of the stellar densities and stellar velocity dispersions as

$$\Delta_{Q{\rm s}+} = \frac{\kappa(\sigma_{\rm s} + \Delta_{\sigma{\rm s}+})}{\pi G(\Sigma_{\rm s} - \Delta_{\rm s})} - Q_{\rm s} \tag{B.19}$$

for the upper error and

$$\Delta_{Q{\rm s}-} = -\left(\frac{\kappa(\sigma_{\rm s} - \Delta_{\sigma{\rm s}-})}{\pi G(\Sigma_{\rm s} + \Delta_{\rm s})} - Q_{\rm s}\right) \tag{B.20}$$

for the lower error.

This in turn gives the margin of error of the effective stability parameter,

$$\Delta_{Q{\rm eff}+} = \frac{Q_{\rm s} + \Delta_{Q{\rm s}+}}{\bar{Q} - \Delta_{\bar{Q}-}} - Q_{\rm eff} \tag{B.21}$$

for the upper error and

$$\Delta_{Q{\rm eff}-} = -\left(\frac{Q_{\rm s} - \Delta_{Q{\rm s}-}}{\bar{Q} + \Delta_{\bar{Q}+}} - Q_{\rm eff}\right) \tag{B.22}$$

for the lower error.

There are other methods for deriving margins of error, deviation and propagation of error. However, the method described above is the more rigorous way of doing it. Also were the differences between length of error bars using different methods found to be much smaller than unity.

B.3 Radial profiles

In this section are the radial profiles for all the galaxies in the chosen samples presented. The columns with R, $\Sigma_{\rm HI}$, $\Sigma_{\rm H_2}$ and $\Sigma_{\rm s}$ are directly from the electronic version of table 7 of the article

Table B.1: Radial profiles for the galaxy HO II ($R_{25} = 3.7$ kpc).

	From Leroy et al. (2008)			Our stability quantities			
R (kpc)	$\Sigma_{\rm HI}$ ($M_\odot {\rm pc}^{-2}$)	$\Sigma_{\rm H_2}$ ($M_\odot {\rm pc}^{-2}$)	$\Sigma_{\rm s}$ ($M_\odot {\rm pc}^{-2}$)	$\mathcal{A}$	$\mathcal{B}$	$Q_{\rm eff}$	$\bar{Q}$
0.1	7.3 ± 2.9	< 1.0	25.6 ± 0.8	$0.285\,^{+0.126}_{-0.118}$	$0.619\,^{+0.010}_{-0.009}$	$3.86\,^{+0.76}_{-0.60}$	$1.43\,^{+0.19}_{-0.18}$
0.2	8.2 ± 3.3	< 1.0	24.8 ± 0.7	$0.331\,^{+0.147}_{-0.138}$	$0.629\,^{+0.009}_{-0.009}$	$3.36\,^{+0.71}_{-0.55}$	$1.49\,^{+0.22}_{-0.21}$
0.4	8.9 ± 3.0	< 1.0	19.7 ± 0.3	$0.452\,^{+0.162}_{-0.157}$	$0.706\,^{+0.005}_{-0.005}$	$2.87\,^{+0.51}_{-0.40}$	$1.62\,^{+0.22}_{-0.21}$
0.6	9.4 ± 2.2	< 1.0	19.5 ± 0.2	$0.482\,^{+0.119}_{-0.117}$	$0.709\,^{+0.004}_{-0.004}$	$2.37\,^{+0.29}_{-0.24}$	$1.66\,^{+0.16}_{-0.16}$
0.7	9.6 ± 1.5	< 1.0	21.4 ± 0.9	$0.449\,^{+0.093}_{-0.085}$	$0.677\,^{+0.015}_{-0.014}$	$2.09\,^{+0.30}_{-0.26}$	$1.63\,^{+0.12}_{-0.11}$
0.9	9.0 ± 1.8	< 1.0	19.1 ± 0.7	$0.471\,^{+0.116}_{-0.108}$	$0.717\,^{+0.014}_{-0.013}$	$1.88\,^{+0.29}_{-0.25}$	$1.64\,^{+0.15}_{-0.14}$
1.1	8.3 ± 2.3	< 1.0	20.4 ± 1.3	$0.407\,^{+0.148}_{-0.130}$	$0.693\,^{+0.023}_{-0.021}$	$1.65\,^{+0.39}_{-0.31}$	$1.56\,^{+0.19}_{-0.17}$
1.2	7.5 ± 2.5	< 1.0	53.5 ± 7.8	$0.140\,^{+0.079}_{-0.059}$	$0.428\,^{+0.035}_{-0.028}$	$1.18\,^{+0.43}_{-0.32}$	$1.25\,^{+0.14}_{-0.10}$
1.4	7.0 ± 2.4	< 1.0	13.0 ± 0.2	$0.538\,^{+0.196}_{-0.190}$	$0.869\,^{+0.007}_{-0.007}$	$1.62\,^{+0.29}_{-0.23}$	$1.62\,^{+0.22}_{-0.22}$
1.6	6.7 ± 2.3	< 1.0	8.4 ± 0.1	$0.798\,^{+0.287}_{-0.280}$	$1.081\,^{+0.006}_{-0.006}$	$1.66\,^{+0.32}_{-0.24}$	$1.74\,^{+0.26}_{-0.26}$
1.7	6.6 ± 2.1	< 1.0	7.4 ± 0.1	$0.892\,^{+0.300}_{-0.292}$	$1.151\,^{+0.008}_{-0.008}$	$1.63\,^{+0.31}_{-0.23}$	$1.77\,^{+0.25}_{-0.25}$
1.9	6.9 ± 2.1	< 1.0	8.1 ± 0.5	$0.852\,^{+0.332}_{-0.294}$	$1.100\,^{+0.036}_{-0.032}$	$1.40\,^{+0.39}_{-0.29}$	$1.77\,^{+0.27}_{-0.25}$
2.1	7.5 ± 2.2	< 1.0	12.0 ± 1.5	$0.625\,^{+0.299}_{-0.232}$	$0.904\,^{+0.062}_{-0.052}$	$1.09\,^{+0.44}_{-0.31}$	$1.69\,^{+0.27}_{-0.23}$
2.2	8.0 ± 2.2	< 1.0	5.3 ± 0.1	$1.509\,^{+0.452}_{-0.435}$	$1.360\,^{+0.013}_{-0.013}$	$1.27\,^{+0.26}_{-0.18}$	$2.08\,^{+0.28}_{-0.31}$
2.4	8.5 ± 2.1	< 1.0	9.8 ± 0.8	$0.867\,^{+0.310}_{-0.264}$	$1.000\,^{+0.044}_{-0.038}$	$0.95\,^{+0.29}_{-0.21}$	$1.87\,^{+0.26}_{-0.24}$
2.6	8.9 ± 1.8	< 1.0	7.6 ± 0.6	$1.171\,^{+0.358}_{-0.305}$	$1.136\,^{+0.048}_{-0.042}$	$0.92\,^{+0.25}_{-0.19}$	$2.03\,^{+0.25}_{-0.24}$
2.7	9.4 ± 1.5	< 1.0	4.7 ± 0.2	$2.000\,^{+0.422}_{-0.388}$	$1.445\,^{+0.032}_{-0.030}$	$0.99\,^{+0.17}_{-0.13}$	$2.31\,^{+0.19}_{-0.21}$
2.9	10.1 ± 1.3	< 1.0	23.8 ± 4.3	$0.424\,^{+0.160}_{-0.111}$	$0.642\,^{+0.067}_{-0.051}$	$0.58\,^{+0.26}_{-0.18}$	$1.62\,^{+0.18}_{-0.14}$
3.0	10.8 ± 1.3	< 1.0	5.8 ± 0.3	$1.862\,^{+0.338}_{-0.305}$	$1.300\,^{+0.035}_{-0.032}$	$0.77\,^{+0.13}_{-0.10}$	$2.39\,^{+0.16}_{-0.18}$
3.2	10.6 ± 1.3	< 1.0	4.5 ± 0.3	$2.356\,^{+0.478}_{-0.418}$	$1.476\,^{+0.052}_{-0.047}$	$0.79\,^{+0.15}_{-0.12}$	$2.47\,^{+0.16}_{-0.17}$
3.4	9.7 ± 1.2	< 1.0	3.0 ± 0.2	$3.233\,^{+0.660}_{-0.577}$	$1.808\,^{+0.063}_{-0.057}$	$0.91\,^{+0.17}_{-0.13}$	$2.49\,^{+0.15}_{-0.16}$
3.5	8.6 ± 1.0	< 1.0	2.6 ± 0.1	$3.308\,^{+0.532}_{-0.493}$	$1.942\,^{+0.038}_{-0.036}$	$0.98\,^{+0.12}_{-0.10}$	$2.39\,^{+0.13}_{-0.13}$
3.7	7.5 ± 0.8	< 1.0	2.7 ± 0.1	$2.778\,^{+0.415}_{-0.385}$	$1.906\,^{+0.036}_{-0.034}$	$0.97\,^{+0.11}_{-0.10}$	$2.24\,^{+0.11}_{-0.12}$
3.9	6.6 ± 0.7	< 1.0	2.2 ± 0.1	$3.000\,^{+0.476}_{-0.435}$	$2.111\,^{+0.050}_{-0.046}$	$1.06\,^{+0.14}_{-0.11}$	$2.16\,^{+0.10}_{-0.11}$
4.0	5.8 ± 0.7	< 1.0	1.9 ± 0.1	$3.053\,^{+0.558}_{-0.503}$	$2.272\,^{+0.062}_{-0.058}$	$1.16\,^{+0.17}_{-0.14}$	$2.08\,^{+0.11}_{-0.12}$
4.2	5.4 ± 0.6	< 1.0	3.3 ± 0.2	$1.636\,^{+0.299}_{-0.265}$	$1.724\,^{+0.055}_{-0.050}$	$0.92\,^{+0.16}_{-0.13}$	$1.88\,^{+0.11}_{-0.12}$
4.4	5.1 ± 0.6	< 1.0	3.7 ± 0.3	$1.378\,^{+0.298}_{-0.253}$	$1.628\,^{+0.070}_{-0.062}$	$0.87\,^{+0.18}_{-0.15}$	$1.79\,^{+0.12}_{-0.12}$

by Leroy et al. (2008). The columns with $\mathcal{A}$, $\mathcal{B}$, $Q_{\rm eff}$ and $\bar{Q}$ were derived in this thesis from the data provided by Leroy et al. (2008) with their methods and the methods described previously in this appendix and in Chapter 4.

The data from Leroy et al. (2008) had been approximated down to one decimal and were used like so to derive the parameters used in this thesis. The $\mathcal{B}$ and $\mathcal{A}$ parameters and corresponding errors were approximated to three decimals and the stability parameters with errors were approximated to two decimals as this was the resolution used in this thesis.

Table B.2: Radial profiles for the galaxy IC 2574 ($R_{25} = 7.5$ kpc).[1]

	From Leroy et al. (2008)			Our stability quantities			
R (kpc)	$\Sigma_{\rm HI}$ ($M_\odot {\rm pc}^{-2}$)	$\Sigma_{\rm H_2}$ ($M_\odot {\rm pc}^{-2}$)	$\Sigma_{\rm s}$ ($M_\odot {\rm pc}^{-2}$)	$\mathcal{A}$	$\mathcal{B}$	$Q_{\rm eff}$	$\bar{Q}$
0.1	10.3 ± 2.5	< 1.0	23.5 ± 0.8	$0.438^{+0.126}_{-0.117}$	$0.488^{+0.009}_{-0.008}$	$0.82^{+0.16}_{-0.13}$	$1.78^{+0.23}_{-0.22}$
0.3	10.7 ± 2.3	< 1.0	19.1 ± 0.3	$0.560^{+0.131}_{-0.127}$	$0.542^{+0.004}_{-0.004}$	$0.83^{+0.13}_{-0.10}$	$1.94^{+0.23}_{-0.22}$
0.5	10.7 ± 1.6	< 1.0	18.2 ± 0.2	$0.588^{+0.095}_{-0.093}$	$0.555^{+0.003}_{-0.003}$	$0.83^{+0.09}_{-0.07}$	$1.97^{+0.16}_{-0.16}$
0.7	9.6 ± 1.3	< 1.0	16.4 ± 0.2	$0.585^{+0.087}_{-0.085}$	$0.585^{+0.004}_{-0.004}$	$0.88^{+0.08}_{-0.07}$	$1.93^{+0.14}_{-0.14}$
0.9	8.2 ± 1.4	< 1.0	16.1 ± 0.2	$0.509^{+0.094}_{-0.092}$	$0.590^{+0.004}_{-0.004}$	$0.94^{+0.10}_{-0.09}$	$1.80^{+0.15}_{-0.15}$
1.1	7.7 ± 1.6	< 1.0	14.2 ± 0.1	$0.542^{+0.117}_{-0.116}$	$0.628^{+0.002}_{-0.002}$	$0.99^{+0.12}_{-0.10}$	$1.81^{+0.18}_{-0.18}$
1.3	8.0 ± 1.7	< 1.0	13.0 ± 0.1	$0.615^{+0.137}_{-0.134}$	$0.657^{+0.003}_{-0.003}$	$0.98^{+0.13}_{-0.10}$	$1.90^{+0.20}_{-0.20}$
1.5	8.5 ± 1.7	< 1.0	13.0 ± 0.2	$0.654^{+0.143}_{-0.139}$	$0.657^{+0.005}_{-0.005}$	$0.94^{+0.13}_{-0.11}$	$1.95^{+0.21}_{-0.20}$
1.6	9.0 ± 1.4	< 1.0	11.0 ± 0.1	$0.818^{+0.136}_{-0.133}$	$0.714^{+0.003}_{-0.003}$	$0.94^{+0.10}_{-0.09}$	$2.12^{+0.18}_{-0.18}$
1.8	9.3 ± 1.1	< 1.0	9.6 ± 0.1	$0.969^{+0.126}_{-0.123}$	$0.764^{+0.004}_{-0.004}$	$0.94^{+0.09}_{-0.07}$	$2.25^{+0.16}_{-0.16}$
2.0	9.2 ± 1.2	< 1.0	8.2 ± 0.1	$1.122^{+0.162}_{-0.158}$	$0.827^{+0.005}_{-0.005}$	$0.96^{+0.10}_{-0.09}$	$2.35^{+0.19}_{-0.18}$
2.2	8.8 ± 1.2	< 1.0	8.3 ± 0.1	$1.060^{+0.159}_{-0.155}$	$0.822^{+0.005}_{-0.005}$	$0.98^{+0.10}_{-0.09}$	$2.28^{+0.18}_{-0.18}$
2.4	7.9 ± 1.1	< 1.0	8.0 ± 0.1	$0.988^{+0.152}_{-0.148}$	$0.837^{+0.005}_{-0.005}$	$1.03^{+0.11}_{-0.09}$	$2.17^{+0.17}_{-0.17}$
2.6	7.2 ± 1.1	< 1.0	9.5 ± 0.5	$0.758^{+0.164}_{-0.148}$	$0.768^{+0.021}_{-0.019}$	$1.04^{+0.19}_{-0.16}$	$1.97^{+0.18}_{-0.17}$
2.8	7.2 ± 1.2	< 1.0	7.0 ± 0.1	$1.029^{+0.189}_{-0.184}$	$0.895^{+0.006}_{-0.006}$	$1.10^{+0.14}_{-0.12}$	$2.15^{+0.20}_{-0.20}$
3.0	7.5 ± 1.3	< 1.0	6.8 ± 0.1	$1.103^{+0.210}_{-0.204}$	$0.908^{+0.007}_{-0.007}$	$1.07^{+0.14}_{-0.12}$	$2.21^{+0.22}_{-0.22}$
3.2	7.9 ± 1.3	< 1.0	5.2 ± 0.1	$1.519^{+0.285}_{-0.274}$	$1.038^{+0.010}_{-0.010}$	$1.09^{+0.16}_{-0.12}$	$2.46^{+0.23}_{-0.25}$
3.4	8.3 ± 1.3	< 1.0	6.9 ± 0.4	$1.203^{+0.274}_{-0.244}$	$0.901^{+0.027}_{-0.025}$	$0.99^{+0.22}_{-0.17}$	$2.33^{+0.26}_{-0.24}$
3.6	8.5 ± 1.1	< 1.0	4.5 ± 0.1	$1.889^{+0.293}_{-0.280}$	$1.116^{+0.013}_{-0.012}$	$1.07^{+0.13}_{-0.10}$	$2.65^{+0.19}_{-0.20}$
3.8	8.7 ± 1.1	< 1.0	4.8 ± 0.1	$1.813^{+0.273}_{-0.261}$	$1.081^{+0.011}_{-0.011}$	$1.03^{+0.12}_{-0.10}$	$2.65^{+0.19}_{-0.20}$
4.0	9.0 ± 1.0	< 1.0	3.9 ± 0.1	$2.308^{+0.324}_{-0.308}$	$1.199^{+0.016}_{-0.015}$	$1.06^{+0.12}_{-0.10}$	$2.81^{+0.17}_{-0.18}$
4.2	9.2 ± 0.9	< 1.0	4.1 ± 0.1	$2.244^{+0.281}_{-0.268}$	$1.169^{+0.015}_{-0.014}$	$1.02^{+0.10}_{-0.09}$	$2.81^{+0.15}_{-0.16}$
4.4	9.3 ± 0.9	< 1.0	3.6 ± 0.1	$2.583^{+0.331}_{-0.313}$	$1.248^{+0.018}_{-0.017}$	$1.05^{+0.11}_{-0.09}$	$2.89^{+0.15}_{-0.16}$

[1]This table continues in table B.3.

Table B.3: Radial profiles for the galaxy IC 2574 ($R_{25} = 7.5$ kpc).[2]

	From Leroy et al. (2008)			Our stability quantities			
R (kpc)	$\Sigma_{\rm HI}$ ($M_\odot {\rm pc}^{-2}$)	$\Sigma_{\rm H_2}$ ($M_\odot {\rm pc}^{-2}$)	$\Sigma_{\rm s}$ ($M_\odot {\rm pc}^{-2}$)	$\mathcal{A}$	$\mathcal{B}$	$Q_{\rm eff}$	$\bar{Q}$
4.6	9.4 ± 0.9	< 1.0	3.5 ± 0.0	$2.686^{+0.257}_{-0.257}$	$1.265^{+0.000}_{-0.000}$	$1.05^{+0.05}_{-0.05}$	$2.92^{+0.14}_{-0.14}$
4.8	9.5 ± 0.9	< 1.0	4.9 ± 0.1	$1.939^{+0.228}_{-0.219}$	$1.069^{+0.011}_{-0.011}$	$0.93^{+0.09}_{-0.07}$	$2.76^{+0.15}_{-0.16}$
4.9	9.7 ± 0.9	< 1.0	11.0 ± 1.6	$0.882^{+0.246}_{-0.183}$	$0.714^{+0.058}_{-0.047}$	$0.77^{+0.29}_{-0.21}$	$2.20^{+0.24}_{-0.20}$
5.1	10.1 ± 1.0	< 1.0	3.8 ± 0.1	$2.658^{+0.342}_{-0.325}$	$1.214^{+0.016}_{-0.016}$	$0.96^{+0.10}_{-0.08}$	$2.99^{+0.16}_{-0.17}$
5.3	10.4 ± 1.0	< 1.0	3.6 ± 0.1	$2.889^{+0.368}_{-0.348}$	$1.248^{+0.018}_{-0.017}$	$0.96^{+0.10}_{-0.08}$	$3.06^{+0.15}_{-0.16}$
5.5	10.4 ± 1.0	< 1.0	5.1 ± 0.4	$2.039^{+0.386}_{-0.330}$	$1.048^{+0.044}_{-0.039}$	$0.85^{+0.18}_{-0.14}$	$2.88^{+0.19}_{-0.20}$
5.7	10.2 ± 1.0	< 1.0	3.3 ± 0.1	$3.091^{+0.409}_{-0.385}$	$1.303^{+0.020}_{-0.019}$	$0.98^{+0.10}_{-0.09}$	$3.06^{+0.15}_{-0.16}$
5.9	9.6 ± 0.9	< 1.0	2.7 ± 0.0	$3.556^{+0.333}_{-0.333}$	$1.441^{+0.000}_{-0.000}$	$1.08^{+0.05}_{-0.04}$	$3.05^{+0.13}_{-0.14}$
6.1	8.6 ± 0.7	< 1.0	2.6 ± 0.1	$3.308^{+0.412}_{-0.382}$	$1.468^{+0.029}_{-0.027}$	$1.14^{+0.12}_{-0.11}$	$2.91^{+0.12}_{-0.13}$
6.3	8.0 ± 0.7	< 1.0	2.0 ± 0.0	$4.000^{+0.350}_{-0.350}$	$1.674^{+0.000}_{-0.000}$	$1.30^{+0.05}_{-0.05}$	$2.89^{+0.11}_{-0.12}$
6.5	7.7 ± 0.8	< 1.0	2.8 ± 0.1	$2.750^{+0.398}_{-0.371}$	$1.415^{+0.026}_{-0.025}$	$1.15^{+0.14}_{-0.11}$	$2.73^{+0.14}_{-0.15}$
6.7	7.5 ± 0.8	< 1.0	2.2 ± 0.1	$3.409^{+0.543}_{-0.496}$	$1.596^{+0.038}_{-0.035}$	$1.27^{+0.17}_{-0.14}$	$2.78^{+0.14}_{-0.15}$
6.9	7.3 ± 0.8	< 1.0	2.3 ± 0.2	$3.174^{+0.683}_{-0.574}$	$1.561^{+0.073}_{-0.064}$	$1.25^{+0.27}_{-0.21}$	$2.73^{+0.16}_{-0.17}$
7.1	6.9 ± 0.7	< 1.0	1.8 ± 0.0	$3.833^{+0.389}_{-0.389}$	$1.765^{+0.000}_{-0.000}$	$1.40^{+0.07}_{-0.06}$	$2.73^{+0.12}_{-0.13}$
7.3	6.5 ± 0.6	< 1.0	2.2 ± 0.1	$2.955^{+0.426}_{-0.389}$	$1.596^{+0.038}_{-0.035}$	$1.32^{+0.17}_{-0.14}$	$2.60^{+0.12}_{-0.13}$
7.5	6.0 ± 0.5	< 1.0	3.9 ± 0.5	$1.538^{+0.373}_{-0.288}$	$1.199^{+0.085}_{-0.070}$	$1.12^{+0.35}_{-0.26}$	$2.27^{+0.17}_{-0.17}$
7.7	5.7 ± 0.5	< 1.0	1.9 ± 0.1	$3.000^{+0.444}_{-0.400}$	$1.718^{+0.047}_{-0.043}$	$1.45^{+0.20}_{-0.17}$	$2.49^{+0.11}_{-0.12}$
7.9	5.6 ± 0.5	< 1.0	1.0 ± 0.0	$5.600^{+0.500}_{-0.500}$	$2.367^{+0.000}_{-0.000}$	$1.90^{+0.08}_{-0.07}$	$2.60^{+0.09}_{-0.10}$
8.0	5.4 ± 0.5	< 1.0	2.4 ± 0.2	$2.250^{+0.432}_{-0.365}$	$1.528^{+0.068}_{-0.060}$	$1.35^{+0.28}_{-0.22}$	$2.36^{+0.13}_{-0.14}$
8.2	5.2 ± 0.5	< 1.0	1.4 ± 0.1	$3.714^{+0.670}_{-0.581}$	$2.001^{+0.076}_{-0.068}$	$1.68^{+0.29}_{-0.23}$	$2.46^{+0.11}_{-0.12}$
8.4	4.9 ± 0.6	< 1.0	1.4 ± 0.0	$3.500^{+0.429}_{-0.429}$	$2.001^{+0.000}_{-0.000}$	$1.70^{+0.10}_{-0.08}$	$2.40^{+0.12}_{-0.13}$
8.6	4.5 ± 0.6	< 1.0	1.4 ± 0.0	$3.214^{+0.429}_{-0.429}$	$2.001^{+0.000}_{-0.000}$	$1.75^{+0.11}_{-0.09}$	$2.31^{+0.13}_{-0.14}$
8.8	4.0 ± 0.5	< 1.0	1.0 ± 0.1	$4.000^{+1.000}_{-0.818}$	$2.367^{+0.128}_{-0.110}$	$2.11^{+0.51}_{-0.39}$	$2.26^{+0.13}_{-0.14}$

[2]Continued from table B.2.

Table B.4: Radial profiles for the galaxy NGC 628 ($R_{25} = 10.4$ kpc).

	From Leroy et al. (2008)			Our stability quantities			
R (kpc)	$\Sigma_{\rm HI}$ ($M_\odot {\rm pc}^{-2}$)	$\Sigma_{\rm H_2}$ ($M_\odot {\rm pc}^{-2}$)	$\Sigma_{\rm s}$ ($M_\odot {\rm pc}^{-2}$)	$\mathcal{A}$	$\mathcal{B}$	$Q_{\rm eff}$	$\bar{Q}$
0.2	1.6 ± 0.3	22.7 ± 1.2	1209.4 ± 18.3	$0.020\,^{+0.002}_{-0.002}$	$0.065\,^{+0.000}_{-0.000}$	$4.53\,^{+0.12}_{-0.12}$	$1.04\,^{+0.00}_{-0.00}$
0.5	2.1 ± 0.3	20.2 ± 1.3	557.8 ± 4.8	$0.040\,^{+0.003}_{-0.003}$	$0.096\,^{+0.000}_{-0.000}$	$5.12\,^{+0.10}_{-0.10}$	$1.08\,^{+0.01}_{-0.01}$
0.9	2.6 ± 0.4	16.1 ± 1.2	313.6 ± 1.0	$0.060\,^{+0.005}_{-0.005}$	$0.128\,^{+0.000}_{-0.000}$	$5.06\,^{+0.08}_{-0.08}$	$1.12\,^{+0.01}_{-0.01}$
1.2	3.1 ± 0.4	12.7 ± 0.8	231.9 ± 0.5	$0.068\,^{+0.005}_{-0.005}$	$0.149\,^{+0.000}_{-0.000}$	$4.80\,^{+0.07}_{-0.07}$	$1.14\,^{+0.01}_{-0.01}$
1.6	3.7 ± 0.3	11.4 ± 1.1	194.3 ± 0.5	$0.078\,^{+0.007}_{-0.007}$	$0.162\,^{+0.000}_{-0.000}$	$4.15\,^{+0.08}_{-0.08}$	$1.16\,^{+0.02}_{-0.02}$
1.9	4.6 ± 0.3	11.1 ± 1.2	163.5 ± 0.7	$0.096\,^{+0.010}_{-0.010}$	$0.177\,^{+0.000}_{-0.000}$	$3.75\,^{+0.10}_{-0.09}$	$1.20\,^{+0.02}_{-0.02}$
2.3	5.3 ± 0.4	11.1 ± 1.7	143.9 ± 0.8	$0.114\,^{+0.015}_{-0.015}$	$0.189\,^{+0.001}_{-0.001}$	$3.23\,^{+0.13}_{-0.12}$	$1.25\,^{+0.04}_{-0.04}$
2.7	5.8 ± 0.5	10.6 ± 1.9	123.5 ± 0.5	$0.133\,^{+0.020}_{-0.020}$	$0.204\,^{+0.000}_{-0.000}$	$2.89\,^{+0.13}_{-0.13}$	$1.29\,^{+0.05}_{-0.05}$
3.0	6.1 ± 0.5	8.9 ± 1.5	107.5 ± 0.4	$0.140\,^{+0.019}_{-0.019}$	$0.218\,^{+0.000}_{-0.000}$	$2.75\,^{+0.12}_{-0.12}$	$1.30\,^{+0.05}_{-0.05}$
3.4	6.5 ± 0.5	7.2 ± 1.2	151.0 ± 10.5	$0.091\,^{+0.019}_{-0.016}$	$0.184\,^{+0.007}_{-0.006}$	$2.24\,^{+0.33}_{-0.29}$	$1.19\,^{+0.04}_{-0.04}$
3.7	7.3 ± 0.7	6.2 ± 1.5	81.6 ± 0.4	$0.165\,^{+0.028}_{-0.028}$	$0.250\,^{+0.001}_{-0.001}$	$2.45\,^{+0.15}_{-0.14}$	$1.36\,^{+0.07}_{-0.07}$
4.1	7.9 ± 0.8	5.9 ± 1.7	68.0 ± 0.4	$0.203\,^{+0.038}_{-0.038}$	$0.274\,^{+0.001}_{-0.001}$	$2.27\,^{+0.18}_{-0.17}$	$1.44\,^{+0.10}_{-0.09}$
4.4	8.1 ± 0.8	5.4 ± 1.5	61.6 ± 0.4	$0.219\,^{+0.039}_{-0.039}$	$0.288\,^{+0.001}_{-0.001}$	$2.17\,^{+0.17}_{-0.16}$	$1.48\,^{+0.10}_{-0.10}$
4.8	7.9 ± 0.9	4.3 ± 1.1	48.3 ± 0.2	$0.253\,^{+0.043}_{-0.042}$	$0.325\,^{+0.001}_{-0.001}$	$2.16\,^{+0.17}_{-0.15}$	$1.54\,^{+0.11}_{-0.10}$
5.1	8.2 ± 1.0	3.1 ± 0.8	41.8 ± 0.2	$0.270\,^{+0.045}_{-0.044}$	$0.350\,^{+0.001}_{-0.001}$	$2.15\,^{+0.17}_{-0.15}$	$1.56\,^{+0.11}_{-0.10}$
5.5	8.5 ± 1.0	2.1 ± 0.7	37.0 ± 0.2	$0.286\,^{+0.048}_{-0.047}$	$0.372\,^{+0.001}_{-0.001}$	$2.09\,^{+0.17}_{-0.15}$	$1.58\,^{+0.11}_{-0.11}$
5.8	8.6 ± 0.8	1.2 ± 0.5	33.2 ± 0.4	$0.295\,^{+0.043}_{-0.042}$	$0.393\,^{+0.002}_{-0.002}$	$2.09\,^{+0.17}_{-0.15}$	$1.58\,^{+0.09}_{-0.09}$
6.2	8.6 ± 0.7	< 1.0	37.0 ± 2.3	$0.232\,^{+0.036}_{-0.031}$	$0.372\,^{+0.012}_{-0.011}$	$2.00\,^{+0.30}_{-0.26}$	$1.46\,^{+0.07}_{-0.06}$
6.5	8.8 ± 0.6	< 1.0	52.9 ± 6.1	$0.166\,^{+0.035}_{-0.027}$	$0.311\,^{+0.020}_{-0.017}$	$1.74\,^{+0.43}_{-0.35}$	$1.34\,^{+0.07}_{-0.06}$
6.9	8.8 ± 0.5	< 1.0	19.5 ± 0.1	$0.451\,^{+0.028}_{-0.028}$	$0.512\,^{+0.001}_{-0.001}$	$2.03\,^{+0.07}_{-0.07}$	$1.78\,^{+0.05}_{-0.05}$
7.3	8.6 ± 0.5	< 1.0	18.9 ± 0.1	$0.455\,^{+0.029}_{-0.029}$	$0.520\,^{+0.001}_{-0.001}$	$1.95\,^{+0.07}_{-0.07}$	$1.78\,^{+0.05}_{-0.05}$
7.6	8.2 ± 0.6	< 1.0	18.7 ± 0.7	$0.439\,^{+0.050}_{-0.047}$	$0.523\,^{+0.010}_{-0.010}$	$1.92\,^{+0.20}_{-0.18}$	$1.75\,^{+0.08}_{-0.08}$
8.0	7.6 ± 0.6	< 1.0	12.9 ± 0.1	$0.589\,^{+0.051}_{-0.051}$	$0.630\,^{+0.002}_{-0.002}$	$2.03\,^{+0.11}_{-0.10}$	$1.88\,^{+0.08}_{-0.08}$
8.3	7.1 ± 0.6	< 1.0	17.6 ± 1.3	$0.403\,^{+0.069}_{-0.059}$	$0.539\,^{+0.021}_{-0.019}$	$1.89\,^{+0.35}_{-0.29}$	$1.67\,^{+0.10}_{-0.09}$
8.7	6.7 ± 0.5	< 1.0	17.0 ± 1.6	$0.394\,^{+0.073}_{-0.061}$	$0.549\,^{+0.028}_{-0.024}$	$1.87\,^{+0.41}_{-0.34}$	$1.65\,^{+0.10}_{-0.09}$
9.0	6.5 ± 0.4	< 1.0	10.8 ± 0.4	$0.602\,^{+0.062}_{-0.057}$	$0.688\,^{+0.013}_{-0.012}$	$2.02\,^{+0.20}_{-0.18}$	$1.84\,^{+0.07}_{-0.07}$
9.4	6.0 ± 0.5	< 1.0	8.0 ± 0.1	$0.750\,^{+0.073}_{-0.071}$	$0.800\,^{+0.005}_{-0.005}$	$2.15\,^{+0.14}_{-0.13}$	$1.93\,^{+0.08}_{-0.08}$
9.7	5.2 ± 0.4	< 1.0	7.5 ± 0.2	$0.693\,^{+0.074}_{-0.070}$	$0.826\,^{+0.011}_{-0.011}$	$2.26\,^{+0.19}_{-0.18}$	$1.83\,^{+0.08}_{-0.08}$
10.1	4.5 ± 0.4	< 1.0	5.0 ± 0.1	$0.900\,^{+0.100}_{-0.096}$	$1.012\,^{+0.010}_{-0.010}$	$2.58\,^{+0.21}_{-0.19}$	$1.89\,^{+0.09}_{-0.09}$
10.4	4.1 ± 0.3	< 1.0	4.1 ± 0.0	$1.000\,^{+0.073}_{-0.073}$	$1.117\,^{+0.000}_{-0.000}$	$2.76\,^{+0.10}_{-0.09}$	$1.89\,^{+0.07}_{-0.07}$
10.8	3.9 ± 0.3	< 1.0	3.6 ± 0.0	$1.083\,^{+0.083}_{-0.083}$	$1.192\,^{+0.000}_{-0.000}$	$2.83\,^{+0.11}_{-0.10}$	$1.90\,^{+0.07}_{-0.07}$
11.1	3.9 ± 0.4	< 1.0	3.9 ± 0.1	$1.000\,^{+0.132}_{-0.125}$	$1.145\,^{+0.015}_{-0.014}$	$2.69\,^{+0.26}_{-0.23}$	$1.87\,^{+0.10}_{-0.10}$
11.5	4.0 ± 0.4	< 1.0	4.4 ± 0.2	$0.909\,^{+0.139}_{-0.126}$	$1.078\,^{+0.025}_{-0.024}$	$2.48\,^{+0.33}_{-0.29}$	$1.84\,^{+0.11}_{-0.10}$
11.9	4.3 ± 0.5	< 1.0	9.5 ± 0.9	$0.453\,^{+0.106}_{-0.087}$	$0.734\,^{+0.037}_{-0.032}$	$1.88\,^{+0.44}_{-0.35}$	$1.60\,^{+0.11}_{-0.10}$
12.2	4.6 ± 0.5	< 1.0	5.8 ± 0.2	$0.793\,^{+0.118}_{-0.110}$	$0.939\,^{+0.017}_{-0.016}$	$2.03\,^{+0.24}_{-0.21}$	$1.84\,^{+0.11}_{-0.10}$

Table B.5: Radial profiles for the galaxy NGC 3184 ($R_{25} = 11.9$ kpc).

	From Leroy et al. (2008)			Our stability quantities			
R (kpc)	$\Sigma_{\rm HI}$ ($M_\odot {\rm pc}^{-2}$)	$\Sigma_{\rm H_2}$ ($M_\odot {\rm pc}^{-2}$)	$\Sigma_{\rm s}$ ($M_\odot {\rm pc}^{-2}$)	$\mathcal{A}$	$\mathcal{B}$	$Q_{\rm eff}$	$\bar{Q}$
0.3	3.7 ± 0.5	44.2 ± 9.6	701.8 ± 22.8	$0.068^{+0.017}_{-0.016}$	$0.084^{+0.001}_{-0.001}$	$1.68^{+0.14}_{-0.14}$	$1.15^{+0.04}_{-0.04}$
0.8	3.2 ± 0.3	20.8 ± 3.3	270.5 ± 1.1	$0.089^{+0.014}_{-0.014}$	$0.135^{+0.000}_{-0.000}$	$2.33^{+0.08}_{-0.08}$	$1.19^{+0.03}_{-0.03}$
1.3	3.3 ± 0.3	14.5 ± 2.0	200.3 ± 0.6	$0.089^{+0.012}_{-0.012}$	$0.156^{+0.000}_{-0.000}$	$2.44^{+0.07}_{-0.07}$	$1.19^{+0.03}_{-0.03}$
1.9	3.8 ± 0.3	11.9 ± 1.6	146.5 ± 1.0	$0.107^{+0.014}_{-0.014}$	$0.183^{+0.001}_{-0.001}$	$2.45^{+0.09}_{-0.09}$	$1.23^{+0.03}_{-0.03}$
2.4	4.7 ± 0.5	12.6 ± 2.0	121.1 ± 0.5	$0.143^{+0.021}_{-0.021}$	$0.201^{+0.000}_{-0.000}$	$2.28^{+0.11}_{-0.11}$	$1.32^{+0.06}_{-0.05}$
3.0	5.5 ± 0.4	12.6 ± 2.1	113.0 ± 0.4	$0.160^{+0.023}_{-0.023}$	$0.208^{+0.000}_{-0.000}$	$2.04^{+0.11}_{-0.10}$	$1.36^{+0.07}_{-0.06}$
3.5	5.7 ± 0.4	11.0 ± 2.1	100.2 ± 0.4	$0.167^{+0.026}_{-0.026}$	$0.221^{+0.000}_{-0.000}$	$1.96^{+0.11}_{-0.11}$	$1.37^{+0.07}_{-0.07}$
4.0	5.9 ± 0.5	9.6 ± 1.9	94.2 ± 0.5	$0.165^{+0.026}_{-0.026}$	$0.228^{+0.001}_{-0.001}$	$1.86^{+0.11}_{-0.11}$	$1.36^{+0.07}_{-0.07}$
4.6	6.5 ± 0.4	7.4 ± 1.0	83.6 ± 0.3	$0.166^{+0.017}_{-0.017}$	$0.242^{+0.000}_{-0.000}$	$1.79^{+0.07}_{-0.07}$	$1.36^{+0.05}_{-0.04}$
5.1	7.3 ± 0.3	6.2 ± 0.6	74.6 ± 0.3	$0.181^{+0.013}_{-0.013}$	$0.256^{+0.001}_{-0.001}$	$1.71^{+0.05}_{-0.05}$	$1.40^{+0.03}_{-0.03}$
5.7	7.5 ± 0.5	5.5 ± 0.9	96.2 ± 6.1	$0.135^{+0.025}_{-0.022}$	$0.226^{+0.008}_{-0.007}$	$1.49^{+0.22}_{-0.19}$	$1.29^{+0.06}_{-0.05}$
6.2	7.8 ± 0.6	4.3 ± 0.8	61.2 ± 0.3	$0.198^{+0.024}_{-0.024}$	$0.283^{+0.001}_{-0.001}$	$1.57^{+0.08}_{-0.08}$	$1.43^{+0.06}_{-0.06}$
6.7	8.1 ± 0.6	2.7 ± 0.5	46.3 ± 0.2	$0.233^{+0.025}_{-0.025}$	$0.325^{+0.001}_{-0.001}$	$1.61^{+0.08}_{-0.07}$	$1.49^{+0.06}_{-0.06}$
7.3	8.0 ± 0.5	1.3 ± 0.3	34.6 ± 0.1	$0.269^{+0.024}_{-0.024}$	$0.376^{+0.001}_{-0.001}$	$1.67^{+0.07}_{-0.06}$	$1.54^{+0.05}_{-0.05}$
7.8	7.3 ± 0.3	< 1.0	27.5 ± 0.1	$0.265^{+0.012}_{-0.012}$	$0.422^{+0.001}_{-0.001}$	$1.81^{+0.04}_{-0.04}$	$1.50^{+0.02}_{-0.02}$
8.3	7.0 ± 0.3	< 1.0	22.4 ± 0.1	$0.313^{+0.015}_{-0.015}$	$0.468^{+0.001}_{-0.001}$	$1.81^{+0.04}_{-0.04}$	$1.56^{+0.03}_{-0.03}$
8.9	7.0 ± 0.3	< 1.0	19.3 ± 0.2	$0.363^{+0.020}_{-0.019}$	$0.504^{+0.003}_{-0.003}$	$1.74^{+0.06}_{-0.06}$	$1.63^{+0.03}_{-0.03}$
9.4	6.7 ± 0.3	< 1.0	14.9 ± 0.1	$0.450^{+0.023}_{-0.023}$	$0.574^{+0.002}_{-0.002}$	$1.78^{+0.06}_{-0.05}$	$1.72^{+0.04}_{-0.04}$
10.0	6.1 ± 0.2	< 1.0	12.9 ± 0.3	$0.473^{+0.027}_{-0.026}$	$0.617^{+0.007}_{-0.007}$	$1.80^{+0.10}_{-0.10}$	$1.72^{+0.04}_{-0.03}$
10.5	5.4 ± 0.2	< 1.0	9.5 ± 0.1	$0.568^{+0.027}_{-0.027}$	$0.718^{+0.004}_{-0.004}$	$1.94^{+0.07}_{-0.07}$	$1.77^{+0.03}_{-0.03}$
11.0	5.0 ± 0.3	< 1.0	7.9 ± 0.1	$0.633^{+0.047}_{-0.045}$	$0.788^{+0.005}_{-0.005}$	$2.00^{+0.10}_{-0.09}$	$1.79^{+0.05}_{-0.05}$
11.6	4.6 ± 0.3	< 1.0	6.6 ± 0.1	$0.697^{+0.057}_{-0.055}$	$0.862^{+0.007}_{-0.006}$	$2.05^{+0.12}_{-0.11}$	$1.80^{+0.06}_{-0.06}$
12.1	4.0 ± 0.2	< 1.0	5.1 ± 0.1	$0.784^{+0.056}_{-0.054}$	$0.981^{+0.010}_{-0.009}$	$2.24^{+0.13}_{-0.12}$	$1.80^{+0.05}_{-0.05}$
12.6	3.3 ± 0.2	< 1.0	4.7 ± 0.1	$0.702^{+0.059}_{-0.056}$	$1.021^{+0.011}_{-0.011}$	$2.39^{+0.15}_{-0.14}$	$1.69^{+0.05}_{-0.05}$
13.2	2.9 ± 0.2	< 1.0	3.7 ± 0.1	$0.784^{+0.077}_{-0.073}$	$1.151^{+0.016}_{-0.015}$	$2.58^{+0.20}_{-0.18}$	$1.68^{+0.06}_{-0.05}$
13.7	2.8 ± 0.2	< 1.0	3.0 ± 0.0	$0.933^{+0.067}_{-0.067}$	$1.279^{+0.000}_{-0.000}$	$2.70^{+0.08}_{-0.08}$	$1.72^{+0.05}_{-0.05}$
14.3	2.7 ± 0.2	< 1.0	3.8 ± 0.1	$0.711^{+0.073}_{-0.070}$	$1.136^{+0.015}_{-0.015}$	$2.43^{+0.18}_{-0.17}$	$1.62^{+0.05}_{-0.05}$

Table B.6: Radial profiles for the galaxy NGC 3198 ($R_{25} = 13.0$ kpc).

	From Leroy et al. (2008)			Our stability quantities			
R (kpc)	$\Sigma_{\rm HI}$ ($M_\odot {\rm pc}^{-2}$)	$\Sigma_{\rm H_2}$ ($M_\odot {\rm pc}^{-2}$)	$\Sigma_{\rm s}$ ($M_\odot {\rm pc}^{-2}$)	$\mathcal{A}$	$\mathcal{B}$	$Q_{\rm eff}$	$\bar{Q}$
0.3	4.0 ± 0.6	20.4 ± 9.1	503.1 ± 35.7	$0.048\,^{+0.024}_{-0.021}$	$0.086\,^{+0.003}_{-0.003}$	$1.70\,^{+0.27}_{-0.24}$	$1.10\,^{+0.06}_{-0.05}$
1.0	3.3 ± 0.3	7.0 ± 3.1	164.2 ± 2.4	$0.063\,^{+0.022}_{-0.021}$	$0.150\,^{+0.001}_{-0.001}$	$2.49\,^{+0.16}_{-0.16}$	$1.13\,^{+0.05}_{-0.05}$
1.7	3.6 ± 0.3	2.5 ± 0.9	105.0 ± 1.0	$0.058\,^{+0.012}_{-0.012}$	$0.187\,^{+0.001}_{-0.001}$	$2.73\,^{+0.10}_{-0.10}$	$1.12\,^{+0.03}_{-0.03}$
2.3	4.1 ± 0.2	1.7 ± 0.6	84.6 ± 0.7	$0.069\,^{+0.010}_{-0.010}$	$0.209\,^{+0.001}_{-0.001}$	$2.64\,^{+0.08}_{-0.08}$	$1.14\,^{+0.02}_{-0.02}$
3.0	4.9 ± 0.5	2.6 ± 0.7	77.2 ± 0.4	$0.097\,^{+0.016}_{-0.016}$	$0.218\,^{+0.001}_{-0.001}$	$2.30\,^{+0.09}_{-0.09}$	$1.20\,^{+0.04}_{-0.04}$
3.7	5.9 ± 0.5	3.7 ± 0.8	71.8 ± 0.4	$0.134\,^{+0.019}_{-0.019}$	$0.226\,^{+0.001}_{-0.001}$	$1.97\,^{+0.09}_{-0.09}$	$1.29\,^{+0.05}_{-0.04}$
4.3	6.2 ± 0.4	3.9 ± 0.9	62.7 ± 0.4	$0.161\,^{+0.022}_{-0.022}$	$0.242\,^{+0.001}_{-0.001}$	$1.81\,^{+0.09}_{-0.09}$	$1.35\,^{+0.06}_{-0.05}$
5.0	6.3 ± 0.3	3.1 ± 0.6	54.2 ± 0.3	$0.173\,^{+0.018}_{-0.017}$	$0.261\,^{+0.001}_{-0.001}$	$1.70\,^{+0.07}_{-0.07}$	$1.37\,^{+0.05}_{-0.04}$
5.7	6.5 ± 0.3	2.1 ± 0.4	45.0 ± 0.2	$0.191\,^{+0.016}_{-0.016}$	$0.286\,^{+0.001}_{-0.001}$	$1.64\,^{+0.06}_{-0.06}$	$1.41\,^{+0.04}_{-0.04}$
6.4	6.6 ± 0.4	1.2 ± 0.3	34.8 ± 0.2	$0.224\,^{+0.022}_{-0.021}$	$0.325\,^{+0.001}_{-0.001}$	$1.62\,^{+0.07}_{-0.07}$	$1.47\,^{+0.05}_{-0.05}$
7.0	6.6 ± 0.4	< 1.0	28.3 ± 0.2	$0.233\,^{+0.016}_{-0.016}$	$0.361\,^{+0.001}_{-0.001}$	$1.66\,^{+0.06}_{-0.06}$	$1.47\,^{+0.03}_{-0.03}$
7.7	6.7 ± 0.5	< 1.0	21.4 ± 0.1	$0.313\,^{+0.025}_{-0.025}$	$0.415\,^{+0.001}_{-0.001}$	$1.60\,^{+0.06}_{-0.06}$	$1.60\,^{+0.05}_{-0.05}$
8.4	6.8 ± 0.5	< 1.0	17.7 ± 0.1	$0.384\,^{+0.031}_{-0.030}$	$0.456\,^{+0.001}_{-0.001}$	$1.51\,^{+0.07}_{-0.06}$	$1.71\,^{+0.06}_{-0.06}$
9.0	7.0 ± 0.5	< 1.0	14.8 ± 0.1	$0.473\,^{+0.037}_{-0.037}$	$0.499\,^{+0.002}_{-0.002}$	$1.44\,^{+0.07}_{-0.07}$	$1.84\,^{+0.07}_{-0.07}$
9.7	6.9 ± 0.5	< 1.0	12.2 ± 0.1	$0.566\,^{+0.046}_{-0.045}$	$0.549\,^{+0.002}_{-0.002}$	$1.39\,^{+0.07}_{-0.07}$	$1.94\,^{+0.08}_{-0.08}$
10.4	6.4 ± 0.4	< 1.0	10.3 ± 0.1	$0.621\,^{+0.045}_{-0.044}$	$0.598\,^{+0.003}_{-0.003}$	$1.39\,^{+0.07}_{-0.07}$	$1.97\,^{+0.07}_{-0.07}$
11.0	6.0 ± 0.3	< 1.0	8.2 ± 0.0	$0.732\,^{+0.037}_{-0.037}$	$0.670\,^{+0.000}_{-0.000}$	$1.41\,^{+0.04}_{-0.04}$	$2.05\,^{+0.05}_{-0.05}$
11.7	6.3 ± 0.4	< 1.0	7.3 ± 0.1	$0.863\,^{+0.068}_{-0.066}$	$0.710\,^{+0.005}_{-0.005}$	$1.32\,^{+0.08}_{-0.08}$	$2.18\,^{+0.09}_{-0.09}$
12.4	6.4 ± 0.4	< 1.0	5.9 ± 0.0	$1.085\,^{+0.068}_{-0.068}$	$0.790\,^{+0.000}_{-0.000}$	$1.28\,^{+0.05}_{-0.04}$	$2.36\,^{+0.09}_{-0.09}$
13.0	5.9 ± 0.3	< 1.0	4.5 ± 0.0	$1.311\,^{+0.067}_{-0.067}$	$0.904\,^{+0.000}_{-0.000}$	$1.34\,^{+0.04}_{-0.04}$	$2.45\,^{+0.07}_{-0.07}$
13.7	5.1 ± 0.3	< 1.0	3.3 ± 0.0	$1.545\,^{+0.091}_{-0.091}$	$1.056\,^{+0.000}_{-0.000}$	$1.48\,^{+0.05}_{-0.05}$	$2.46\,^{+0.08}_{-0.08}$
14.4	4.6 ± 0.4	< 1.0	3.5 ± 0.1	$1.314\,^{+0.156}_{-0.148}$	$1.025\,^{+0.015}_{-0.014}$	$1.47\,^{+0.16}_{-0.14}$	$2.28\,^{+0.13}_{-0.13}$
15.1	4.2 ± 0.4	< 1.0	2.5 ± 0.1	$1.680\,^{+0.237}_{-0.218}$	$1.213\,^{+0.025}_{-0.024}$	$1.61\,^{+0.21}_{-0.17}$	$2.36\,^{+0.14}_{-0.14}$

Table B.7: Radial profiles for the galaxy NGC 3521 ($R_{25} = 12.9$ kpc).

	From Leroy et al. (2008)			Our stability quantities			
R (kpc)	$\Sigma_{\rm HI}$ ($M_\odot {\rm pc}^{-2}$)	$\Sigma_{\rm H_2}$ ($M_\odot {\rm pc}^{-2}$)	$\Sigma_{\rm s}$ ($M_\odot {\rm pc}^{-2}$)	$\mathcal{A}$	$\mathcal{B}$	$Q_{\rm eff}$	$\bar{Q}$
0.3	4.5 ± 0.2	25.7 ± 4.7	4545.9 ± 287.3	$0.007\,^{+0.002}_{-0.001}$	$0.030\,^{+0.001}_{-0.001}$	$1.65\,^{+0.17}_{-0.15}$	$1.01\,^{+0.00}_{-0.00}$
0.8	4.8 ± 0.3	35.4 ± 5.5	1442.2 ± 23.0	$0.028\,^{+0.005}_{-0.004}$	$0.053\,^{+0.000}_{-0.000}$	$2.27\,^{+0.08}_{-0.07}$	$1.06\,^{+0.01}_{-0.01}$
1.3	5.7 ± 0.6	43.4 ± 3.0	929.8 ± 8.9	$0.053\,^{+0.004}_{-0.004}$	$0.066\,^{+0.000}_{-0.000}$	$2.21\,^{+0.05}_{-0.05}$	$1.11\,^{+0.01}_{-0.01}$
1.8	7.1 ± 0.7	44.6 ± 1.5	589.1 ± 5.4	$0.088\,^{+0.005}_{-0.004}$	$0.083\,^{+0.000}_{-0.000}$	$2.08\,^{+0.12}_{-0.11}$	$1.24\,^{+0.05}_{-0.05}$
2.3	8.3 ± 0.8	41.5 ± 2.1	462.9 ± 2.9	$0.108\,^{+0.007}_{-0.007}$	$0.094\,^{+0.000}_{-0.000}$	$1.81\,^{+0.12}_{-0.11}$	$1.35\,^{+0.07}_{-0.07}$
2.9	8.7 ± 0.8	36.8 ± 2.7	381.3 ± 2.0	$0.119\,^{+0.010}_{-0.010}$	$0.103\,^{+0.000}_{-0.000}$	$1.63\,^{+0.13}_{-0.11}$	$1.38\,^{+0.09}_{-0.09}$
3.4	8.7 ± 0.6	30.6 ± 2.6	322.9 ± 1.9	$0.122\,^{+0.011}_{-0.011}$	$0.112\,^{+0.000}_{-0.000}$	$1.59\,^{+0.12}_{-0.11}$	$1.33\,^{+0.09}_{-0.08}$
3.9	8.9 ± 0.8	24.6 ± 2.3	250.8 ± 1.8	$0.134\,^{+0.013}_{-0.013}$	$0.127\,^{+0.000}_{-0.000}$	$1.58\,^{+0.10}_{-0.12}$	$1.34\,^{+0.10}_{-0.07}$
4.4	9.9 ± 0.9	22.2 ± 2.0	212.3 ± 1.4	$0.151\,^{+0.015}_{-0.015}$	$0.138\,^{+0.000}_{-0.000}$	$1.45\,^{+0.12}_{-0.11}$	$1.41\,^{+0.10}_{-0.09}$
4.9	10.6 ± 0.6	21.0 ± 2.1	192.2 ± 1.3	$0.164\,^{+0.015}_{-0.015}$	$0.145\,^{+0.000}_{-0.000}$	$1.32\,^{+0.11}_{-0.09}$	$1.46\,^{+0.10}_{-0.09}$
5.4	10.5 ± 0.5	17.5 ± 2.4	169.7 ± 1.1	$0.165\,^{+0.018}_{-0.018}$	$0.155\,^{+0.001}_{-0.000}$	$1.31\,^{+0.09}_{-0.10}$	$1.43\,^{+0.11}_{-0.08}$
6.0	10.2 ± 0.4	12.5 ± 2.5	134.7 ± 1.0	$0.169\,^{+0.023}_{-0.023}$	$0.174\,^{+0.001}_{-0.001}$	$1.34\,^{+0.08}_{-0.11}$	$1.40\,^{+0.10}_{-0.07}$
6.5	10.2 ± 0.5	8.4 ± 2.0	106.7 ± 0.8	$0.174\,^{+0.025}_{-0.025}$	$0.195\,^{+0.001}_{-0.001}$	$1.38\,^{+0.09}_{-0.09}$	$1.41\,^{+0.09}_{-0.07}$
7.0	9.4 ± 0.3	5.2 ± 1.4	82.4 ± 0.7	$0.177\,^{+0.022}_{-0.022}$	$0.222\,^{+0.001}_{-0.001}$	$1.46\,^{+0.08}_{-0.08}$	$1.40\,^{+0.07}_{-0.06}$
7.5	8.6 ± 0.4	3.2 ± 0.9	66.1 ± 0.6	$0.179\,^{+0.021}_{-0.021}$	$0.248\,^{+0.001}_{-0.001}$	$1.53\,^{+0.08}_{-0.08}$	$1.39\,^{+0.06}_{-0.05}$
8.0	8.4 ± 0.5	2.1 ± 0.6	55.4 ± 0.5	$0.190\,^{+0.022}_{-0.021}$	$0.271\,^{+0.001}_{-0.001}$	$1.55\,^{+0.08}_{-0.08}$	$1.41\,^{+0.06}_{-0.05}$
8.6	8.5 ± 0.5	1.7 ± 0.5	47.7 ± 0.4	$0.214\,^{+0.023}_{-0.023}$	$0.292\,^{+0.001}_{-0.001}$	$1.50\,^{+0.08}_{-0.08}$	$1.46\,^{+0.06}_{-0.06}$
9.1	8.6 ± 0.5	1.6 ± 0.5	41.7 ± 0.3	$0.245\,^{+0.026}_{-0.026}$	$0.312\,^{+0.001}_{-0.001}$	$1.45\,^{+0.08}_{-0.07}$	$1.53\,^{+0.07}_{-0.06}$
9.6	8.5 ± 0.6	1.2 ± 0.4	35.8 ± 0.3	$0.271\,^{+0.030}_{-0.030}$	$0.337\,^{+0.001}_{-0.001}$	$1.44\,^{+0.09}_{-0.08}$	$1.57\,^{+0.07}_{-0.07}$
10.1	8.2 ± 0.6	< 1.0	30.5 ± 0.2	$0.269\,^{+0.022}_{-0.021}$	$0.365\,^{+0.001}_{-0.001}$	$1.50\,^{+0.06}_{-0.06}$	$1.54\,^{+0.05}_{-0.05}$
10.6	8.1 ± 0.7	< 1.0	27.1 ± 0.2	$0.299\,^{+0.028}_{-0.028}$	$0.387\,^{+0.001}_{-0.001}$	$1.47\,^{+0.07}_{-0.07}$	$1.59\,^{+0.06}_{-0.06}$
11.2	8.1 ± 0.8	< 1.0	25.4 ± 0.2	$0.319\,^{+0.034}_{-0.034}$	$0.400\,^{+0.002}_{-0.002}$	$1.41\,^{+0.08}_{-0.08}$	$1.63\,^{+0.07}_{-0.07}$
11.7	8.2 ± 0.9	< 1.0	22.9 ± 0.2	$0.358\,^{+0.043}_{-0.042}$	$0.421\,^{+0.002}_{-0.002}$	$1.37\,^{+0.09}_{-0.09}$	$1.69\,^{+0.09}_{-0.09}$
12.2	8.3 ± 0.9	< 1.0	20.0 ± 0.2	$0.415\,^{+0.050}_{-0.049}$	$0.450\,^{+0.002}_{-0.002}$	$1.33\,^{+0.10}_{-0.09}$	$1.78\,^{+0.10}_{-0.10}$
12.7	8.2 ± 0.9	< 1.0	17.4 ± 0.1	$0.471\,^{+0.055}_{-0.054}$	$0.483\,^{+0.001}_{-0.001}$	$1.32\,^{+0.09}_{-0.08}$	$1.85\,^{+0.10}_{-0.10}$
13.2	8.0 ± 0.9	< 1.0	15.7 ± 0.1	$0.510\,^{+0.061}_{-0.060}$	$0.508\,^{+0.002}_{-0.002}$	$1.31\,^{+0.09}_{-0.08}$	$1.89\,^{+0.11}_{-0.11}$
13.7	7.9 ± 1.0	< 1.0	14.4 ± 0.1	$0.549\,^{+0.074}_{-0.073}$	$0.531\,^{+0.002}_{-0.002}$	$1.29\,^{+0.11}_{-0.09}$	$1.94\,^{+0.13}_{-0.13}$
14.3	7.7 ± 0.9	< 1.0	13.3 ± 0.1	$0.579\,^{+0.073}_{-0.071}$	$0.552\,^{+0.002}_{-0.002}$	$1.27\,^{+0.10}_{-0.09}$	$1.96\,^{+0.12}_{-0.12}$
14.8	7.1 ± 0.8	< 1.0	12.0 ± 0.1	$0.592\,^{+0.072}_{-0.071}$	$0.582\,^{+0.002}_{-0.002}$	$1.30\,^{+0.10}_{-0.09}$	$1.95\,^{+0.12}_{-0.11}$
15.3	6.5 ± 0.6	< 1.0	10.9 ± 0.1	$0.596\,^{+0.061}_{-0.060}$	$0.610\,^{+0.003}_{-0.003}$	$1.34\,^{+0.09}_{-0.08}$	$1.92\,^{+0.09}_{-0.09}$

Table B.8: Radial profiles for the galaxy NGC 5055 ($R_{25} = 17.4$ kpc).

	From Leroy et al. (2008)			Our stability quantities			
R (kpc)	$\Sigma_{\rm HI}$ ($M_\odot {\rm pc}^{-2}$)	$\Sigma_{\rm H_2}$ ($M_\odot {\rm pc}^{-2}$)	$\Sigma_{\rm s}$ ($M_\odot {\rm pc}^{-2}$)	$\mathcal{A}$	$\mathcal{B}$	$Q_{\rm eff}$	$\bar{Q}$
0.2	5.6 ± 0.7	142.7 ± 19.4	4742.4 ± 251.1	$0.031^{+0.006}_{-0.006}$	$0.028^{+0.001}_{-0.001}$	$2.32^{+0.50}_{-0.47}$	$1.18^{+0.19}_{-0.13}$
0.7	5.8 ± 0.5	98.8 ± 16.1	1627.7 ± 11.4	$0.064^{+0.011}_{-0.011}$	$0.048^{+0.000}_{-0.000}$	$2.16^{+0.41}_{-0.30}$	$1.45^{+0.22}_{-0.22}$
1.2	5.9 ± 0.4	62.2 ± 8.5	987.4 ± 4.6	$0.069^{+0.009}_{-0.009}$	$0.061^{+0.000}_{-0.000}$	$2.27^{+0.28}_{-0.26}$	$1.26^{+0.15}_{-0.13}$
1.7	5.9 ± 0.2	43.7 ± 3.9	758.0 ± 2.2	$0.065^{+0.006}_{-0.006}$	$0.070^{+0.000}_{-0.000}$	$2.14^{+0.03}_{-0.06}$	$1.14^{+0.03}_{-0.01}$
2.2	6.2 ± 0.3	36.6 ± 2.3	569.7 ± 1.7	$0.075^{+0.005}_{-0.005}$	$0.080^{+0.000}_{-0.000}$	$1.90^{+0.03}_{-0.03}$	$1.16^{+0.01}_{-0.01}$
2.7	6.6 ± 0.4	32.1 ± 2.5	417.9 ± 1.1	$0.093^{+0.007}_{-0.007}$	$0.094^{+0.000}_{-0.000}$	$1.75^{+0.03}_{-0.09}$	$1.20^{+0.06}_{-0.02}$
3.2	6.4 ± 0.4	25.3 ± 2.7	325.4 ± 0.9	$0.097^{+0.010}_{-0.010}$	$0.106^{+0.000}_{-0.000}$	$1.65^{+0.04}_{-0.05}$	$1.22^{+0.03}_{-0.02}$
3.7	6.2 ± 0.5	20.3 ± 2.3	264.3 ± 0.8	$0.100^{+0.011}_{-0.011}$	$0.118^{+0.000}_{-0.000}$	$1.57^{+0.04}_{-0.04}$	$1.22^{+0.03}_{-0.03}$
4.2	6.5 ± 0.5	19.1 ± 2.1	230.7 ± 0.7	$0.111^{+0.012}_{-0.012}$	$0.126^{+0.000}_{-0.000}$	$1.45^{+0.04}_{-0.04}$	$1.25^{+0.03}_{-0.03}$
4.7	7.2 ± 0.6	18.6 ± 2.1	194.9 ± 0.5	$0.132^{+0.014}_{-0.014}$	$0.137^{+0.000}_{-0.000}$	$1.35^{+0.05}_{-0.08}$	$1.30^{+0.08}_{-0.04}$
5.1	8.2 ± 0.7	18.8 ± 2.1	169.5 ± 0.4	$0.159^{+0.017}_{-0.017}$	$0.147^{+0.000}_{-0.000}$	$1.22^{+0.09}_{-0.09}$	$1.42^{+0.11}_{-0.09}$
5.6	8.7 ± 0.5	17.3 ± 1.8	150.6 ± 0.4	$0.173^{+0.016}_{-0.016}$	$0.156^{+0.000}_{-0.000}$	$1.14^{+0.08}_{-0.07}$	$1.46^{+0.09}_{-0.09}$
6.1	8.7 ± 0.5	13.4 ± 1.1	133.4 ± 0.4	$0.166^{+0.013}_{-0.012}$	$0.166^{+0.000}_{-0.000}$	$1.17^{+0.04}_{-0.06}$	$1.40^{+0.06}_{-0.04}$
6.6	8.5 ± 0.6	10.9 ± 1.0	109.1 ± 0.3	$0.178^{+0.015}_{-0.015}$	$0.184^{+0.000}_{-0.000}$	$1.17^{+0.05}_{-0.05}$	$1.43^{+0.06}_{-0.05}$
7.1	8.5 ± 0.5	10.3 ± 1.0	94.0 ± 0.2	$0.200^{+0.016}_{-0.016}$	$0.198^{+0.000}_{-0.000}$	$1.12^{+0.05}_{-0.05}$	$1.49^{+0.07}_{-0.06}$
7.6	8.6 ± 0.5	10.0 ± 1.2	84.5 ± 0.3	$0.220^{+0.021}_{-0.021}$	$0.209^{+0.000}_{-0.000}$	$1.06^{+0.06}_{-0.06}$	$1.55^{+0.08}_{-0.08}$
8.1	8.5 ± 0.5	8.7 ± 1.3	75.3 ± 0.3	$0.228^{+0.025}_{-0.025}$	$0.221^{+0.000}_{-0.000}$	$1.04^{+0.07}_{-0.06}$	$1.57^{+0.09}_{-0.08}$
8.6	7.9 ± 0.4	6.2 ± 1.0	62.6 ± 0.1	$0.225^{+0.023}_{-0.023}$	$0.242^{+0.000}_{-0.000}$	$1.10^{+0.05}_{-0.05}$	$1.53^{+0.07}_{-0.07}$
9.1	7.5 ± 0.4	4.3 ± 0.8	52.0 ± 0.1	$0.227^{+0.024}_{-0.023}$	$0.266^{+0.000}_{-0.000}$	$1.16^{+0.05}_{-0.05}$	$1.51^{+0.07}_{-0.06}$
9.5	7.4 ± 0.5	3.1 ± 0.6	44.5 ± 0.1	$0.236^{+0.025}_{-0.025}$	$0.287^{+0.000}_{-0.000}$	$1.19^{+0.06}_{-0.06}$	$1.52^{+0.07}_{-0.07}$
10.0	7.2 ± 0.7	2.1 ± 0.5	40.8 ± 0.1	$0.228^{+0.030}_{-0.030}$	$0.300^{+0.000}_{-0.000}$	$1.21^{+0.07}_{-0.06}$	$1.49^{+0.08}_{-0.07}$
10.5	7.3 ± 0.8	1.5 ± 0.4	36.8 ± 0.1	$0.239^{+0.033}_{-0.033}$	$0.316^{+0.000}_{-0.000}$	$1.20^{+0.07}_{-0.07}$	$1.51^{+0.08}_{-0.08}$
11.0	7.5 ± 0.9	1.1 ± 0.4	33.4 ± 0.1	$0.257^{+0.040}_{-0.040}$	$0.332^{+0.000}_{-0.000}$	$1.17^{+0.08}_{-0.08}$	$1.54^{+0.10}_{-0.09}$
11.5	7.3 ± 0.7	< 1.0	60.4 ± 5.4	$0.121^{+0.025}_{-0.021}$	$0.247^{+0.012}_{-0.010}$	$1.03^{+0.19}_{-0.17}$	$1.25^{+0.06}_{-0.05}$
12.0	6.7 ± 0.5	< 1.0	59.2 ± 5.7	$0.113^{+0.021}_{-0.018}$	$0.249^{+0.013}_{-0.011}$	$1.01^{+0.20}_{-0.17}$	$1.23^{+0.05}_{-0.04}$
12.5	6.4 ± 0.5	< 1.0	24.8 ± 0.1	$0.258^{+0.021}_{-0.021}$	$0.385^{+0.001}_{-0.001}$	$1.23^{+0.05}_{-0.04}$	$1.51^{+0.05}_{-0.05}$
13.0	6.2 ± 0.5	< 1.0	21.2 ± 0.1	$0.292^{+0.025}_{-0.025}$	$0.417^{+0.001}_{-0.001}$	$1.23^{+0.05}_{-0.05}$	$1.56^{+0.05}_{-0.05}$
13.5	5.7 ± 0.5	< 1.0	18.7 ± 0.1	$0.305^{+0.029}_{-0.028}$	$0.443^{+0.001}_{-0.001}$	$1.26^{+0.06}_{-0.05}$	$1.56^{+0.06}_{-0.06}$
14.0	5.1 ± 0.4	< 1.0	17.3 ± 0.1	$0.295^{+0.025}_{-0.025}$	$0.461^{+0.001}_{-0.001}$	$1.29^{+0.05}_{-0.05}$	$1.53^{+0.05}_{-0.05}$
14.4	4.5 ± 0.4	< 1.0	18.0 ± 0.5	$0.250^{+0.030}_{-0.028}$	$0.452^{+0.006}_{-0.006}$	$1.30^{+0.11}_{-0.10}$	$1.45^{+0.05}_{-0.05}$
14.9	4.2 ± 0.5	< 1.0	13.8 ± 0.0	$0.304^{+0.036}_{-0.036}$	$0.516^{+0.000}_{-0.000}$	$1.37^{+0.06}_{-0.06}$	$1.51^{+0.06}_{-0.06}$
15.4	3.9 ± 0.6	< 1.0	13.2 ± 0.1	$0.295^{+0.048}_{-0.047}$	$0.528^{+0.002}_{-0.002}$	$1.38^{+0.10}_{-0.09}$	$1.49^{+0.08}_{-0.08}$
15.9	3.7 ± 0.5	< 1.0	11.8 ± 0.0	$0.314^{+0.042}_{-0.042}$	$0.558^{+0.000}_{-0.000}$	$1.40^{+0.07}_{-0.06}$	$1.50^{+0.07}_{-0.07}$
16.4	3.2 ± 0.4	< 1.0	10.7 ± 0.0	$0.299^{+0.037}_{-0.037}$	$0.586^{+0.000}_{-0.000}$	$1.46^{+0.06}_{-0.06}$	$1.46^{+0.06}_{-0.06}$
16.9	2.8 ± 0.4	< 1.0	9.8 ± 0.0	$0.286^{+0.041}_{-0.041}$	$0.613^{+0.000}_{-0.000}$	$1.52^{+0.07}_{-0.06}$	$1.43^{+0.06}_{-0.06}$
17.4	2.6 ± 0.4	< 1.0	9.2 ± 0.0	$0.283^{+0.043}_{-0.043}$	$0.632^{+0.000}_{-0.000}$	$1.54^{+0.07}_{-0.07}$	$1.42^{+0.07}_{-0.07}$
17.9	2.5 ± 0.3	< 1.0	8.4 ± 0.0	$0.298^{+0.036}_{-0.036}$	$0.662^{+0.000}_{-0.000}$	$1.56^{+0.06}_{-0.05}$	$1.42^{+0.05}_{-0.05}$
18.4	2.4 ± 0.3	< 1.0	8.4 ± 0.1	$0.286^{+0.040}_{-0.039}$	$0.662^{+0.004}_{-0.004}$	$1.53^{+0.09}_{-0.08}$	$1.41^{+0.06}_{-0.05}$
18.9	2.1 ± 0.2	< 1.0	7.7 ± 0.1	$0.273^{+0.030}_{-0.029}$	$0.691^{+0.005}_{-0.004}$	$1.59^{+0.08}_{-0.07}$	$1.38^{+0.04}_{-0.04}$
19.3	1.7 ± 0.2	< 1.0	7.4 ± 0.2	$0.230^{+0.034}_{-0.032}$	$0.705^{+0.010}_{-0.009}$	$1.67^{+0.13}_{-0.12}$	$1.31^{+0.04}_{-0.04}$
19.8	1.4 ± 0.2	< 1.0	7.1 ± 0.2	$0.197^{+0.035}_{-0.033}$	$0.720^{+0.010}_{-0.010}$	$1.73^{+0.14}_{-0.13}$	$1.26^{+0.04}_{-0.04}$
20.3	1.3 ± 0.2	< 1.0	13.2 ± 1.0	$0.098^{+0.024}_{-0.021}$	$0.528^{+0.021}_{-0.019}$	$1.35^{+0.21}_{-0.18}$	$1.16^{+0.04}_{-0.03}$
20.8	1.2 ± 0.2	< 1.0	12.4 ± 1.4	$0.097^{+0.030}_{-0.024}$	$0.545^{+0.034}_{-0.028}$	$1.36^{+0.31}_{-0.25}$	$1.15^{+0.04}_{-0.04}$

Table B.9: Radial profiles for the galaxy NGC 5194 ($R_{25} = 9.0$ kpc).

	From Leroy et al. (2008)			Our stability quantities			
R (kpc)	$\Sigma_{\rm HI}$ ($M_\odot {\rm pc}^{-2}$)	$\Sigma_{\rm H_2}$ ($M_\odot {\rm pc}^{-2}$)	$\Sigma_{\rm s}$ ($M_\odot {\rm pc}^{-2}$)	$\mathcal{A}$	$\mathcal{B}$	$Q_{\rm eff}$	$\bar{Q}$
0.2	4.5 ± 0.4	197.4 ± 35.0	4912.2 ± 111.6	$0.041\,^{+0.008}_{-0.008}$	$0.029\,^{+0.000}_{-0.000}$	$1.77\,^{+0.46}_{-0.32}$	$1.46\,^{+0.27}_{-0.26}$
0.6	5.5 ± 0.4	207.7 ± 33.5	2352.5 ± 15.3	$0.091\,^{+0.015}_{-0.015}$	$0.042\,^{+0.000}_{-0.000}$	$1.26\,^{+0.25}_{-0.18}$	$2.23\,^{+0.35}_{-0.35}$
1.0	6.1 ± 0.4	181.6 ± 30.5	1251.1 ± 6.5	$0.150\,^{+0.026}_{-0.025}$	$0.058\,^{+0.000}_{-0.000}$	$1.10\,^{+0.22}_{-0.16}$	$2.71\,^{+0.43}_{-0.43}$
1.4	6.1 ± 0.6	134.5 ± 41.2	703.1 ± 3.8	$0.200\,^{+0.061}_{-0.060}$	$0.077\,^{+0.000}_{-0.000}$	$1.15\,^{+0.46}_{-0.26}$	$2.74\,^{+0.78}_{-0.77}$
1.7	6.7 ± 0.6	106.8 ± 33.8	471.8 ± 1.3	$0.241\,^{+0.074}_{-0.073}$	$0.094\,^{+0.000}_{-0.000}$	$1.19\,^{+0.47}_{-0.27}$	$2.74\,^{+0.78}_{-0.77}$
2.1	7.9 ± 0.6	94.8 ± 19.2	417.5 ± 1.6	$0.246\,^{+0.049}_{-0.048}$	$0.100\,^{+0.000}_{-0.000}$	$1.08\,^{+0.24}_{-0.17}$	$2.66\,^{+0.48}_{-0.47}$
2.5	8.5 ± 0.9	72.6 ± 15.7	394.9 ± 1.9	$0.205\,^{+0.043}_{-0.043}$	$0.103\,^{+0.000}_{-0.000}$	$1.13\,^{+0.27}_{-0.18}$	$2.21\,^{+0.41}_{-0.41}$
2.9	7.5 ± 0.9	40.9 ± 12.2	334.1 ± 1.5	$0.145\,^{+0.040}_{-0.040}$	$0.112\,^{+0.000}_{-0.000}$	$1.53\,^{+0.38}_{-0.29}$	$1.54\,^{+0.35}_{-0.30}$
3.3	6.2 ± 0.7	19.1 ± 5.6	286.9 ± 1.3	$0.088\,^{+0.022}_{-0.022}$	$0.121\,^{+0.000}_{-0.000}$	$1.86\,^{+0.10}_{-0.10}$	$1.19\,^{+0.06}_{-0.05}$
3.7	6.1 ± 0.5	14.6 ± 3.3	253.2 ± 2.0	$0.082\,^{+0.016}_{-0.016}$	$0.129\,^{+0.001}_{-0.001}$	$1.79\,^{+0.08}_{-0.08}$	$1.18\,^{+0.04}_{-0.04}$
4.1	7.2 ± 0.7	22.6 ± 7.5	236.7 ± 1.7	$0.126\,^{+0.036}_{-0.035}$	$0.133\,^{+0.000}_{-0.000}$	$1.52\,^{+0.13}_{-0.24}$	$1.29\,^{+0.22}_{-0.09}$
4.5	9.1 ± 0.9	33.6 ± 10.3	224.2 ± 1.2	$0.190\,^{+0.051}_{-0.051}$	$0.137\,^{+0.000}_{-0.000}$	$1.08\,^{+0.30}_{-0.20}$	$1.69\,^{+0.36}_{-0.35}$
4.8	11.2 ± 0.9	35.9 ± 9.6	227.8 ± 1.4	$0.207\,^{+0.048}_{-0.047}$	$0.136\,^{+0.000}_{-0.000}$	$0.94\,^{+0.22}_{-0.15}$	$1.82\,^{+0.34}_{-0.33}$
5.2	12.8 ± 0.8	28.0 ± 7.0	206.0 ± 1.1	$0.198\,^{+0.039}_{-0.039}$	$0.143\,^{+0.000}_{-0.000}$	$0.97\,^{+0.18}_{-0.14}$	$1.70\,^{+0.26}_{-0.26}$
5.6	12.7 ± 0.8	14.9 ± 4.7	176.5 ± 0.9	$0.156\,^{+0.032}_{-0.032}$	$0.154\,^{+0.000}_{-0.000}$	$1.20\,^{+0.10}_{-0.15}$	$1.38\,^{+0.19}_{-0.10}$
6.0	11.1 ± 0.8	4.3 ± 2.8	148.9 ± 0.8	$0.103\,^{+0.025}_{-0.025}$	$0.168\,^{+0.000}_{-0.000}$	$1.37\,^{+0.08}_{-0.08}$	$1.22\,^{+0.06}_{-0.06}$
6.4	9.4 ± 0.9	1.0 ± 1.1	106.3 ± 0.4	$0.098\,^{+0.019}_{-0.019}$	$0.199\,^{+0.000}_{-0.000}$	$1.54\,^{+0.07}_{-0.06}$	$1.21\,^{+0.05}_{-0.04}$
6.8	8.4 ± 0.9	< 1.0	77.5 ± 0.3	$0.108\,^{+0.012}_{-0.012}$	$0.233\,^{+0.000}_{-0.000}$	$1.67\,^{+0.05}_{-0.05}$	$1.23\,^{+0.03}_{-0.03}$
7.2	7.8 ± 0.9	< 1.0	64.3 ± 0.6	$0.121\,^{+0.015}_{-0.015}$	$0.256\,^{+0.001}_{-0.001}$	$1.70\,^{+0.07}_{-0.07}$	$1.25\,^{+0.04}_{-0.03}$
7.6	7.8 ± 1.0	< 1.0	50.2 ± 0.3	$0.155\,^{+0.021}_{-0.021}$	$0.289\,^{+0.001}_{-0.001}$	$1.72\,^{+0.08}_{-0.08}$	$1.32\,^{+0.05}_{-0.05}$
8.0	7.8 ± 1.1	< 1.0	45.0 ± 0.3	$0.173\,^{+0.026}_{-0.025}$	$0.306\,^{+0.001}_{-0.001}$	$1.68\,^{+0.09}_{-0.09}$	$1.36\,^{+0.06}_{-0.06}$
8.3	7.8 ± 1.2	< 1.0	46.4 ± 0.3	$0.168\,^{+0.027}_{-0.027}$	$0.301\,^{+0.001}_{-0.001}$	$1.61\,^{+0.09}_{-0.09}$	$1.35\,^{+0.06}_{-0.06}$
8.7	7.8 ± 1.2	< 1.0	53.2 ± 0.6	$0.147\,^{+0.024}_{-0.024}$	$0.281\,^{+0.002}_{-0.002}$	$1.48\,^{+0.09}_{-0.09}$	$1.30\,^{+0.06}_{-0.05}$
9.1	7.3 ± 1.1	< 1.0	69.2 ± 1.8	$0.105\,^{+0.019}_{-0.018}$	$0.246\,^{+0.003}_{-0.003}$	$1.33\,^{+0.10}_{-0.09}$	$1.22\,^{+0.04}_{-0.04}$
9.5	6.4 ± 1.0	< 1.0	71.2 ± 1.3	$0.090\,^{+0.016}_{-0.015}$	$0.243\,^{+0.002}_{-0.002}$	$1.29\,^{+0.07}_{-0.07}$	$1.18\,^{+0.04}_{-0.03}$
9.9	5.8 ± 1.0	< 1.0	86.5 ± 1.7	$0.067\,^{+0.013}_{-0.013}$	$0.220\,^{+0.002}_{-0.002}$	$1.17\,^{+0.06}_{-0.06}$	$1.14\,^{+0.03}_{-0.03}$
10.3	5.1 ± 0.9	< 1.0	210.3 ± 11.3	$0.024\,^{+0.006}_{-0.005}$	$0.141\,^{+0.004}_{-0.004}$	$0.78\,^{+0.08}_{-0.07}$	$1.05\,^{+0.01}_{-0.01}$
10.7	4.5 ± 0.9	< 1.0	102.7 ± 3.1	$0.044\,^{+0.010}_{-0.010}$	$0.202\,^{+0.003}_{-0.003}$	$1.04\,^{+0.07}_{-0.07}$	$1.09\,^{+0.02}_{-0.02}$

Table B.10: Radial profiles for the galaxy NGC 6946 ($R_{25} = 9.8$ kpc).

	From Leroy et al. (2008)			Our stability quantities			
R (kpc)	$\Sigma_{\rm HI}$ ($M_\odot {\rm pc}^{-2}$)	$\Sigma_{\rm H_2}$ ($M_\odot {\rm pc}^{-2}$)	$\Sigma_{\rm s}$ ($M_\odot {\rm pc}^{-2}$)	$\mathcal{A}$	$\mathcal{B}$	$Q_{\rm eff}$	$\bar{Q}$
0.1	6.1 ± 1.1	548.6 ± 68.4	5937.7 ± 348.7	$0.093\,^{+0.018}_{-0.016}$	$0.028\,^{+0.001}_{-0.001}$	$0.36\,^{+0.10}_{-0.08}$	$3.37\,^{+0.53}_{-0.50}$
0.4	6.4 ± 1.1	390.7 ± 81.2	1125.9 ± 7.7	$0.353\,^{+0.076}_{-0.075}$	$0.065\,^{+0.000}_{-0.000}$	$0.44\,^{+0.12}_{-0.08}$	$5.58\,^{+1.15}_{-1.15}$
0.7	6.4 ± 1.0	214.2 ± 54.9	708.0 ± 4.5	$0.312\,^{+0.081}_{-0.080}$	$0.082\,^{+0.000}_{-0.000}$	$0.69\,^{+0.23}_{-0.14}$	$3.99\,^{+0.98}_{-0.98}$
1.0	5.9 ± 0.7	110.4 ± 31.1	496.6 ± 2.6	$0.234\,^{+0.066}_{-0.065}$	$0.097\,^{+0.000}_{-0.000}$	$1.11\,^{+0.39}_{-0.23}$	$2.61\,^{+0.66}_{-0.66}$
1.3	5.5 ± 0.6	64.2 ± 17.4	405.6 ± 1.8	$0.172\,^{+0.045}_{-0.045}$	$0.108\,^{+0.000}_{-0.000}$	$1.56\,^{+0.46}_{-0.30}$	$1.82\,^{+0.41}_{-0.41}$
1.6	5.5 ± 0.5	46.4 ± 10.6	390.4 ± 4.7	$0.133\,^{+0.030}_{-0.030}$	$0.110\,^{+0.001}_{-0.001}$	$1.79\,^{+0.36}_{-0.30}$	$1.45\,^{+0.26}_{-0.22}$
1.9	5.8 ± 0.4	39.9 ± 7.0	356.3 ± 1.9	$0.128\,^{+0.022}_{-0.021}$	$0.115\,^{+0.000}_{-0.000}$	$1.79\,^{+0.21}_{-0.22}$	$1.37\,^{+0.18}_{-0.13}$
2.1	6.4 ± 0.4	37.9 ± 5.4	313.6 ± 0.9	$0.141\,^{+0.019}_{-0.019}$	$0.123\,^{+0.000}_{-0.000}$	$1.71\,^{+0.20}_{-0.17}$	$1.43\,^{+0.15}_{-0.15}$
2.4	6.9 ± 0.4	36.9 ± 4.9	287.1 ± 1.0	$0.153\,^{+0.019}_{-0.019}$	$0.128\,^{+0.000}_{-0.000}$	$1.56\,^{+0.17}_{-0.15}$	$1.48\,^{+0.14}_{-0.14}$
2.7	7.4 ± 0.4	35.2 ± 4.3	258.4 ± 1.0	$0.165\,^{+0.019}_{-0.019}$	$0.135\,^{+0.000}_{-0.000}$	$1.46\,^{+0.15}_{-0.13}$	$1.52\,^{+0.13}_{-0.13}$
3.0	7.8 ± 0.4	32.4 ± 3.5	236.2 ± 1.5	$0.170\,^{+0.018}_{-0.017}$	$0.141\,^{+0.000}_{-0.000}$	$1.39\,^{+0.13}_{-0.11}$	$1.52\,^{+0.12}_{-0.11}$
3.3	8.2 ± 0.5	29.7 ± 3.3	212.1 ± 0.9	$0.179\,^{+0.019}_{-0.019}$	$0.149\,^{+0.000}_{-0.000}$	$1.34\,^{+0.12}_{-0.10}$	$1.53\,^{+0.12}_{-0.12}$
3.6	8.7 ± 0.6	28.1 ± 3.9	200.8 ± 1.5	$0.183\,^{+0.024}_{-0.024}$	$0.153\,^{+0.001}_{-0.001}$	$1.26\,^{+0.14}_{-0.12}$	$1.54\,^{+0.15}_{-0.14}$
3.9	9.3 ± 0.8	27.5 ± 4.9	276.6 ± 12.8	$0.133\,^{+0.028}_{-0.026}$	$0.130\,^{+0.003}_{-0.003}$	$1.17\,^{+0.17}_{-0.21}$	$1.32\,^{+0.18}_{-0.08}$
4.1	9.5 ± 1.0	25.9 ± 5.7	187.3 ± 1.8	$0.189\,^{+0.038}_{-0.037}$	$0.159\,^{+0.001}_{-0.001}$	$1.15\,^{+0.18}_{-0.16}$	$1.55\,^{+0.22}_{-0.20}$
4.4	9.5 ± 1.1	22.8 ± 5.6	159.7 ± 1.3	$0.202\,^{+0.044}_{-0.043}$	$0.172\,^{+0.001}_{-0.001}$	$1.15\,^{+0.18}_{-0.16}$	$1.57\,^{+0.24}_{-0.20}$
4.7	9.6 ± 1.1	19.2 ± 5.1	146.3 ± 1.0	$0.197\,^{+0.044}_{-0.043}$	$0.179\,^{+0.001}_{-0.001}$	$1.16\,^{+0.15}_{-0.16}$	$1.52\,^{+0.22}_{-0.16}$
5.0	9.6 ± 1.1	15.6 ± 4.4	127.2 ± 0.7	$0.198\,^{+0.045}_{-0.044}$	$0.192\,^{+0.001}_{-0.001}$	$1.19\,^{+0.14}_{-0.15}$	$1.49\,^{+0.20}_{-0.14}$
5.3	9.5 ± 1.1	12.2 ± 3.7	110.4 ± 0.6	$0.197\,^{+0.045}_{-0.044}$	$0.207\,^{+0.001}_{-0.001}$	$1.22\,^{+0.13}_{-0.14}$	$1.47\,^{+0.17}_{-0.13}$
5.6	9.3 ± 0.9	9.4 ± 2.7	97.4 ± 0.4	$0.192\,^{+0.038}_{-0.038}$	$0.220\,^{+0.000}_{-0.000}$	$1.25\,^{+0.11}_{-0.11}$	$1.45\,^{+0.13}_{-0.11}$
5.9	9.3 ± 0.8	7.5 ± 1.9	184.5 ± 10.5	$0.091\,^{+0.021}_{-0.019}$	$0.160\,^{+0.005}_{-0.004}$	$1.04\,^{+0.14}_{-0.12}$	$1.19\,^{+0.05}_{-0.04}$
6.1	9.3 ± 0.8	6.3 ± 1.5	105.3 ± 2.0	$0.148\,^{+0.025}_{-0.024}$	$0.211\,^{+0.002}_{-0.002}$	$1.20\,^{+0.09}_{-0.09}$	$1.33\,^{+0.07}_{-0.06}$
6.4	9.1 ± 0.8	5.1 ± 1.4	99.9 ± 4.4	$0.142\,^{+0.030}_{-0.027}$	$0.217\,^{+0.005}_{-0.005}$	$1.19\,^{+0.15}_{-0.14}$	$1.31\,^{+0.08}_{-0.07}$
6.7	8.8 ± 0.8	4.1 ± 1.4	85.8 ± 3.8	$0.150\,^{+0.034}_{-0.031}$	$0.234\,^{+0.005}_{-0.005}$	$1.21\,^{+0.16}_{-0.15}$	$1.33\,^{+0.09}_{-0.07}$
7.0	8.4 ± 0.8	3.2 ± 1.4	71.1 ± 1.1	$0.163\,^{+0.034}_{-0.033}$	$0.257\,^{+0.002}_{-0.002}$	$1.25\,^{+0.11}_{-0.10}$	$1.35\,^{+0.09}_{-0.08}$
7.3	8.1 ± 0.9	2.3 ± 1.5	59.1 ± 0.5	$0.176\,^{+0.042}_{-0.042}$	$0.282\,^{+0.001}_{-0.001}$	$1.29\,^{+0.12}_{-0.11}$	$1.37\,^{+0.11}_{-0.10}$
7.6	8.0 ± 1.0	1.6 ± 1.3	49.0 ± 0.4	$0.196\,^{+0.049}_{-0.048}$	$0.310\,^{+0.001}_{-0.001}$	$1.32\,^{+0.13}_{-0.12}$	$1.41\,^{+0.12}_{-0.11}$
7.9	8.0 ± 1.1	< 1.0	40.7 ± 0.3	$0.197\,^{+0.029}_{-0.028}$	$0.340\,^{+0.001}_{-0.001}$	$1.41\,^{+0.08}_{-0.08}$	$1.39\,^{+0.06}_{-0.06}$
8.2	7.9 ± 1.0	< 1.0	43.0 ± 1.0	$0.184\,^{+0.028}_{-0.027}$	$0.331\,^{+0.004}_{-0.004}$	$1.34\,^{+0.11}_{-0.10}$	$1.37\,^{+0.06}_{-0.06}$
8.4	7.4 ± 0.9	< 1.0	35.2 ± 0.9	$0.210\,^{+0.032}_{-0.030}$	$0.366\,^{+0.005}_{-0.005}$	$1.40\,^{+0.12}_{-0.11}$	$1.41\,^{+0.07}_{-0.06}$
8.7	6.9 ± 0.8	< 1.0	32.4 ± 0.9	$0.213\,^{+0.031}_{-0.030}$	$0.381\,^{+0.005}_{-0.005}$	$1.41\,^{+0.13}_{-0.12}$	$1.41\,^{+0.06}_{-0.06}$
9.0	6.3 ± 0.7	< 1.0	30.4 ± 1.1	$0.207\,^{+0.032}_{-0.029}$	$0.394\,^{+0.007}_{-0.007}$	$1.43\,^{+0.15}_{-0.13}$	$1.39\,^{+0.06}_{-0.06}$
9.3	5.8 ± 0.6	< 1.0	22.6 ± 0.5	$0.257\,^{+0.033}_{-0.032}$	$0.456\,^{+0.005}_{-0.005}$	$1.53\,^{+0.12}_{-0.11}$	$1.46\,^{+0.06}_{-0.06}$
9.6	5.3 ± 0.6	< 1.0	26.8 ± 0.8	$0.198\,^{+0.029}_{-0.027}$	$0.419\,^{+0.006}_{-0.006}$	$1.46\,^{+0.13}_{-0.12}$	$1.36\,^{+0.05}_{-0.05}$
9.9	4.8 ± 0.5	< 1.0	36.6 ± 1.9	$0.131\,^{+0.022}_{-0.019}$	$0.359\,^{+0.010}_{-0.009}$	$1.32\,^{+0.15}_{-0.14}$	$1.25\,^{+0.04}_{-0.04}$
10.2	4.5 ± 0.5	< 1.0	86.9 ± 6.3	$0.052\,^{+0.010}_{-0.009}$	$0.233\,^{+0.009}_{-0.008}$	$0.94\,^{+0.13}_{-0.11}$	$1.10\,^{+0.02}_{-0.02}$
10.4	4.1 ± 0.5	< 1.0	20.4 ± 0.5	$0.201\,^{+0.030}_{-0.029}$	$0.480\,^{+0.006}_{-0.006}$	$1.56\,^{+0.12}_{-0.11}$	$1.35\,^{+0.05}_{-0.05}$
10.7	3.9 ± 0.5	< 1.0	17.3 ± 0.4	$0.225\,^{+0.035}_{-0.033}$	$0.522\,^{+0.006}_{-0.006}$	$1.61\,^{+0.13}_{-0.12}$	$1.37\,^{+0.06}_{-0.06}$
11.0	3.7 ± 0.4	< 1.0	17.2 ± 0.5	$0.215\,^{+0.030}_{-0.029}$	$0.523\,^{+0.008}_{-0.007}$	$1.59\,^{+0.13}_{-0.12}$	$1.35\,^{+0.05}_{-0.05}$
11.3	3.6 ± 0.4	< 1.0	17.8 ± 0.7	$0.202\,^{+0.032}_{-0.029}$	$0.514\,^{+0.010}_{-0.010}$	$1.55\,^{+0.15}_{-0.14}$	$1.34\,^{+0.05}_{-0.05}$
11.6	3.6 ± 0.4	< 1.0	12.9 ± 0.3	$0.279\,^{+0.038}_{-0.037}$	$0.604\,^{+0.007}_{-0.007}$	$1.66\,^{+0.13}_{-0.12}$	$1.42\,^{+0.06}_{-0.05}$

Table B.11: Radial profiles for the galaxy NGC 7331 ($R_{25} = 19.6$ kpc).

	From Leroy et al. (2008)			Our stability quantities			
R (kpc)	$\Sigma_{\rm HI}$ ($M_\odot {\rm pc}^{-2}$)	$\Sigma_{\rm H_2}$ ($M_\odot {\rm pc}^{-2}$)	$\Sigma_{\rm s}$ ($M_\odot {\rm pc}^{-2}$)	$\mathcal{A}$	$\mathcal{B}$	$Q_{\rm eff}$	$\bar{Q}$
0.4	3.6 ± 1.3	15.6 ± 3.9	3990.1 ± 206.5	$0.005\,^{+0.002}_{-0.001}$	$0.030\,^{+0.001}_{-0.001}$	$2.04\,^{+0.17}_{-0.16}$	$1.01\,^{+0.00}_{-0.00}$
1.1	3.1 ± 0.7	17.7 ± 5.3	1558.3 ± 38.7	$0.013\,^{+0.004}_{-0.004}$	$0.048\,^{+0.001}_{-0.001}$	$2.37\,^{+0.11}_{-0.11}$	$1.03\,^{+0.01}_{-0.01}$
1.8	3.3 ± 0.6	24.7 ± 5.4	860.5 ± 10.8	$0.033\,^{+0.007}_{-0.007}$	$0.064\,^{+0.000}_{-0.000}$	$2.33\,^{+0.08}_{-0.08}$	$1.07\,^{+0.02}_{-0.02}$
2.5	4.5 ± 0.8	33.3 ± 3.9	655.2 ± 5.2	$0.058\,^{+0.008}_{-0.008}$	$0.074\,^{+0.000}_{-0.000}$	$1.99\,^{+0.05}_{-0.05}$	$1.12\,^{+0.02}_{-0.02}$
3.2	5.6 ± 0.8	33.8 ± 4.2	538.0 ± 3.9	$0.073\,^{+0.010}_{-0.010}$	$0.081\,^{+0.000}_{-0.000}$	$1.72\,^{+0.05}_{-0.07}$	$1.16\,^{+0.04}_{-0.02}$
3.9	5.9 ± 0.5	28.7 ± 4.4	395.8 ± 3.7	$0.087\,^{+0.013}_{-0.013}$	$0.095\,^{+0.000}_{-0.000}$	$1.62\,^{+0.07}_{-0.12}$	$1.19\,^{+0.07}_{-0.03}$
4.6	6.5 ± 0.4	25.3 ± 3.8	307.5 ± 3.1	$0.103\,^{+0.015}_{-0.015}$	$0.108\,^{+0.001}_{-0.001}$	$1.51\,^{+0.07}_{-0.14}$	$1.23\,^{+0.10}_{-0.04}$
5.3	6.5 ± 0.3	18.6 ± 3.6	231.9 ± 2.3	$0.108\,^{+0.018}_{-0.018}$	$0.124\,^{+0.001}_{-0.001}$	$1.50\,^{+0.08}_{-0.09}$	$1.24\,^{+0.06}_{-0.04}$
6.1	6.6 ± 0.5	11.4 ± 2.7	161.9 ± 1.5	$0.111\,^{+0.021}_{-0.021}$	$0.148\,^{+0.001}_{-0.001}$	$1.55\,^{+0.09}_{-0.09}$	$1.25\,^{+0.06}_{-0.05}$
6.8	7.3 ± 0.6	6.8 ± 1.3	121.2 ± 1.0	$0.116\,^{+0.017}_{-0.017}$	$0.172\,^{+0.001}_{-0.001}$	$1.59\,^{+0.07}_{-0.07}$	$1.25\,^{+0.04}_{-0.04}$
7.5	8.1 ± 0.7	5.8 ± 1.0	98.5 ± 0.8	$0.141\,^{+0.019}_{-0.018}$	$0.190\,^{+0.001}_{-0.001}$	$1.52\,^{+0.08}_{-0.07}$	$1.32\,^{+0.05}_{-0.05}$
8.2	8.5 ± 0.5	4.8 ± 0.9	83.8 ± 0.8	$0.159\,^{+0.018}_{-0.018}$	$0.206\,^{+0.001}_{-0.001}$	$1.46\,^{+0.08}_{-0.07}$	$1.36\,^{+0.05}_{-0.05}$
8.9	8.2 ± 0.6	3.5 ± 0.5	66.6 ± 0.5	$0.176\,^{+0.018}_{-0.018}$	$0.231\,^{+0.001}_{-0.001}$	$1.47\,^{+0.07}_{-0.07}$	$1.39\,^{+0.05}_{-0.05}$
9.6	8.3 ± 0.7	2.4 ± 0.5	54.8 ± 0.4	$0.195\,^{+0.023}_{-0.023}$	$0.255\,^{+0.001}_{-0.001}$	$1.46\,^{+0.08}_{-0.08}$	$1.43\,^{+0.06}_{-0.06}$
10.3	8.8 ± 0.7	1.6 ± 0.5	47.4 ± 0.4	$0.219\,^{+0.027}_{-0.027}$	$0.274\,^{+0.001}_{-0.001}$	$1.41\,^{+0.09}_{-0.08}$	$1.49\,^{+0.07}_{-0.07}$
11.0	8.6 ± 0.6	1.1 ± 0.4	40.4 ± 0.3	$0.240\,^{+0.027}_{-0.026}$	$0.297\,^{+0.001}_{-0.001}$	$1.39\,^{+0.08}_{-0.08}$	$1.53\,^{+0.07}_{-0.07}$
11.8	8.1 ± 0.6	< 1.0	34.3 ± 0.3	$0.236\,^{+0.020}_{-0.019}$	$0.322\,^{+0.001}_{-0.001}$	$1.43\,^{+0.06}_{-0.06}$	$1.50\,^{+0.05}_{-0.05}$
12.5	7.4 ± 0.6	< 1.0	29.3 ± 0.4	$0.253\,^{+0.024}_{-0.024}$	$0.349\,^{+0.002}_{-0.002}$	$1.44\,^{+0.08}_{-0.08}$	$1.52\,^{+0.06}_{-0.05}$
13.2	6.9 ± 0.5	< 1.0	24.9 ± 0.2	$0.277\,^{+0.022}_{-0.022}$	$0.378\,^{+0.002}_{-0.002}$	$1.45\,^{+0.06}_{-0.06}$	$1.55\,^{+0.05}_{-0.05}$
13.9	7.2 ± 0.5	< 1.0	22.6 ± 0.2	$0.319\,^{+0.025}_{-0.025}$	$0.397\,^{+0.002}_{-0.002}$	$1.38\,^{+0.07}_{-0.06}$	$1.63\,^{+0.05}_{-0.05}$
14.6	7.1 ± 0.4	< 1.0	22.0 ± 0.2	$0.323\,^{+0.021}_{-0.021}$	$0.403\,^{+0.002}_{-0.002}$	$1.33\,^{+0.06}_{-0.05}$	$1.63\,^{+0.04}_{-0.04}$
15.3	7.1 ± 0.4	< 1.0	20.1 ± 0.2	$0.353\,^{+0.024}_{-0.023}$	$0.421\,^{+0.002}_{-0.002}$	$1.29\,^{+0.06}_{-0.05}$	$1.68\,^{+0.05}_{-0.05}$
16.0	7.2 ± 0.5	< 1.0	18.5 ± 0.2	$0.389\,^{+0.032}_{-0.031}$	$0.439\,^{+0.002}_{-0.002}$	$1.24\,^{+0.07}_{-0.06}$	$1.74\,^{+0.06}_{-0.06}$
16.7	7.3 ± 0.6	< 1.0	16.7 ± 0.1	$0.437\,^{+0.039}_{-0.038}$	$0.462\,^{+0.001}_{-0.001}$	$1.20\,^{+0.06}_{-0.06}$	$1.81\,^{+0.08}_{-0.07}$
17.5	6.9 ± 0.6	< 1.0	15.3 ± 0.1	$0.451\,^{+0.042}_{-0.042}$	$0.483\,^{+0.002}_{-0.002}$	$1.20\,^{+0.07}_{-0.06}$	$1.81\,^{+0.08}_{-0.08}$
18.2	6.5 ± 0.6	< 1.0	15.4 ± 0.4	$0.422\,^{+0.051}_{-0.049}$	$0.481\,^{+0.006}_{-0.006}$	$1.18\,^{+0.11}_{-0.10}$	$1.76\,^{+0.09}_{-0.09}$
18.9	6.4 ± 0.7	< 1.0	19.4 ± 1.4	$0.330\,^{+0.065}_{-0.056}$	$0.429\,^{+0.016}_{-0.015}$	$1.10\,^{+0.21}_{-0.18}$	$1.63\,^{+0.12}_{-0.10}$
19.6	6.1 ± 0.7	< 1.0	13.1 ± 0.4	$0.466\,^{+0.070}_{-0.066}$	$0.522\,^{+0.008}_{-0.008}$	$1.16\,^{+0.14}_{-0.12}$	$1.80\,^{+0.12}_{-0.11}$
20.3	5.5 ± 0.7	< 1.0	9.4 ± 0.1	$0.585\,^{+0.082}_{-0.080}$	$0.616\,^{+0.003}_{-0.003}$	$1.26\,^{+0.11}_{-0.10}$	$1.89\,^{+0.12}_{-0.12}$
21.0	4.5 ± 0.6	< 1.0	9.0 ± 0.3	$0.500\,^{+0.086}_{-0.081}$	$0.630\,^{+0.011}_{-0.010}$	$1.35\,^{+0.17}_{-0.15}$	$1.75\,^{+0.12}_{-0.12}$
21.7	3.6 ± 0.5	< 1.0	7.2 ± 0.1	$0.500\,^{+0.077}_{-0.075}$	$0.704\,^{+0.005}_{-0.005}$	$1.51\,^{+0.13}_{-0.12}$	$1.69\,^{+0.10}_{-0.10}$
22.4	3.1 ± 0.4	< 1.0	6.4 ± 0.1	$0.484\,^{+0.071}_{-0.069}$	$0.747\,^{+0.006}_{-0.006}$	$1.60\,^{+0.13}_{-0.12}$	$1.63\,^{+0.09}_{-0.09}$
23.2	2.7 ± 0.3	< 1.0	6.2 ± 0.1	$0.435\,^{+0.056}_{-0.055}$	$0.758\,^{+0.006}_{-0.006}$	$1.65\,^{+0.12}_{-0.11}$	$1.56\,^{+0.07}_{-0.07}$

Appendix C

Numerical methods: thick discs

As mentioned in Appendix A, MATLAB was used for the numerical computations done in this thesis.

The problem described in Chapter 5 consists of: (1) comparing the marginal stability curves for discs of different thickness for given values of our parameters $\mathcal{A}$ and $\mathcal{B}$; (2) finding the two-phase region and studying how the thickness affects this; and (3) determining the stability threshold and again study how the thickness affects this.

C.1 Computing the marginal stability curve

Romeo (1992) had derived a polyonomial in the fourth order to derive the marginal stability curve for a two-component thick disc numerically. However, note that it was more convient at that time to compute Q^2 instead of Q for reasons as there would not appear any imaginary roots to the polynomial. Today it is more convenient to derive Q directly instead as it is more helpful in simulations and observations. For simplicity was the polynomial again handled in the fourth order and the square root of the solutions were then presented.

The marginal stability curve is thus given by

$$A \cdot Q^8 + B \cdot Q^6 + C \cdot Q^4 + D \cdot Q^2 + E = 0 \tag{C.1}$$

where the coefficients are

$$A = \mathcal{B}^2 \cdot \mathcal{U}_\mathrm{s}\mathcal{U}_\mathrm{g} \tag{C.2}$$

$$B = 2\Lambda \left[2\Lambda(1+\mathcal{B}^2)\mathcal{U}_\mathrm{s}\mathcal{U}_\mathrm{g} + \mathcal{B}^2(\mathcal{U}_\mathrm{s}+\mathcal{U}_\mathrm{g})\right] \tag{C.3}$$

$$C = 4\Lambda^2 \left\{4\Lambda^2\mathcal{U}_\mathrm{s}\mathcal{U}_\mathrm{g} + 2\Lambda(1+\mathcal{B}^2)(\mathcal{U}_\mathrm{s}+\mathcal{U}_\mathrm{g}) + [\mathcal{B}^2 - 2(\mathcal{A}\mathcal{U}_\mathrm{s} + \mathcal{B}^2\mathcal{U}_\mathrm{g})]\right\} \tag{C.4}$$

$$D = 16\Lambda^3 \left\{2\Lambda^2(\mathcal{U}_\mathrm{s}+\mathcal{U}_\mathrm{g}) + \Lambda[(1+\mathcal{B}^2) - 2(\mathcal{A}\mathcal{U}_\mathrm{s}+\mathcal{U}_\mathrm{g})] - (\mathcal{A}+\mathcal{B}^2)\right\} \tag{C.5}$$

$$E = 64\Lambda^5 \left[\Lambda - (\mathcal{A}+1)\right]. \tag{C.6}$$

The parameters denoted $\mathcal{U}_\mathrm{i}$ are in turn given by

$$\mathcal{U}_{\rm s} = \frac{\mathcal{D}_{\rm s}^2}{1+\mathcal{A}} \frac{h_{\rm effs}}{2h_{\rm Es}} \tag{C.7}$$

and

$$\mathcal{U}_{\rm g} = \frac{\mathcal{B}^2\mathcal{D}_{\rm g}^2}{1+\mathcal{A}} \frac{h_{\rm effg}}{2h_{\rm Eg}} \tag{C.8}$$

where $h_{\rm effi}$ is the effective scale height and $h_{\rm Ei}$ is the exponential scale height of each fluid disc. These are studied quite extensively in Chapter 8 of Romeo (1990). However, here we are content with knowing that they are given by computing for the stellar component

$$\frac{h_{\rm effs}}{2h_{\rm Es}} = \frac{1}{2}\sqrt{1+\gamma\mathcal{B}_{\rm z}^2} \int_0^1 \frac{du}{\left[(1-u)+\gamma\mathcal{B}_{\rm z}^2(1-u^{\mathcal{B}_{\rm z}^{-2}})\right]^{1/2}} \tag{C.9}$$

and for the gaseous component

$$\frac{h_{\rm effg}}{2h_{\rm Eg}} = \frac{1}{2}\sqrt{1+\gamma\mathcal{B}_{\rm z}^2} \int_0^1 \frac{dv}{\left[(1-v^{\mathcal{B}_{\rm z}^2})+\gamma\mathcal{B}_{\rm z}^2(1-v)\right]^{1/2}} \tag{C.10}$$

where the u and v are integration factors. The $\mathcal{B}_{\rm z}$ is a vertical velocity dispersion ratio parameter defined as

$$\mathcal{B}_{\rm z} \equiv \frac{\sigma_{\rm zg}}{\sigma_{\rm zs}} = \mathcal{B}\frac{\mathcal{D}_{\rm g}}{\mathcal{D}_{\rm s}} \tag{C.11}$$

because we can remember from Chapter 5 that

$$\mathcal{D}_{\rm i} = \frac{\sigma_{\rm zi}}{\sigma_{\rm i}}, \tag{C.12}$$

the ratio between the vertical and radial velocity dispersions for each component.

The $\mathcal{B}_z$ is possible to relate numerically with our density parameter $\mathcal{A}$ (Romeo 1992) by using the γ seen in equations (C.9) and (C.10) which is defined to be

$$\gamma \equiv \frac{\rho_{0\rm g}}{\rho_{0\rm s}} \tag{C.13}$$

where $\rho_{0\rm i}$ is the volume density for each component.

It is then possible to find when $\gamma < 1$ and $\mathcal{B}_{\rm z} > 2.5 \cdot 10^{-3}$ that

$$\mathcal{A} = \gamma\mathcal{B}_{\rm z}^{6/5} \tag{C.14}$$

which is denoted as the *fit approximation* by Romeo (1992). This approximation was used to derive γ for the integrals (C.9) and (C.10).

Finally, to derive the marginal stability curve is the polynomial (5.9) solved for every Λ in our range, again $1+\mathcal{A}$. The integrals were solved only once for each marginal stability curve as they do not depend on Λ. This was done by using the predefined MATLAB-function quad which uses recursive adaptive Simpson quadrature to approximate the integral of a given function within an

error of 10^{-6}. This is usually the most efficient integral solving function in MATLAB and as all the predefined functions gave the same solution within some small error this was chosen for the thesis.

The polynomial was solved by using the predefined function fzero. This functions uses a user-defined "guess" to try and find a zero of the polynomial in its vicinity by searching for when the polynomial changes sign. Our polynomial has four solutions to Q^2 for each value of our parameters and only one of them is physically correct. This function only gives out one answer so the choice of guess-value is quite important. Our obvious choice here was the corresponding zero-thickness Q^2 solution och Chapter 3, this is closest to the physical correct thick disc-value of Q^2.

Worth mentioning is that MATLAB had at the time this thesis was written two predefined functions for solving polynomials, roots and fzero. Roots seems simpler and uses a polynomial solving routine where it defines a matrix containing the coefficients of the polynomial where the eigenvalues of the matrix is, due to how the matrix is defined, the roots of the polynomial. Thus giving all four solutions to each Q^2. This however, gave complicated solutions as the routine does not understand what is physical and not physical which resulted in the curves being a mix of solutions. Thus was roots never used for this thesis.

As the fzero gave Q^2 of the polyonomial for each Λ in the wanted $\mathcal{B} - \mathcal{A}$ range and we want $Q(\Lambda)$ was just the square root applied to each solution. These were then saved in a vector that could easily be plotted against Λ and the marginal stability curve was obtained.

C.2 Finding the two-phase region

In the two-component thin case it was a simple matter of deriving the marginal stability curve and having a routine that could study how the curve behaved for each $\mathcal{A}$ and $\mathcal{B}$ and finding the two-phase region that way. However, in the thick disc case to derive that many marginal stability curves in the whole $\mathcal{B} - \mathcal{A}$ space with the same resolution would take days of computations on normal computers. In the thin case I used 1000 points of resolution for $\mathcal{A}$, $\mathcal{B}$ and in Λ. That would require that the computer solves the polynomial one billion times to find three transition lines. To effectivise this several solutions were attempted. Some had good resolution and acceptable amount of computation time, usually in the range of 30 to 60 minutes for the whole region. However, the solution I ended up with only requires five minutes for each transition line.

The obvious way of shortening the calculation time is to lower the resolution. This however will make it very difficult for the routine to find the gaseous peak of the marginal stability curve at the lowest defined $\mathcal{A}$'s and $\mathcal{B}$'s. In the thick cases considered this peak can be extremely small and not finding it will result in the two-phase region to be shifted to higher $\mathcal{A}$ in those parts of the parameter space. The simple solution that was used is just to define the Λ to be logarithmic in the range 10^{-4} to 1.2 (actually $10^{0.08}$) with one hundred points instead of the linear one thousand points used earlier. One hundred points to a logarithmic scaled Λ gave sufficient resolution so the routine is both better at finding the low valued gaseous peak and quicker. It was also discovered that using only one hundred points on a logarithmic scaled $\mathcal{B}$ between 10^{-2} to 1 gave a sufficient resolution.

However, it is still not possible (with realistic amount of time) to compute the marginal stability curve in the whole $\mathcal{B}-\mathcal{A}$ plane. This still requires ten million computations of the polynomial. Instead I defined three different scenarios so that the routine only derives the marginal stability curve in the vicinity of each transition line. See figure C.1 for a flowchart of the following description.

Fortunetaly there is a predefined function in MATLAB denoted findpeaks which returns a vector containing the values for each peak of the function it samples. So in this case it gives either a vector containing one or two elements as the curve will only have one peak outside the region and two inside it.

To find the lower transition of the two-phase region, i.e. sampling from low $\mathcal{A}$ to find where the gaseous peak first appears I simply let the routine stop as soon as the vector given by findpeaks contains two elements (the blue parts of figure C.1). The routine then continues on the next defined $\mathcal{B}$ value and sample from five $\mathcal{A}$ elements below the previous stop, i.e. $i-5$ in figure C.1. All the $\mathcal{A}$ values where the routine is stopped are saved in a vector that corresponds to the lowest transition line.

The main transition line, i.e. the transition between stellar dominated instabilities and gas dominated instabilities, or just simply where the two peaks exhibited by the marginal stability curve is of equal Q is found in a similar fashion (the yellow parts of figure C.1). The routine samples the parameter space from low $\mathcal{A}$ until it finds with the help of findpeaks two peaks and that the difference in height between the peaks are less than 0.0001. This is just an arbitary number to counter any numerical errors, e.g. using 0 resulted in no transition found at all. The $\mathcal{A}$ value is again saved in a vector and the next point is found by sampling on the next $\mathcal{B}$ value from just five $\mathcal{A}$ elements below the previously found point.

The upper transition is when the marginal stability curve exhibits one peak, only the gaseous peak. This is easiest to find when sampling $\mathcal{A}$ from large values instead (the green parts of figure C.1). This is exactly the same manner as with the low transition, sampling the curves until the routine finds that it exhibits two peaks. Then it continues on the next defined $\mathcal{B}$ value and samples from just five $\mathcal{A}$ values above the previously found point. The found points are of course saved in a third vector.

What we obtain are three vectors for each chosen thickness that are the different transition lines of the two-phase region.

C.3 Determining the stability threshold

To find the different two-phase regions we were only required to derive the marginal stability curves for the different thick cases in the proximity of the specific transition curves in the $\mathcal{B}-\mathcal{A}$ space. However, to compute the stability threshold in the same fashion as with the thin discs we again need to compute the marginal stability curve for the whole parameter space for all four chosen thick cases.

For the thin case we used 1000 elements for each parameter, now we instead only have 1000 $\mathcal{A}$ elements and 100 $\mathcal{B}$ elements. Unfortunetaly it would still take an unrealistic amount of time to derive the marginal stability curve for all $\mathcal{A}$ and $\mathcal{B}$ values and for all the four thick cases we

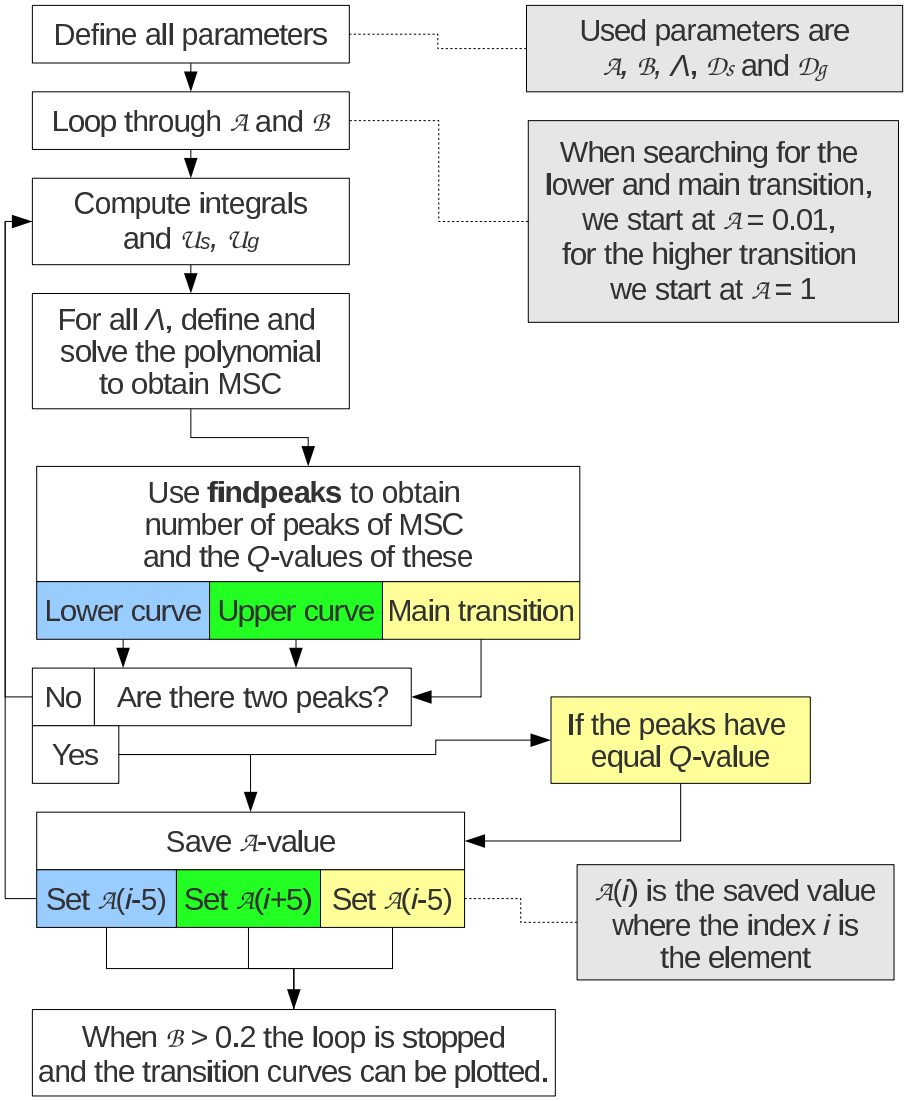

Figure C.1: Flowchart describing the routine used to find the two-phase region of the thick discs. More details are found in the text of Appendix C.2.

are considering on a normal computer. Constraints were required and so only a few specific contour-lines were computed instead so that the marginal stability curve could be computed in the vicinity of these.

Again are there several ways of deriving the specific contour-lines in an effective way. However, I decided to use the one I found most effective, which was not exactly as precise as some other methods that were tried. The other methods that had higher precision in finding the specific contour-lines had however very cumbersome codes and also required at least four to five times longer time to find each line while this method I decided to use only required around five minutes.

The same method for deriving the marginal stability curve as for the two-phase region was used again, i.e. using a logarithmic scale for the wavelengths from 10^{-4} to 1.2. However, this time the routine was devised so that it would find only the global maxima of the marginal stability curve from the lowest defined $\mathcal{A}$ and $\mathcal{B}$ with the command max until it reaches a $\bar{Q}$ larger than the predefined contour-line value (see figure C.2). The first $\bar{Q}$ that is found to be larger than the wanted predefined value is saved in a vector and the routine continues to compute the marginal stability curves from the next predefined $\mathcal{B}$ and only five (as with the two-phase region) predefined $\mathcal{A}$ elements (again denoted by the index i in figure C.2) below the saved one.

What we obtain is one vector in MATLAB for each contour-line. The problem is that this method does not use the predefined MATLAB-command contour as it instead derives an approximate contour-line. To be able to use the contour command the routine has to compute the marginal stability curves in a wider range above and below the wanted $\bar{Q}$ so that there are no empty regions or discontinuities in the contour-lines. This gives a higher precision and also took much more time. And it required alot of code to optimise the process.

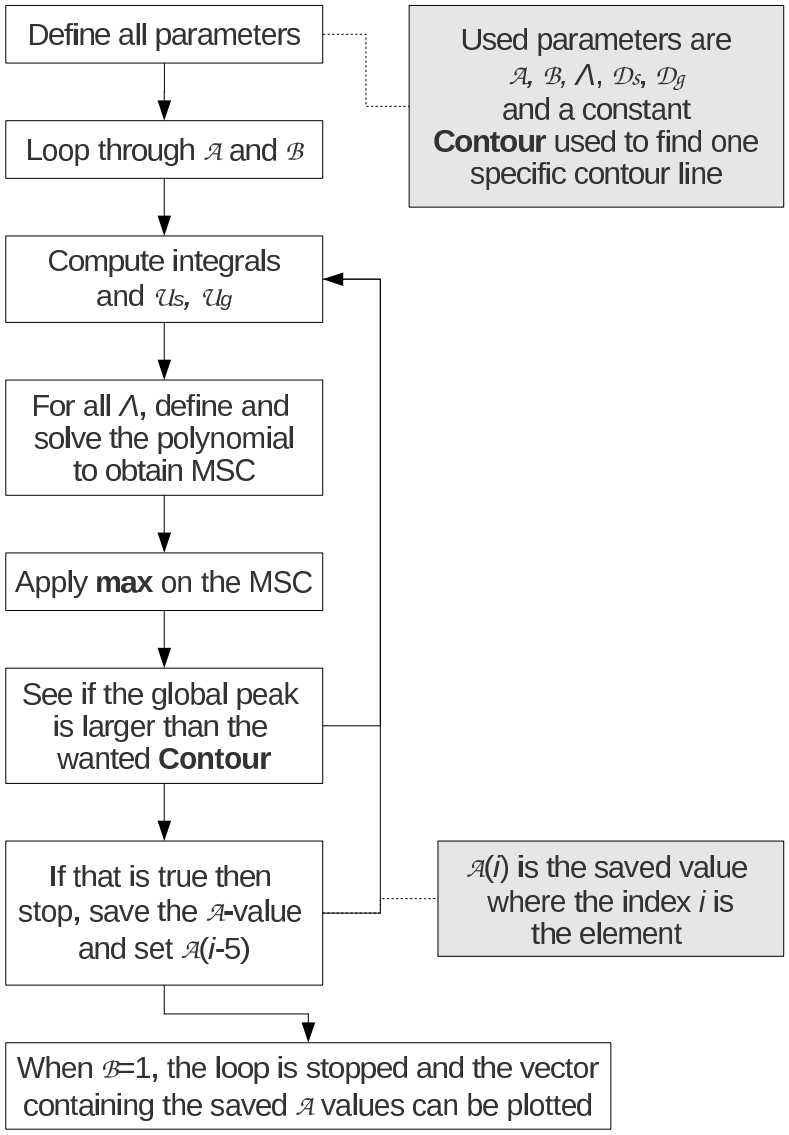

Figure C.2: Flowchart describing the routine used to find the determine contour lines of the stability threshold for thick discs as described in Appendix C.3.

Bibliography

Arp, H. 1966, ApJS, 14, 1

Bertin, G. & Romeo, A. B. 1988, A&A, 195, 105

Binney, J. & Tremaine, S. 2008, Galactic Dynamics: Second Edition (Princeton University Press)

Burkert, A. 2009, in IAU Symposium, Vol. 254, IAU Symposium, ed. J. Andersen, J. Bland-Hawthorn, & B. Nordström, 437–444

Burkert, A., Genzel, R., Bouche, N., Cresci, G., Khochfar, S., Sommer-Larsen, J., Sternberg, A., Naab, T., Foerster-Schreiber, N., Tacconi, L., Shapiro, K., Hicks, E., Lutz, D., Davies, R., Buschkamp, P., & Genel, S. 2009, ArXiv e-prints

Elmegreen, B. G. 1999, in Star Formation 1999, ed. T. Nakamoto, 3–5

Fridman, A. M., Polyachenko, V. L., Aries, A. B., & Poliakoff, I. N. 1984, Physics of gravitating systems. I. Equilibrium and stability. (Springer-Verlag)

Gerssen, J., Kuijken, K., & Merrifield, M. R. 1997, MNRAS, 288, 618

Helfer, T. T., Thornley, M. D., Regan, M. W., Wong, T., Sheth, K., Vogel, S. N., Blitz, L., & Bock, D. 2003, ApJS, 145, 259

Hitschfeld, M., Kramer, C., Schuster, K. F., Garcia-Burillo, S., & Stutzki, J. 2009, A&A, 495, 795

Jarrett, T. H., Chester, T., Cutri, R., Schneider, S. E., & Huchra, J. P. 2003, AJ, 125, 525

Jog, C. J. 1996, MNRAS, 278, 209

Jog, C. J. & Solomon, P. M. 1984, ApJ, 276, 114

Kennicutt, Jr., R. C., Armus, L., Bendo, G., Calzetti, D., Dale, D. A., Draine, B. T., Engelbracht, C. W., Gordon, K. D., Grauer, A. D., Helou, G., Hollenbach, D. J., Jarrett, T. H., Kewley, L. J., Leitherer, C., Li, A., Malhotra, S., Regan, M. W., Rieke, G. H., Rieke, M. J., Roussel, H., Smith, J., Thornley, M. D., & Walter, F. 2003, PASP, 115, 928

Krumholz, M. R. & Burkert, A. 2010, ArXiv e-prints

Leroy, A. K., Walter, F., Brinks, E., Bigiel, F., de Blok, W. J. G., Madore, B., & Thornley, M. D. 2008, AJ, 136, 2782

Martin, C. L. & Kennicutt, Jr., R. C. 2001, ApJ, 555, 301

McKee, C. F. & Ostriker, E. C. 2007, ARAA, 45, 565

Polyachenko, V. L., Polyachenko, E. V., & Strel'Nikov, A. V. 1997, Astronomy Letters, 23, 483

Prada, F., Gutierrez, C., Peletier, R. F., & McKeith, C. D. 1996, ArXiv Astrophysics e-prints

Puech, M. 2010, MNRAS, 689

Rafikov, R. R. 2001, MNRAS, 323, 445

Romeo, A. B. 1990, PhD thesis, SISSA, Trieste, Italy

—. 1992, MNRAS, 256, 307

—. 1994, A&A, 286, 799

Safronov, V. S. 1960, Annales d'Astrophysique, 23, 979

Schmidt, M. 1959, ApJ, 129, 243

Toomre, A. 1964, ApJ, 139, 1217

van der Kruit, P. C. & de Grijs, R. 1999, A&A, 352, 129

Vandervoort, P. O. 1970, ApJ, 161, 87

Walter, F., Brinks, E., de Blok, W. J. G., Bigiel, F., Kennicutt, R. C., Thornley, M. D., & Leroy, A. 2008, AJ, 136, 2563

Wang, B. & Silk, J. 1994, ApJ, 427, 759

Wong, T., Hughes, A., Fukui, Y., Kawamura, A., Mizuno, N., Ott, J., Muller, E., Pineda, J. L., Welty, D. E., Kim, S., Mizuno, Y., Murai, M., & Onishi, T. 2009, ApJ, 696, 370

Yang, C., Gruendl, R. A., Chu, Y., Mac Low, M., & Fukui, Y. 2007, ApJ, 671, 374
toc